

國立交通大學

電機學院通訊與網路科技產業研發碩士班

碩士論文

IEEE 802.16m 之初始下行同步

Initial Downlink Synchronization for IEEE 802.16m



研究生：陸凱暉

指導教授：林大衛 博士

張文鐘 博士

中華民國九十九年二月

IEEE 802.16m 之初始下行同步
Initial Downlink Synchronization for IEEE 802.16m


研究生：陸凱暉

Student : Kai-Wei Lu

指導教授：林大衛

Advisor : Dr. David W. Lin

國立交通大學
電機學院通訊與網路科技產業研發碩士班
碩士論文



A Thesis
Submitted to College of Electrical and Computer Engineering
National Chiao Tung University
in partial Fulfillment of the Requirements
for the Degree of
Master
in

Industrial Technology R & D Master Program on
Communication Engineering

February 2010

Hsinchu, Taiwan, Republic of China

中華民國九十九年二月

IEEE 802.16m 之初始下行同步

學生：陸凱暉

指導教授：林大衛 博士
張文鐘 博士

國立交通大學電機學院產業研發碩士班

摘要

當一個行動電話開始要進入網路的時候，我們必須與基地台做初始的同步。在初始的同步中，包含了符元時間偏移、載波偏移和前置符元序號(preamble index)需要同步估測。我們利用前置符元的功率較一般資料符元(data symbol)大的特性做功率移動累加，藉由找到累加結果的峰值來估測前置符元的起始位置。由此起始位置向後推算一個符元長度以當作我們所估測出來的前置符元，而與真實的前置符元存在一個相位性錯誤(phase error)。我們利用此估測出來的前置符元推導其近似最大可能性估測(quasi maximum likelihood)以求得小數部分載波偏移和導出前置符元的通道估測的式子。我們在頻域上將此通道估測的式子經由估測出來的小數部分載波偏移補償之後，代入由合理範圍的整數部分載波偏移和不同的前置符元而得到的通道脈衝響應。再計算這些通道脈衝響應不同的精準符碼時間偏移序號 64 點功率和並且選出最大的那一個，其所在的整數部分載波偏移、前置符元和精準符碼時間偏移序號即為此聯合估測的結果。

本篇論文介紹 IEEE 802.16m 系統裡關於下行初始同步的問題、演算法推導、以及程式模擬方面的議題。首先簡介 IEEE 802.16m 下行的標準機制及相關架構，接著提出同步問題並提供演算法的設計發想及推導，而後將整個演算法的流程用浮點數運算來驗證，設計出一個合理的 IEEE 802.16m 接收訊號模型，在可加性白色高斯雜訊(additive white Gaussian noise, AWGN)通道之下得到的數據來驗證演算法的特性，然後在多路徑衰減(multipath fading)通道傳輸中使用數種不同多路徑通道、相對移動車速以及訊雜比(signal to noise ratio, SNR)來測試演算法對多路徑效應、通道衰減以及相對速度引起的都普勒頻移(Doppler shifts)所產生的影響。

Initial Downlink Synchronization for IEEE 802.16m

Student: Kai-Wei Lu

Advisor: Dr. David W. Lin

Dr. Wen-Thong Chang

Industrial Technology R & D Master Program of
Electrical and Computer Engineering College
National Chiao Tung University

ABSTRACT

This thesis introduces some topics about initial downlink synchronization, algorithm derivations, and program simulations of IEEE 802.16m system.

When a mobile station entering to the network, it needs to perform initial synchronization, including of symbol timing offset, carrier frequency offset and preamble index. We utilize the trait which the power of preamble is larger than it of the common data symbol to compute the moving power sum, and then estimate the left boundary of preamble by finding out the peak value of moving power sum. A symbol period from this estimated boundary is regarded as the estimated preamble, which has a phase noise with the exact preamble. We derive the quasi maximum likelihood estimation from the likelihood function of the estimated preamble to obtain fractional carrier frequency offset (FCFO) and the formula of channel estimation. After compensating the estimated fractional carrier frequency offset to the formula of channel estimation, we substitute several reasonable integral carrier frequency offsets (ICFOs) and primary advanced preambles (PA-Preambles) into this formula and obtain channel impulse responses (CIRs). After that, we compute different fine timing offset index 64-points power sum of these CIRs and find out the peak value whose ICFO, PA-Preamble index, and fine timing offset index are regarded as the result of the joint estimation.

In terms of simulations, above all, we present a reasonable received signal model of IEEE 802.16m, and then simulate our algorithm in floating point under AWGN (additive white Gaussian noise) channel to verify its performance. Moreover, we test this algorithm under different multipath fading channels, Pedestrian B and SUI-5, at different speed which cause Doppler shifts, and signal to noise ratio (SNR) to observe the effect on this algorithm.

誌謝

這篇論文能夠順利完成，首先要感謝的人是我的指導教授林大衛老師以及張文鐘老師。在兩年半的研究所生涯當中，由於老師的細心指導及在專業領域的博學精深，令我在研究的精神與方法上獲益良多且終身受用。

此外，感謝通訊電子與訊號處理實驗室所有的成員，包含各位師長、同學、學長姐與學弟妹們。感謝洪崑健學長、林鴻志學長、吳俊榮學長、王柏森學長以及王海薇學姐給予我在研究過程上的指導與建議，還有劭學、志偉、豐進、世榮、清德、振偉、重佑和藹璇等同學，因為能和你們共同討論、分享求學的經驗及一路上的相互扶持，讓這兩年半的研究生涯充滿歡樂與回憶。

最後，我要感謝我的家人們以及女友，感謝他們一直都在背後支持我，在求學過程中總是不斷的鼓勵、體諒及包容，是我精神與實質上最大的支柱，沒有他們無保留的給予，一切的美好與榮耀將不復存在。

在此，虔誠的將此篇論文獻給所有陪伴著我走過這一段歲月的每一個人。

陸凱暉

民國九十九年二月 於風城·新竹

Contents

1	Introduction	1
2	Overview of the IEEE 802.16m Standard	3
2.1	Overview of OFDMA [1], [2]	3
2.1.1	Cyclic Prefix	4
2.1.2	Discrete-Time Baseband Equivalent System Model	5
2.2	Basic OFDMA Symbol Structure in IEEE 802.16m [3]	6
2.2.1	OFDMA Basic Terms	7
2.2.2	Frequency Domain Description	8
2.2.3	Primitive Parameters	8
2.2.4	Derived Parameters	8
2.2.5	Frame Structure	9
2.3	Downlink Transmission in IEEE 802.16m [3]	11
2.3.1	Subband Partitioning	12
2.3.2	Miniband Permutation	13
2.3.3	Frequency Partitioning	15
2.4	Cell-Specific Resource Mapping [3]	19
2.4.1	CRU/DRU Allocation	19
2.4.2	Subcarrier Permutation	20
2.4.3	Random Sequence Generation	22
2.5	Advanced Preamble Structure (A-Preamble) [3]	22
2.5.1	Primary Advanced Preamble (PA-Preamble)	23
2.5.2	Secondary Advanced Preamble (SA-Preamble)	25

3	Initial Downlink Synchronization	28
3.1	The Initial Synchronization Problem	28
3.2	Derivation of the Initial Synchronization Procedure	29
3.2.1	Coarse Timing Synchronization	30
3.2.2	Estimation of Fractional Carrier Frequency Offset	32
3.2.3	Jointly Integral CFO, PA-Preamble Index, Channel Estimation and Fine Timing Offset Searching	40
3.2.4	Overall Block Diagram	41
3.3	Identification of the SA-Preamble	41
4	Simulation Study	45
4.1	System Parameters and Channel Environments	45
4.1.1	System Parameters	45
4.1.2	Power Delay Profiles	45
4.2	Simulation Results	47
4.2.1	Coarse Timing Estimation	47
4.2.2	Fractional CFO	49
4.2.3	Joint Estimation of Integral CFO, PA-Preamble Index, Channel Response and Fine Timing	50
4.2.4	Overall Timing Estimation	52
5	Conclusion and Future Work	69
5.1	Conclusion	69
5.2	Future Work	70

List of Figures

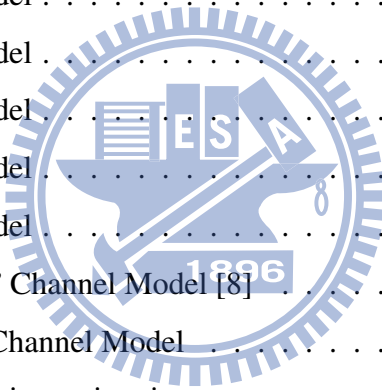
2.1	Discrete-time model of the baseband OFDMA system (from [1]).	4
2.2	OFDMA symbol time structure (Fig. 428 in [3]).	5
2.3	Discrete-time baseband equivalent of an OFDMA system with M users (from [2]).	6
2.4	OFDMA parameters (Table 647 in [3]).	9
2.5	More OFDMA parameters (Table 647 in [3]).	10
2.6	Basic frame structure for 5, 10 and 20 MHz channel bandwidths (Fig. 430 in [3]).	10
2.7	Example of downlink physical structure (Fig. 449 in [3]).	12
2.8	Mapping between SAC and K_{SB} for 10 or 20 MHz band (Table 649 in [3]).	14
2.9	Mapping between SAC and K_{SB} for 5 MHz band (Table 650 in [3]). . . .	14
2.10	PRU to PRU_{SB} and PRU_{MB} mapping for BW = 5 MHz, and $K_{SB}=3$ (Fig. 450 in [3]).	15
2.11	Mapping from PRUs to PRU_{SB} and $PPRU_{MB}$ for BW = 5 MHz and K_{SB} = 3 (Fig. 451 in [3]).	16
2.12	Mapping between DFPC and frequency partitioning for 10 or 20 MHz band (Table 651 in [3]).	17
2.13	Mapping between DFPC and frequency partitioning for 5 MHz band (Ta- ble 652 in [3]).	17
2.14	Frequency partitioning for BW = 5 MHz, $K_{SB} = 3$, FPCT = 2, FPS = 12, and FPSC = 1 (Fig. 452 in [3]).	18
2.15	Location of the A-Preamble symbol (re-arranged from Fig. 500 in [3]). . .	23
2.16	PA-Preamble symbol structure of 5-MHz system (Fig. 501 in [3]).	24

2.17	PA-Preamble symbol structure of 10 MHz system.	24
2.18	PA-Preamble symbol structure of 20 MHz system.	24
2.19	PA-Preamble Series (Table 780 in [3]).	25
2.20	SA-Preamble symbol structure of 5 MHz.	26
2.21	The allocation of sequence block for each FFT size (Fig. 503 in [3]).	27
2.22	SA-Preamble symbol structure for 512-FFT (Fig. 504 in [3]).	27
3.1	Window sliding structure.	29
3.2	576 points power sum under AWGN in 0 dB.	31
3.3	576 points power sum under AWGN in 10 dB.	32
3.4	576 points power sum under PB at mobility 350 km/h in 0 dB.	33
3.5	576 points power sum under PB at mobility 350 km/h in 10 dB.	34
3.6	576 points power sum under SUI-5 at mobility 350 km/h in 0 dB.	35
3.7	576 points power sum under SUI-5 at mobility 350 km/h in 10 dB.	36
3.8	Channel impulse response of PB channel.	37
3.9	Channel impulse response of SUI-5 channel.	38
3.10	The estimated CIR with accurate ICFO, 8, compensating and correct PA-Preamble index, 1, under PB channel with 120 km/h, 0dB in SNR.	41
3.11	The CIR with the inaccurate ICFO, 6, compensating and incorrect PA-Preamble index, 0, under PB channel with 120 km/h, 0dB in SNR.	42
3.12	Block diagram of initial DL synchronization.	43
4.1	Histogram of coarse timing estimation under AWGN channel in 0 dB.	49
4.2	Histogram of coarse timing estimation under AWGN channel in 10 dB.	50
4.3	Histogram of coarse timing estimation under PB at 3 km/h in 0 dB.	51
4.4	Histogram of coarse timing estimation under PB at 3 km/h in 10 dB.	52
4.5	Histogram of coarse timing estimation under PB at 120 km/h in 0 dB.	53
4.6	Histogram of coarse timing estimation under PB at 120 km/h in 10 dB.	54
4.7	Histogram of coarse timing estimation under SUI-5 at 3 km/h in 0 dB.	54
4.8	Histogram of coarse timing estimation under SUI-5 at 3 km/h in 10 dB.	55
4.9	Histogram of coarse timing estimation under SUI-5 at 120 km/h in 0 dB.	55

4.10	Histogram of coarse timing estimation under SUI-5 at 120 km/h in 10 dB.	56
4.11	Simulation results of FCFO estimation under PB, SUI5 and AWGN channel.	57
4.12	Histogram of fine timing estimation under AWGN channel in 0 dB.	58
4.13	Histogram of fine timing estimation under AWGN channel in 10 dB.	58
4.14	Histogram of fine timing estimation under PB at 3 km/h in 0 dB.	59
4.15	Histogram of fine timing estimation under PB at 3 km/h in 10 dB.	59
4.16	Histogram of fine timing estimation under PB at 120 km/h in 0 dB.	60
4.17	Histogram of fine timing estimation under PB at 120 km/h in 10 dB.	60
4.18	Histogram of fine timing estimation under SUI-5 at 3 km/h in 0 dB.	61
4.19	Histogram of fine timing estimation under SUI-5 at 3 km/h in 10 dB.	61
4.20	Histogram of fine timing estimation under SUI-5 at 120 km/h in 0 dB.	62
4.21	Histogram of fine timing estimation under SUI-5 at 120 km/h in 10 dB.	62
4.22	Histogram of ICFO estimation under SUI-5 at 120 km/h in 0 dB.	63
4.23	Histogram of PID estimation under SUI-5 at 120 km/h in 0 dB.	63
4.24	Histogram of timing estimation under AWGN in 0 dB.	64
4.25	Histogram of timing estimation under AWGN in 10 dB.	64
4.26	Histogram of timing estimation under PB at 3 km/h in 0 dB.	65
4.27	Histogram of timing estimation under PB at 3 km/h in 10 dB.	65
4.28	Histogram of timing estimation under PB at 120 km/h in 0 dB.	66
4.29	Histogram of timing estimation under PB at 120 km/h in 10 dB.	66
4.30	Histogram of timing estimation under SUI-5 at 3 km/h in 0 dB.	67
4.31	Histogram of timing estimation under SUI-5 at 3 km/h in 10 dB.	67
4.32	Histogram of timing estimation under SUI-5 at 120 km/h in 0 dB.	68
4.33	Histogram of timing estimation under SUI-5 at 120 km/h in 10 dB.	68

List of Tables

2.1	PRU Structure for Different Types of Subframes	7
4.1	System Parameters Used in Our Study	46
4.2	SUI-1 Channel Model	46
4.3	SUI-2 Channel Model	46
4.4	SUI-3 Channel Model	47
4.5	SUI-4 Channel Model	47
4.6	SUI-5 Channel Model	47
4.7	SUI-6 Channel Model	48
4.8	ETSI “Vehicular A” Channel Model [8]	48
4.9	Pedestrian B (PB) Channel Model	49
4.10	The error rate of timing estimation.	53



Chapter 1

Introduction

ITU-R defined the criterion of the fourth-generation (4G) mobile communication standard IMT-Advanced formally in June 2003, that the data rate need be higher than 100 Mbps in the environment with the high mobility and 1 Gbps in the static environment. Therefore, IEEE 802.16m Task Group (TGm) has set up the 802.16m (i.e., Advanced WiMAX or WiMAX 2) since December 2006 in order to compete for the fourth-generation standard. The new frame structure developed by IEEE 802.16m is such that it can be compatible with IEEE 802.16e, reduce communication latency, support relay and coexist with other radio access techniques, so that it can become one of the promising candidates of 4G.

In this thesis, we consider the IEEE 802.16m system in time-division duplex (TDD) mode, where downlink (DL) and uplink (UL) transmissions are time multiplexed in each frame. Our study focuses on the techniques of downlink initial synchronization, including problem formulation, algorithm derivation and computer simulation. In this, we utilize the special structure of the primary advanced preamble (PA-Preamble) defined in the draft IEEE 802.16m standard. The synchronization work involves frequency recovery, timing recovery and bandwidth detection, where bandwidth detection is accomplished by identifying the PA-Preamble index. In the procedure that we have developed, channel estimation is also obtained simultaneously.

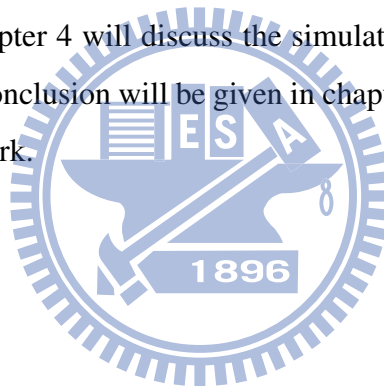
The contributions of this work are as follows:

- We establish a received signal model of IEEE 802.16m and estimate the coarse

timing by the difference of power between the PA-Preamble and other data symbols.

- In order to estimate fractional carrier frequency offset (FCFO), we derive a simplified maximum likelihood estimation and get a result which is the same with the Moose algorithm.
- From the process of FCFO estimation, we can get the least-square estimation of channel impulse response of the PA-Preamble and utilize its characteristic of power centralization to search integral carrier frequency offset (ICFO), preamble index (PID) and the fine timing offset jointly.

This thesis is organized as follows. We will first introduce the IEEE 802.16m standard briefly in chapter 2. We will analyze the synchronization problems and present the overall procedure in chapter 3. Chapter 4 will discuss the simulation results under the different environments. Finally, the conclusion will be given in chapter 5, where we will also point out some potential future work.



Chapter 2

Overview of the IEEE 802.16m Standard

The IEEE 802.16m standard is based on orthogonal frequency division multiplexing (OFDM) and orthogonal frequency division multiple access (OFDMA). The IEEE 802.16m Task Group intends to complete the first version of the standard in 2010. In this chapter, we first introduce some basic concepts regarding OFDM and OFDMA. Then we give an overview of the draft IEEE 802.16m standard. For the sake of simplicity, we only introduce the specifications that are most relevant to our study.

2.1 Overview of OFDMA [1], [2]

OFDMA is considered one most appropriate scheme for future wireless systems, including 4G broadband wireless networks. In a typical OFDMA system, users simultaneously transmit their data by modulating mutually exclusive sets of orthogonal subcarriers, so that each user's signal can be separated in the frequency domain. One typical structure is subband OFDMA, where all available subcarriers are divided into a number of subbands and each user is allowed to use one or more subbands for the data transmission. Usually, pilot symbols are employed for the estimation of channel state information (CSI) within the subband. IEEE 802.16e and 802.16m are examples of such systems. Figure 2.1 shows an OFDMA system in which active users simultaneously communicate

with the base station (BS).

2.1.1 Cyclic Prefix

Cyclic prefix (CP) or guard time is used in OFDM and OFDMA systems to overcome the intersymbol and interchannel intercarrier problems. The multiuser channel is usually assumed to be substantially invariant within one-block (or one-symbol) duration. The channel delay spread plus symbol timing mismatch is usually assumed to be smaller than the CP duration. In this condition, users do not interfere with each other in the frequency domain when their signals are properly synchronized in frequency and in time.

A CP is a copy of the last part of the OFDMA symbol (see Fig. 2.2). A copy of the last T_g of the useful symbol period is used to collect multipaths while maintaining the orthogonality of subcarriers. However, the transmitter energy increases with the length of the guard time while the receiver energy remains the same (the CP is discarded in the receiver). So there is a $10 \log(1 - T_g/(T_b + T_g))/\log(10)$ dB loss in E_b/N_0 .

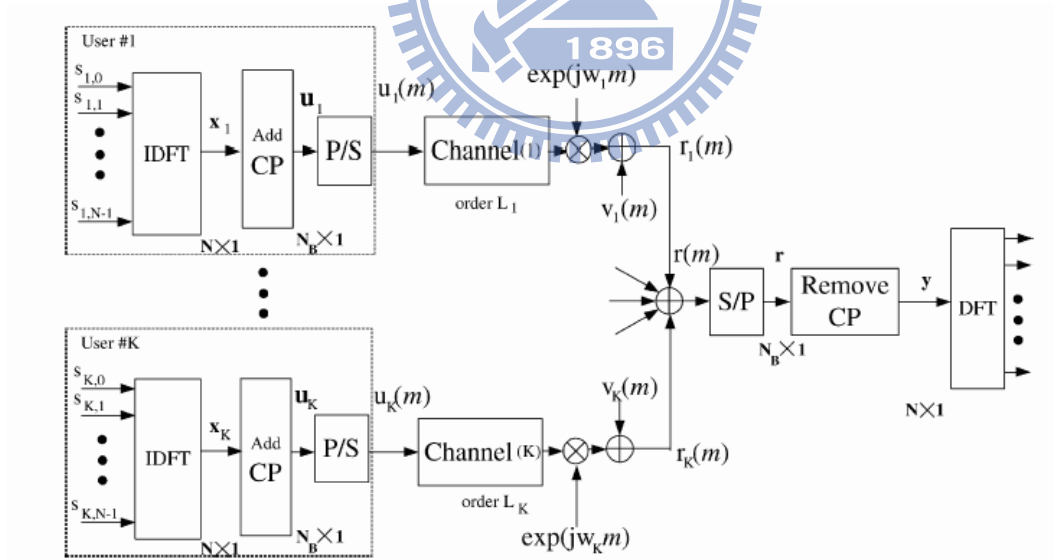


Figure 2.1: Discrete-time model of the baseband OFDMA system (from [1]).

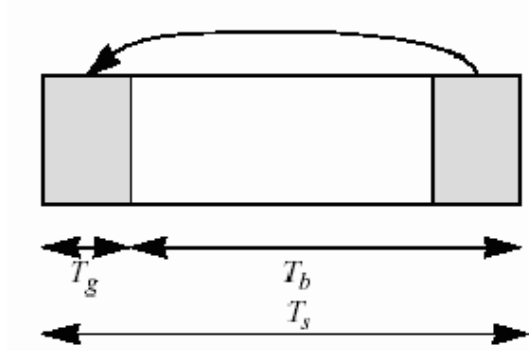


Figure 2.2: OFDMA symbol time structure (Fig. 428 in [3]).

2.1.2 Discrete-Time Baseband Equivalent System Model

The material in this subsection is mainly taken from [2]. Consider an OFDMA system with M active users sharing a bandwidth of $B = \frac{1}{T}$ Hz (T is the sampling period) as shown in Fig. 2.3. The system consists of K subcarriers of which K_u are useful subcarriers (excluding guard bands and DC subcarrier). The users are allocated non-overlapping subcarriers according to their needs.

Let the discrete-time baseband channel consists of L multipath components as

$$h(l) = \sum_{m=0}^{L-1} h_m \delta(l - l_m), \quad (2.1)$$

where h_m is a zero-mean complex Gaussian random variable with $E[h_i h_j^*] = 0$ for $i \neq j$. In the frequency domain,

$$\mathbf{H} = \mathbf{F}\mathbf{h}, \quad (2.2)$$

where $\mathbf{H} = [H_0, H_1, \dots, H_{K-1}]^T$, $\mathbf{h} = [h_0, \dots, h_{L-1}, 0, \dots, 0]^T$ and \mathbf{F} is K -point discrete Fourier transform (DFT) matrix. The impulse response length l_{L-1} is upper bounded by the length of CP (L_{cp}).

The received signal in the frequency domain is given by

$$\mathbf{Y}_n = \sum_{i=1}^M \mathbf{X}_{i,n} \mathbf{H}_{i,n} + \mathbf{V}_n, \quad (2.3)$$

where $\mathbf{X}_{i,n} = \text{diag}(X_{i,n,0}, \dots, X_{i,n,K-1})$ is $K \times K$ diagonal data matrix and $\mathbf{H}_{i,n}$ is the $K \times 1$ channel vector (2.2) corresponding to the i th user in the n th symbol. The noise vector \mathbf{V}_n is distributed as $CN(0, \sigma^2 I_K)$.

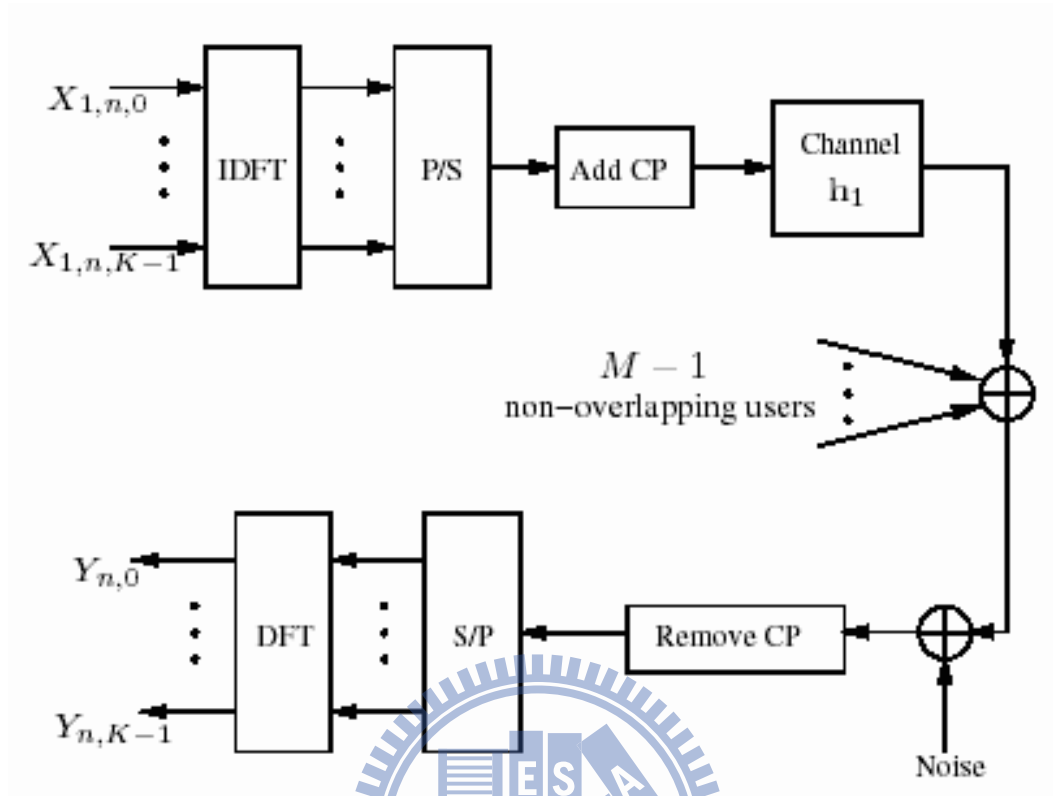


Figure 2.3: Discrete-time baseband equivalent of an OFDMA system with M users (from [2]).

2.2 Basic OFDMA Symbol Structure in IEEE 802.16m [3]

The Advanced Air Interface defined by IEEE 802.16m is designed for nonline-of-sight (NLOS) operation in the licensed frequency bands below 6 GHz. The Advanced Air Interface supports time-division-duplexing (TDD) and frequency-division-duplexing (FDD) duplex modes, including half FDD (H-FDD) mobile station (MS) operation. Unless otherwise specified, the frame structure attributes and baseband processing are common for all duplex modes.

The Advanced Air Interface uses OFDMA as the multiple access scheme in the down-link and uplink. The material of this section is mainly taken from [3].

2.2.1 OFDMA Basic Terms

We introduce some basic terms in the OFDMA physical layer (PHY) of IEEE 802.16m. These definitions help us understand the concepts of subcarrier allocation and transmission in IEEE 802.16m.

- **Physical and logical resource units:** A physical resource unit (PRU) is the basic physical unit for resource allocation. It comprises P_{sc} consecutive subcarriers by N_{sym} consecutive OFDMA symbols, where $P_{sc} = 18$ and $N_{sym} = 6$ for type-1 subframes, $N_{sym} = 7$ for type-2 subframes, and $N_{sym} = 5$ for type-3 subframes. Table 2.2.1 illustrates the PRU's sizes for different subframe types. A logical resource unit (LRU) is the basic logical unit for distributed and localized resource allocations. An LRU is $P_{sc} \cdot N_{sym}$ subcarriers for type-1, type-2, and type-3 subframes. The LRU includes the pilots that are used in a PRU. The effective number of data subcarriers in an LRU depends on the number of allocated pilots.
- **Distributed resource unit:** A distributed resource unit (DRU) contains a group of subcarriers which are spread across the distributed resource allocations within a frequency partition. The size of DRU equals the size of PRU, i.e., P_{sc} subcarriers by N_{sym} OFDMA symbols.
- **Contiguous resource unit:** The localized resource unit, also known as contiguous resource unit (CRU), contains a group of subcarriers which are contiguous across the localized resource allocations. The size of CRU equals the size of PRU, i.e., P_{sc} subcarriers by N_{sym} OFDMA symbols.

Table 2.1: PRU Structure for Different Types of Subframes

Subframe Type	Number of Subcarriers	Number of Symbols
1	18	6
2	18	7
3	18	5

2.2.2 Frequency Domain Description

The frequency domain description includes the basic structure of an OFDMA symbol. An OFDMA symbol is made up of subcarriers, the number of which determines the DFT size used. There are several subcarrier types:

- Data subcarriers: for data transmission.
- Pilot subcarriers: for various estimation purposes.
- Null subcarriers: no transmission at all, for guard bands and DC subcarrier.

The purpose of the guard bands is to help enable proper bandlimiting.

2.2.3 Primitive Parameters

Four primitive parameters characterize the OFDMA symbols:

- BW : the nominal channel bandwidth.
- N_{used} : number of used subcarriers (which includes the DC subcarrier).
- n : sampling factor. This parameter, in conjunction with BW and N_{used} , determines the subcarrier spacing and the useful symbol time. This value is given in Figs. 2.4 and 2.5 for each nominal bandwidth.
- G : This is the ratio of CP time to “useful” time, i.e., T_{cp}/T_s . The following values are supported: 1/16, 1/8, and 1/4.

2.2.4 Derived Parameters

The following parameters are defined in terms of the primitive parameters.

- N_{FFT} : smallest power of two greater than N_{used} .
- Sampling frequency: $F_s = \lfloor n \cdot BW/8000 \rfloor \times 8000$.
- Subcarrier spacing: $\Delta f = F_s/N_{FFT}$.

- Useful symbol time: $T_b = 1/\Delta f$.
- CP time: $T_g = G \times T_b$.
- OFDMA symbol time: $T_s = T_b + T_g$.
- Sampling time: T_b/N_{FFT} .

2.2.5 Frame Structure

The advanced air interface basic frame structure is illustrated in Fig. 2.6. Each 20-ms superframe is divided into four 5-ms radio frames. When using the same OFDMA parameters as in Figs. 2.4 and 2.5 with channel bandwidth of 5, 10, or 20 MHz, each

The nominal channel bandwidth, BW (MHz)		5	7	8.75	10	20	
Sampling factor, n		28/25	8/7	8/7	28/25	28/25	
Sampling frequency, F_s (MHz)		5.6	8	10	11.2	22.4	
FFT size, N_{FFT}		512	1024	1024	1024	2048	
Subcarrier spacing, Δf (kHz)		10.94	7.81	9.77	10.94	10.94	
Useful symbol time, T_b (μ s)		91.4	128	102.4	91.4	91.4	
CP ratio, $G = 1/8$	OFDMA symbol time, T_s (μ s)	102.857	144	115.2	102.857	102.857	
	FDD	Number of OFDMA symbols per 5ms frame	48	34	43	48	48
		Idle time (μ s)	62.857	104	46.40	62.857	62.857
	TDD	Number of OFDMA symbols per 5ms frame	47	33	42	47	47
		TTG + RTG (μ s)	165.714	248	161.6	165.714	165.714
CP ratio, $G = 1/16$	OFDMA symbol time, T_s (μ s)	97.143	136	108.8	97.143	97.143	
	FDD	Number of OFDMA symbols per 5ms frame	51	36	45	51	51
		Idle time (μ s)	45.71	104	104	45.71	45.71
	TDD	Number of OFDMA symbols per 5ms frame	50	35	44	50	50
		TTG + RTG (μ s)	142.853	240	212.8	142.853	142.853

Figure 2.4: OFDMA parameters (Table 647 in [3]).

CP ratio, $G = 1/4$	OFDMA symbol time, T_s (μs)		114.286	160	128	114.286	114.286
	FDD	Number of OFDMA symbols per 5ms frame	43	31	39	43	43
		Idle time (μs)	85.694	40	8	85.694	85.694
	TDD	Number of OFDMA symbols per 5ms frame	42	30	38	42	42
		TTG + RTG (μs)	199.98	200	136	199.98	199.98
Number of Guard Sub-Carriers		Left	40	80	80	80	160
		Right	39	79	79	79	159
Number of Used Sub-Carriers			433	865	865	865	1729
Number of Physical Resource Unit (18x6) in a type-1 sub-frame.			24	48	48	48	96

Figure 2.5: More OFDMA parameters (Table 647 in [3]).

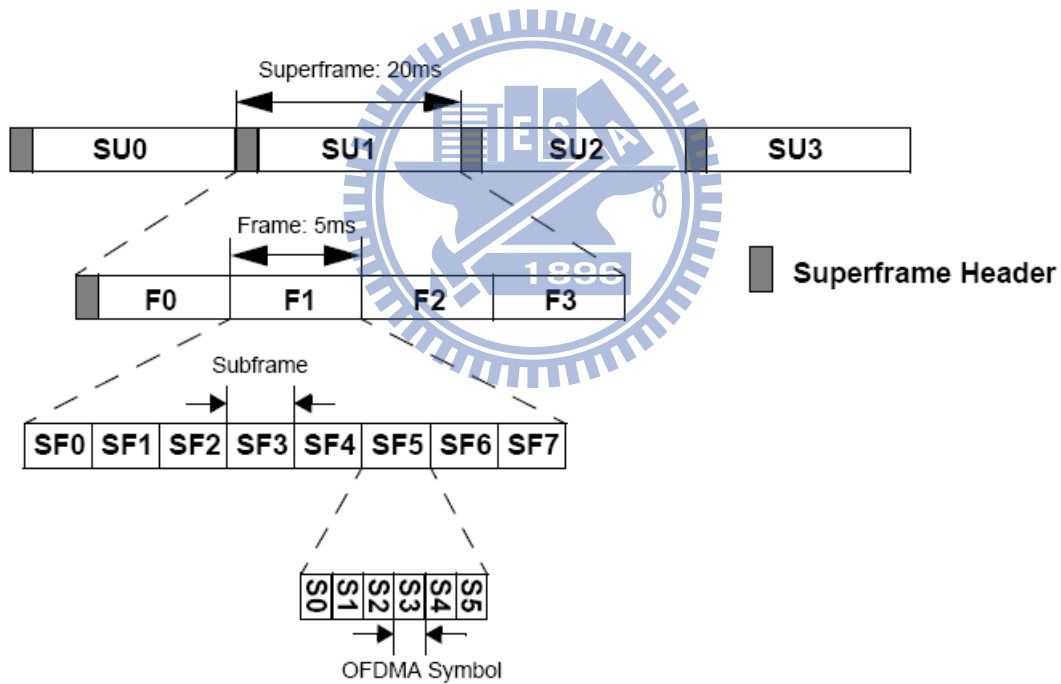


Figure 2.6: Basic frame structure for 5, 10 and 20 MHz channel bandwidths (Fig. 430 in [3]).

5-ms radio frame further consists of eight subframes, for $G = 1/8$ and $1/16$. With channel bandwidth of 8.75 or 7 MHz, each 5-ms radio frame further consists of seven and six subframes, respectively for $G = 1/8$ and $1/16$. In the case of $G = 1/4$, the number

of subframes per frame is one less than that of other CP lengths for each bandwidth case. A subframe forms the unit of assignment for either downlink (DL) or uplink (UL) transmission. There are four types of subframes:

- Type-1 subframe consists of six OFDMA symbols.
- Type-2 subframe consists of seven OFDMA symbols.
- Type-3 subframe consists of five OFDMA symbols.
- Type-4 subframe consists of nine OFDMA symbols. This type shall be applied only to UL subframe for the 8.75 MHz channel bandwidth when supporting the WirelessMAN-OFDMA frames.

The basic frame structure is applied to FDD and TDD duplexing schemes, including H-FDD MS operation. The number of switching points in each radio frame in TDD systems shall be two, where a switching point is defined as a change of directionality, i.e., from DL to UL or from UL to DL.

A data burst shall occupy either one subframe (i.e., the default transmission time interval [TTI] transmission) or contiguous multiple subframes (i.e., the long TTI transmission). The long TTI in FDD shall be 4 subframes for both DL and UL. The long TTI in TDD shall be the whole DL (UL) subframes for DL (UL) in a frame. Every superframe shall contain a superframe header (SFH). The SFH shall be located in the first DL subframe of the superframe and shall include broadcast channels.

2.3 Downlink Transmission in IEEE 802.16m [3]

Again, this section is mainly taken from [3]. Each DL subframe is divided into 4 or fewer frequency partitions, each partition consisting of a set of physical resource units across the total number of OFDMA symbols available in the subframe. Each frequency partition can include contiguous (localized) and/or non-contiguous (distributed) physical resource units (PRUs). Each frequency partition can be used for different purposes such as fractional frequency reuse (FFR) or multicast and broadcast services (MBS). Fig. 2.7

illustrates the downlink physical structure in an example of two frequency partitions with frequency partition 2 including both contiguous and distributed resource allocations.

2.3.1 Subband Partitioning

The PRUs are first subdivided into subbands and minibands where a subband comprises N_1 adjacent PRUs and a miniband comprises N_2 adjacent PRUs, where $N_1 = 4$ and $N_2 = 1$. Subbands are suitable for frequency selective allocations as they provide a contiguous allocation of PRUs in frequency. Minibands are suitable for frequency diverse allocation and are permuted in frequency.

The number of subbands reserved is denoted by K_{SB} . The number of PRUs allocated to subbands is denoted by L_{SB} , where $L_{SB} = N_1 \cdot K_{SB}$, depending on system bandwidth. A 4 or 3-bit field called Subband Allocation Count (SAC) determines the value of K_{SB} . The remainder of the PRUs are allocated to minibands. The number of minibands in an allocation is denoted by K_{MB} . The number of PRUs allocated to minibands is denoted by L_{MB} , where $L_{MB} = N_2 \cdot K_{MB}$. The total number of PRUs is denoted N_{PRU} where $N_{PRU} = L_{SB} + L_{MB}$. The maximum number of subbands that can be formed is denoted

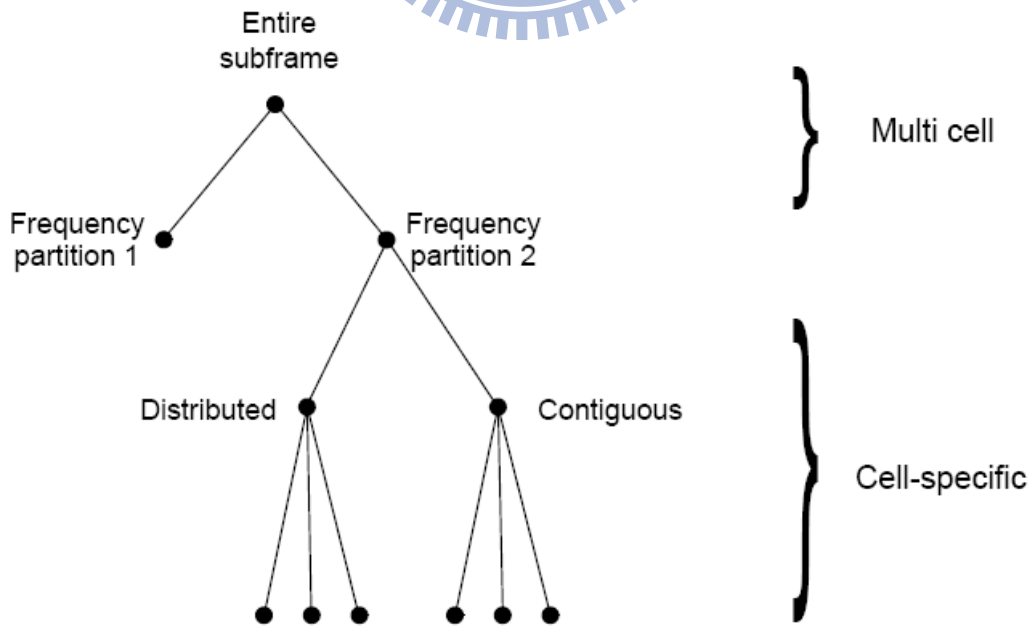


Figure 2.7: Example of downlink physical structure (Fig. 449 in [3]).

N_{sub} where $N_{sub} = NPRU/N_1$.

Figs. 2.8 and 2.9 show the mapping between SAC and K_{SB} for the 10 and 20 MHz bands and the 5 MHz band, respectively.

PRUs are partitioned and reordered into two groups called subband PRUs and mini-band PRUs and denoted PRU_{SB} and PRU_{MB} , respectively. The set PRU_{SB} is numbered from 0 to $L_{SB}-1$, and the set PRU_{MB} is numbered from 0 to $L_{MB}-1$. Equation (2.4) defines the mapping of PRUs to PRU_{SB} , and (2.6) the mapping of PRUs to PRU_{MB} . Fig. 2.10 illustrates the PRU to PRU_{SB} and PRU_{MB} mappings for a 5 MHz bandwidth with K_{SB} equal to 3.

$$PRU_{SB}[j] = PRU[i], \quad j = 0, 1, \dots, L_{SB} - 1, \quad (2.4)$$

where

$$i = N_1 \cdot \left\{ \left\lceil \frac{N_{sub}}{K_{SB}} \right\rceil \cdot \left\lfloor \frac{j}{N_1} \right\rfloor + \left\lfloor \frac{j}{N_1} \right\rfloor \cdot \frac{GCD(N_{sub}, \lceil \frac{N_{sub}}{K_{SB}} \rceil)}{N_{sub}} \right\} \bmod N_{sub} + j \cdot N_1 \quad (2.5)$$

with $GCD(x, y)$ being the greatest common divisor of x and y .

$$PRU_{MB}[k] = PRU[i], \quad k = 0, 1, \dots, L_{MB} - 1, \quad (2.6)$$

where

$$i = \begin{cases} N_1 \cdot \left\{ \left\lceil \frac{N_{sub}}{K_{SB}} \right\rceil \cdot \left\lfloor \frac{k+L_{SB}}{N_1} \right\rfloor + \left\lfloor \frac{k+L_{SB}}{N_1} \right\rfloor \cdot \frac{GCD(N_{sub}, \lceil \frac{N_{sub}}{K_{SB}} \rceil)}{N_{sub}} \right\} \bmod N_{sub} & K_{SB} > 0, \\ + (k + L_{SB}) \bmod N_1, & \\ i = k, & K_{SB} = 0. \end{cases} \quad (2.7)$$

2.3.2 Miniband Permutation

The miniband permutation maps the PRU_{MBS} to Permuted PRU_{MBS} ($PPRU_{MBS}$) to ensure that frequency diverse PRUs are allocated to each frequency partition. Fig. 2.11 shows an example. The following gives the mapping between PRU_{MB} and $PPRU_{MB}$:

$$PRU_{MB}[j] = PRU[i], \quad j = 0, 1, \dots, L_{MB} - 1, \quad (2.8)$$

where

$$i = (q(j) \bmod D) \cdot P + \left\lfloor \frac{q(j)}{D} \right\rfloor, \quad (2.9)$$

SAC	# of subbands allocated (K_{SB})	SAC	# of subbands allocated (K_{SB})
0	0	8	10
1	1	9	12
2	2	10	14
3	3	11	16
4	4	12	18
5	5	13	20
6	6	14	22
7	8	15	24

Figure 2.8: Mapping between SAC and K_{SB} for 10 or 20 MHz band (Table 649 in [3]).

SAC	# of subbands allocated (K_{SB})	SAC	# of subbands allocated (K_{SB})
0	0	4	4
1	1	5	5
2	2	6	6
3	3	7	N.A

Figure 2.9: Mapping between SAC and K_{SB} for 5 MHz band (Table 650 in [3]).

$$P = \min(K_{MB}, N_1/N_2), \quad (2.10)$$

$$r(j) = \max(j - ((K_{MB} \bmod P) \cdot D), 0), \quad (2.11)$$

$$q(j) = j + \lfloor \frac{r(j)}{D-1} \rfloor, \quad (2.12)$$

$$D = \lfloor \frac{K_{MB}}{P} + 1 \rfloor. \quad (2.13)$$

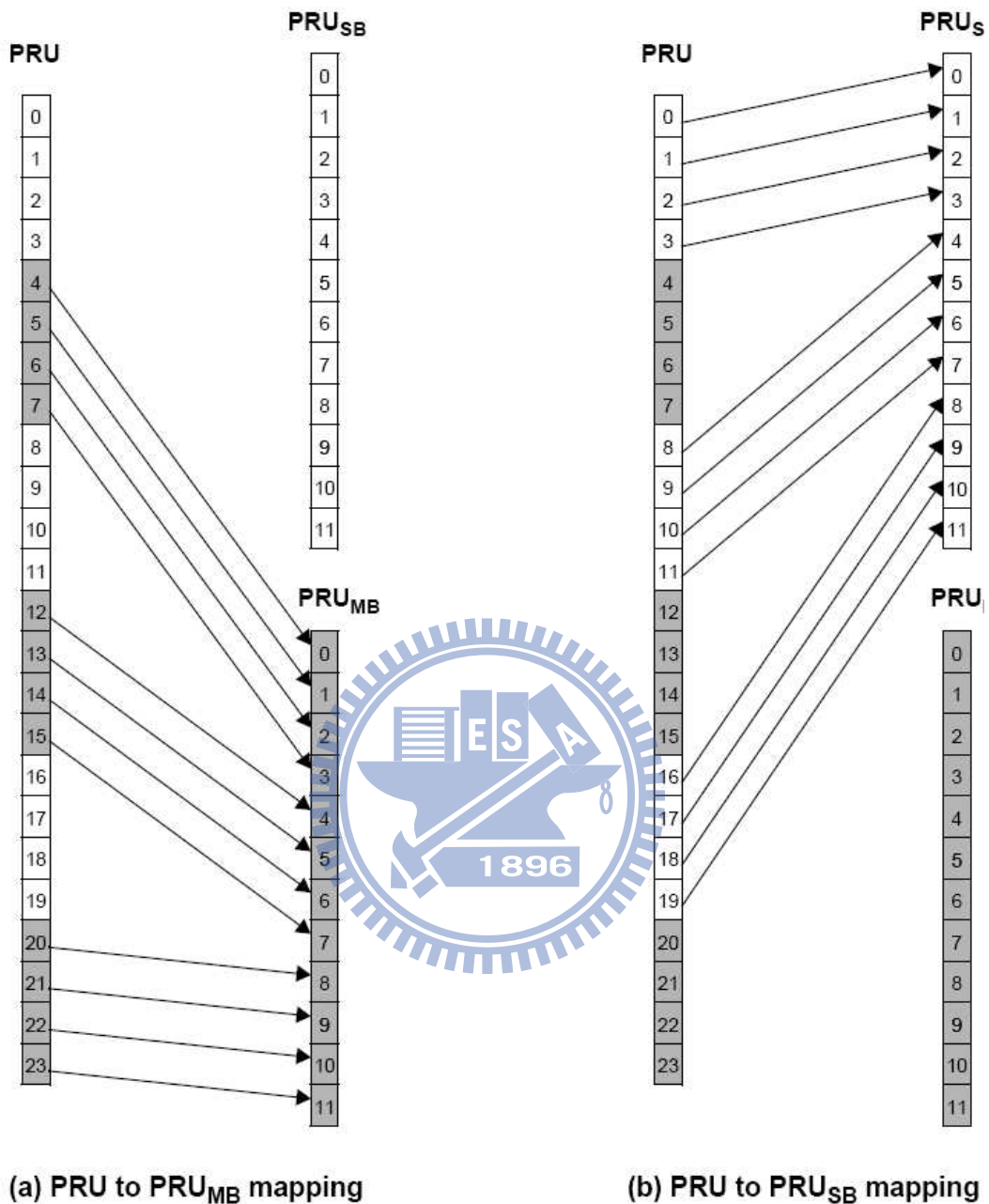


Figure 2.10: PRU to PRU_{SB} and PRU_{MB} mapping for $BW = 5$ MHz, and $K_{SB}=3$ (Fig. 450 in [3]).

2.3.3 Frequency Partitioning

The PRU_{SB} and PRU_{MB} are allocated to one or more frequency partitions. The frequency partition configuration is transmitted in the SFH in a 4 or 3-bit called the Downlink Frequency Partition Configuration (DFPC) depending on system bandwidth. Frequency

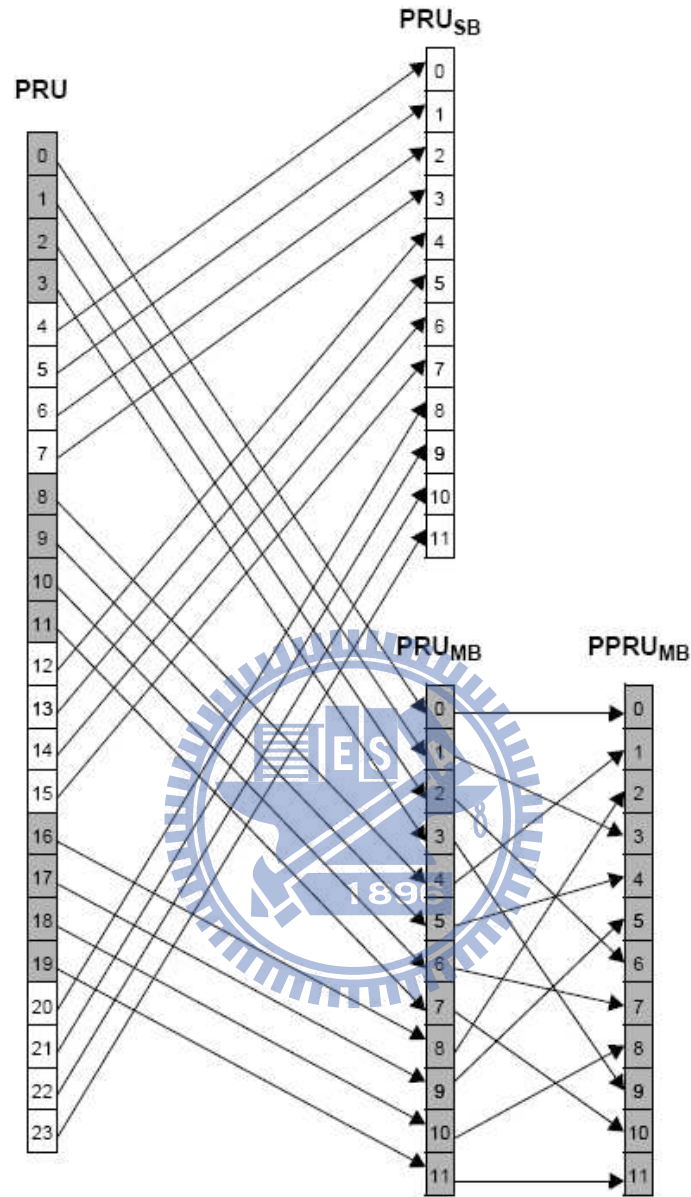


Figure 2.11: Mapping from PRUs to PRU_{SB} and $PPRU_{MB}$ for $BW = 5$ MHz and $K_{SB} = 3$ (Fig. 451 in [3]).

Partition Count (FPCT) defines the number of frequency partitions. Frequency Partition Size (FPSi) defines the number of PRUs allocated to FP_i . FPCT and FPSi are determined from FPC as shown in Figs. 2.12 and 2.13. A 3, 2, or 1-bit parameter called the Downlink Frequency Partition Subband Count (DFPSC) defines the number of subbands allocated to FP_i , $i > 0$. Fig. 2.14 continues the examples in Figs. 2.10 and 2.11 and shows how

PRU_{SB} and $PPRU_{MB}$ can be mapped to frequency partitions.

The number of subbands in the i th frequency partition is denoted by K_{SB,FP_i} . The number of minibands is denoted by K_{MB,FP_i} , which is determined by FPS and FPSC fields. The number of subband PRUs in each frequency partition is denoted by L_{SB,FP_i} , which is given by $L_{SB,FP_i} = N_1 \cdot K_{SB,FP_i}$. The number of miniband PRUs in each frequency partition is denoted by L_{MB,FP_i} , which is given by $L_{MB,FP_i} = N_2 \cdot K_{MB,FP_i}$.

$$K_{SB,FP_i} = \begin{cases} K_{SB}, & i = 0, \\ FPS_C, & i > 0, \end{cases} \quad (2.14)$$

DFPC	Freq. Partitioning (FP ₀ :FP ₁ :FP ₂ :FP ₃)	FPCT	FPS ₀	FPS _{<i>i</i>>0}
0	1:0:0:0	1	N _{PRU}	0
1	0:1:1:1	3	0	N _{PRU} * 1/3
2	1:1:1:1	4	N _{PRU} * 1/4	N _{PRU} * 1/4
3	3:1:1:1	4	N _{PRU} * 1/2	N _{PRU} * 1/6
4	5:1:1:1	4	N _{PRU} * 5/8	N _{PRU} * 1/8
5	9:1:1:1	4	N _{PRU} * 9/12	N _{PRU} * 1/12
6	9:5:5:5	4	N _{PRU} * 3/8	N _{PRU} * 5/12
7-15	<i>Reserved</i>			

Figure 2.12: Mapping between DFPC and frequency partitioning for 10 or 20 MHz band (Table 651 in [3]).

FPC	Freq. Partitioning (FP ₀ :FP ₁ :FP ₂ :FP ₃)	FPCT	FPS ₀	FPS _{<i>i</i>>0}
0	1:0:0:0	1	N _{PRU}	0
1	0:1:1:1	3	0	N _{PRU} * 1/3
2	1:1:1:1	4	N _{PRU} * 1/4	N _{PRU} * 1/4
3	3:1:1:1	4	N _{PRU} * 1/2	N _{PRU} * 1/6
4-7	<i>Reserved</i>			

Figure 2.13: Mapping between DFPC and frequency partitioning for 5 MHz band (Table 652 in [3]).

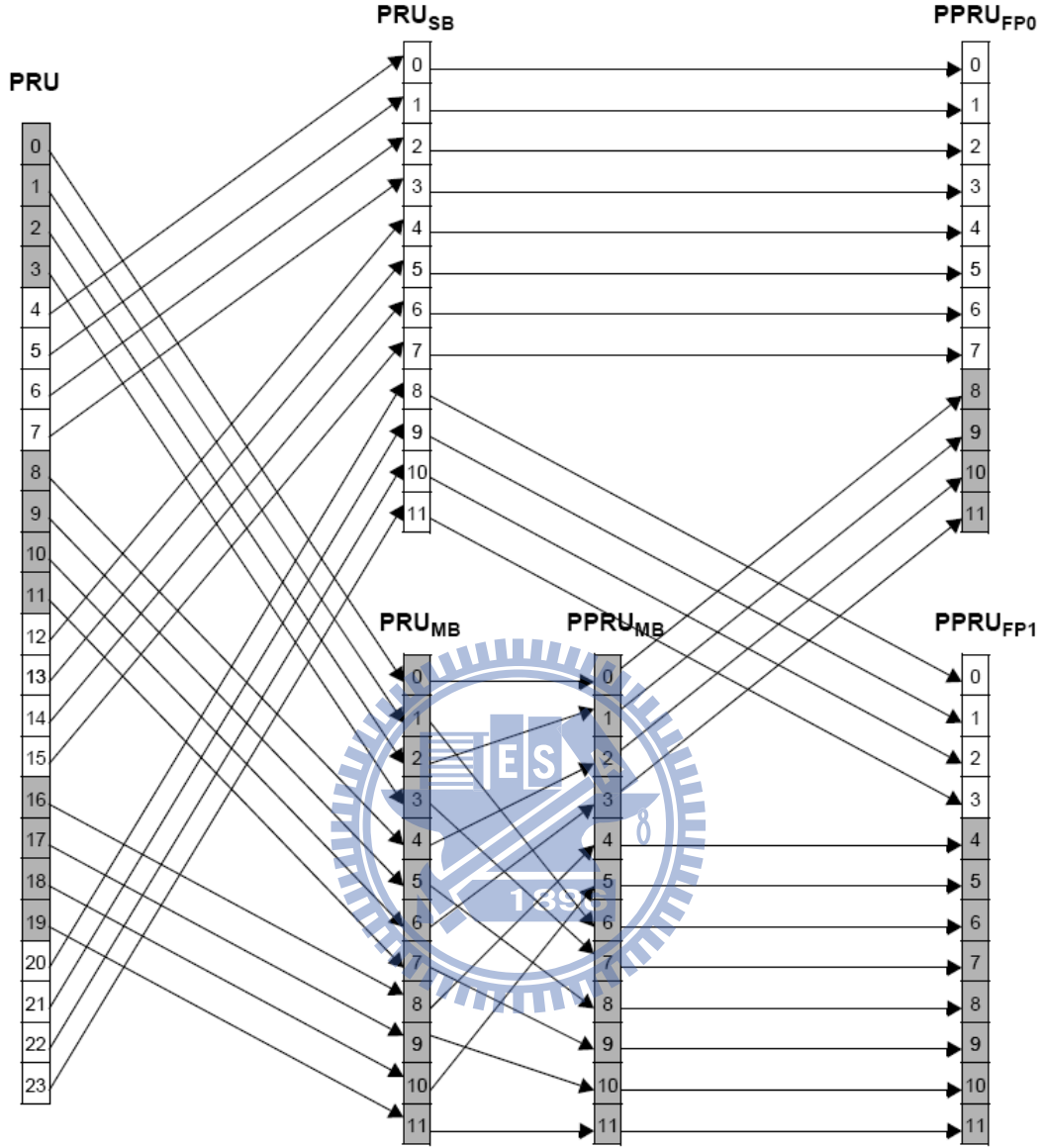


Figure 2.14: Frequency partitioning for $BW = 5$ MHz, $K_{SB} = 3$, $FPCT = 2$, $FPS = 12$, and $FPSC = 1$ (Fig. 452 in [3]).

$$K_{MB,FPi} = (FPS_i - K_{SB,FPi} \cdot N_1) / N_2, \quad 0 \leq i < FPCT. \quad (2.15)$$

The mapping of subband PRUs and miniband PRUs to the frequency partition is given by

$$PRU_{FPi}(j) = \begin{cases} PRU_{SB}(k_1), & 0 \leq j < L_{SB,FPi}, \\ PPRU_{MB}(k_2), & L_{SB,FPi} \leq j < (L_{SB,FPi} + L_{MB,FPi}), \end{cases} \quad (2.16)$$

where

$$k_1 = \sum_{m=0}^{i-1} L_{SB,FPm} + j \quad (2.17)$$

and

$$k_2 = \sum_{m=0}^{i-1} L_{SB,FPm} + j - L_{SB,FPi}. \quad (2.18)$$

2.4 Cell-Specific Resource Mapping [3]

The content of this section is mainly taken from [3]. PRU_{FPi} s are mapped to LRUs. All further PRU and subcarrier permutation are constrained to the PRUs of a frequency partition.

2.4.1 CRU/DRU Allocation

The partition between CRUs and DRUs is done on a sector specific basis. A 4 or 3-bit Downlink subband-based CRU Allocation Size ($DCAS_{S_{Bi}}$) field is sent in the SFH for each allocated frequency partition. $DCAS_{S_{Bi}}$ indicates the number of allocated CRUs for partition FP_i in unit of subband size. A 5, 4 or 3-bit Downlink miniband-based CRU Allocation Size ($DCAS_{MB}$) is sent in the SFH only for partition FP_0 depending on system bandwidth, which indicates the number of allocated miniband-based CRUs for partition FP_0 . The number of CRUs in each frequency partition is denoted $L_{CRU,FPi}$, where

$$L_{CRU,FPi} = \begin{cases} CAS_{S_{Bi}} \cdot N_1 + CAS_{MB} \cdot N_2, & i = 0, \\ CAS_{S_{Bi}} \cdot N_1, & 0 < i < FPCT. \end{cases} \quad (2.19)$$

The number of DRUs in each frequency partition is denoted $L_{DRU,FPi}$, where $L_{DRU,FPi} = FPS_i - L_{CRU,FPi}$ for $0 \leq i < FPCT$ and FPS_i is the number of PRUs allocated to FP_i .

The mapping of PRU_{FPi} to CRU_{FPi} is given by

$$CRU_{FPi}[j] = \begin{cases} PRU_{FPi}[j], & 0 \leq j < CAS_{S_{Bi}} \cdot N_1, & 0 \leq i < FPCT, \\ PRU_{FPi}[k + CAS_{S_{Bi}} \cdot N_1], & CAS_{S_{Bi}} \cdot N_1 \leq j < L_{CRU,FPi}, & 0 \leq i < FPCT, \end{cases} \quad (2.20)$$

where $k = s[j - CAS_{S_{Bi}} \cdot N_1]$, with $s[\]$ being the CRU/DRU allocation sequence defined as

$$s[j] = \{PermSeq(j) + DL_PermBase\} \bmod \{FPS_i - CAS_{S_{Bi}} \cdot N_1\}. \quad (2.21)$$

where $PermSeq()$ is the permutation sequence of length $(FPS_i - CAS_{S_{Bi}} \cdot N_1)$ and is determined by $SEED = ID_{cell} \cdot 343 \bmod 2$, $DL_PermBase$ is an interger ranging from 0 to 31, which is set to preamble ID_{cell} . The mapping of PRU_{FPi} to DRU_{FPi} is given by

$$DRU_{FPi}[j] = PRU_{FPi}[k + CAS_{S_{Bi}} \cdot N_1], \quad 0 \leq j < L_{DRU,FPi}. \quad (2.22)$$

where $k = s^c[j]$, with $s^c[]$ being the sequence which is obtained by renumbering the remainders of the PRUs which are not allocated for CRU from 0 to $L_{DRU,FPi} - 1$.

2.4.2 Subcarrier Permutation

The subcarrier permutation defined for the DL distributed resource allocations within a frequency partition spreads the subcarriers of the DRU across the whole distributed resource allocations. The granularity of the subcarrier permutation is equal to a pair of subcarriers.

After mapping all pilots, the remainder of the used subcarriers are used to define the distributed LRUs. To allocate the LRUs, the remaining subcarriers are paired into contiguous tone-pairs. Each LRU consists of a group of tone-pairs.

Let $L_{SC,l}$ denote the number of data subcarriers in l th OFDMA symbol within a PRU, i.e., $L_{SC,l} = P_{SC} - N_l$, where n_l denotes the number of pilot subcarriers in the l th OFDMA symbol within a PRU. Let $L_{SP,l}$ denote the number of data subcarrier-pairs in the l th OFDMA symbol within a PRU and is equal to $L_{SC,l}/2$. A permutation sequence $PermSeq()$ is defined by (TBD) to perform the DL subcarrier permutation as follows. For each l th OFDMA symbol in the subframe:

1. Allocate the n_l pilots within each DRU as described in Section (TBD). Denote the data subcarriers of $DRU_{FPi}[j]$ in the l th OFDMA symbol as

$$SC_{DRU,j,l}^{FPi}[k], \quad 0 \leq j < L_{DRU,FPi}, \quad 0 \leq k < L_{SC,l}. \quad (2.23)$$

2. Renumber the $L_{DRU,FPi} \cdot L_{SC,l}$ data subcarriers of the DRUs in order, from 0 to $L_{DRU,FPi} \cdot L_{SC,l} - 1$. Group these contiguous and logically renumbered subcarriers into $L_{DRU,FPi} \cdot L_{SP,l}$ pairs and renumber them from 0 to $L_{DRU,FPi} \cdot L_{SP,l} - 1$. The

renumbered subcarrier pairs in the l th OFDMA symbol are denoted as

$$RSP_{FPi,l}[u] = \{SC_{DRUj,l}^{FPi}[2v], SC_{DRUj,l}^{FPi}[2v+1]\}, \quad 0 \leq u < L_{DRU,FPi}L_{SP,l}, \quad (2.24)$$

where $j = \lfloor u/L_{SP,l} \rfloor$ and $v = \{u\} \bmod (L_{SP,l})$.

3. Apply the subcarrier permutation formula to map $RSP_{FPi,l}$ into the s th distributed LRU, $s = 0, 1, \dots, L_{DRU,FPi} - 1$, where the subcarrier permutation formula is given by

$$SC_{LRUs,l}^{FPi}[m] = RSP_{FPi,l}[k], \quad 0 \leq m \leq L_{SP,l}, \quad (2.25)$$

where

$$k = L_{DRU,FPi} \cdot f(m, s) + g(PermSeq(), s, m, l, t). \quad (2.26)$$

In the above,

1. $SC_{LRUs,l}^{FPi}[m]$ is the m th subcarrier pair in the l th OFDMA symbol in the s th distributed LRU of the t th subframe;
2. m is the subcarrier pair index, 0 to $L_{SP,l} - 1$;
3. l is the OFDMA symbol index, 0 to $N_{sym} - 1$;
4. s is the distributed LRU index, 0 to $L_{DRU,FPi} - 1$;
5. t is the subframe index with respect to the frame;
6. $PermSeq()$ is the permutation sequence of length $L_{DRU,FPi}$ and is determined by $SEED = \{ID_{cell} * 1367\} \bmod 2^{10}$; and
7. $g(PermSeq(), s, m, l, t)$ is a function with value from the set $[0, L_{DRU,FPi} - 1]$, which is defined according to

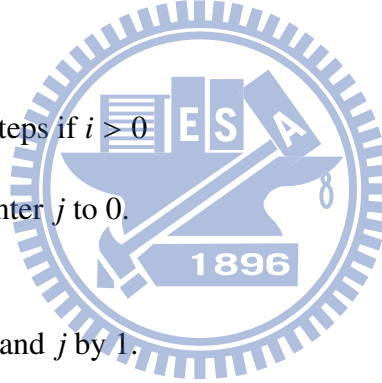
$$g(PermSeq(), s, m, l, t) = \{PermSeq[\{f(m, s) + s + l\} \bmod \{L_{DRU,FPi}\}] + DL_PermBase\} \bmod L_{DRU,FPi}. \quad (2.27)$$

where $DL_PermBase$ is an integer ranging from 0 to 31(TBD), which is set to preamble ID_{cell}, and $f(m, s) = (m + 13 * s) \bmod L_{SP,l}$.

2.4.3 Random Sequence Generation

The permutation sequence generation algorithm with 10-bit SEED ($S_{n-10}, S_{n-9}, \dots, S_{n-1}$) shall generate a permutation sequence of size M according to the following process:

- Initialization
 1. Initialize the variables of the first order polynomial equation with the 10-bit seed, $SEED$. Set $d_1 = \lfloor SEED/2^5 \rfloor + 1$ and $d_2 = SEED \bmod 2^5$.
 2. Initialize the maximum iteration number, $N = 4$.
 3. Initialize an array A with size M to contents $0, 1, \dots, M - 1$ (i.e., $A[i] = i$, for $0 \leq i < M$).
 4. Initialize the counter i to $M - 1$.
 5. Initialize x to -1 .
- Repeat the following steps if $i > 0$
 1. Initialize the counter j to 0.
 2. Loop as follows:
 - (a) Increment x and j by 1.
 - (b) Calculate the output variable of $y = \{(d_1 \cdot x + d_2) \bmod 1031\} \bmod M$.
 - (c) Repeat the above steps (a) and (b), if $y \leq i$ and $j < N$.
 - (d) If $y \leq i$, set $y = y \bmod i$.
 - (e) Swap the i th and the y th elements in the array, i.e., perform the steps $Temp = A[i], A[i] = A[y],$ and $A[y] = Temp$.
 - (f) Decrement i by 1.



Then $PermSeq[i] = A[i]$, where $0 \leq i < M$.

2.5 Advanced Preamble Structure (A-Preamble) [3]

The material in this subsection is mainly taken from [3]. There are two types of Advanced Preamble (A-Preamble): primary advanced preamble (PA-Preamble) and sec-

ondary advanced preamble (SA-Preamble). One PA-Preamble symbol and three SA-Preamble symbols exist within the superframe. The location of the A-Preamble symbol is specified as the first symbol of frame. PA-Preamble is located at the first symbol of second frame in a superframe while SA-Preamble is located at the first symbol of remaining three frames. Fig. 2.15 depicts the location of A-Preamble symbols.

2.5.1 Primary Advanced Preamble (PA-Preamble)

The length of sequence for PA-Preamble is 216 regardless of the FFT size. PA-Preamble carries the information of ABS type, system bandwidth, and carrier configuration.

Take, for example, a 5-MHz system where the subcarrier index 256 is the DC subcarrier. The set of PA-Preamble subcarriers are given by

$$PA_{PreambleCarrierSet} = 2 \cdot k + 41, \quad (2.28)$$

where k is a running index from 0 to 215. Figs. 2.16, 2.17, and 2.18 depict the structures of

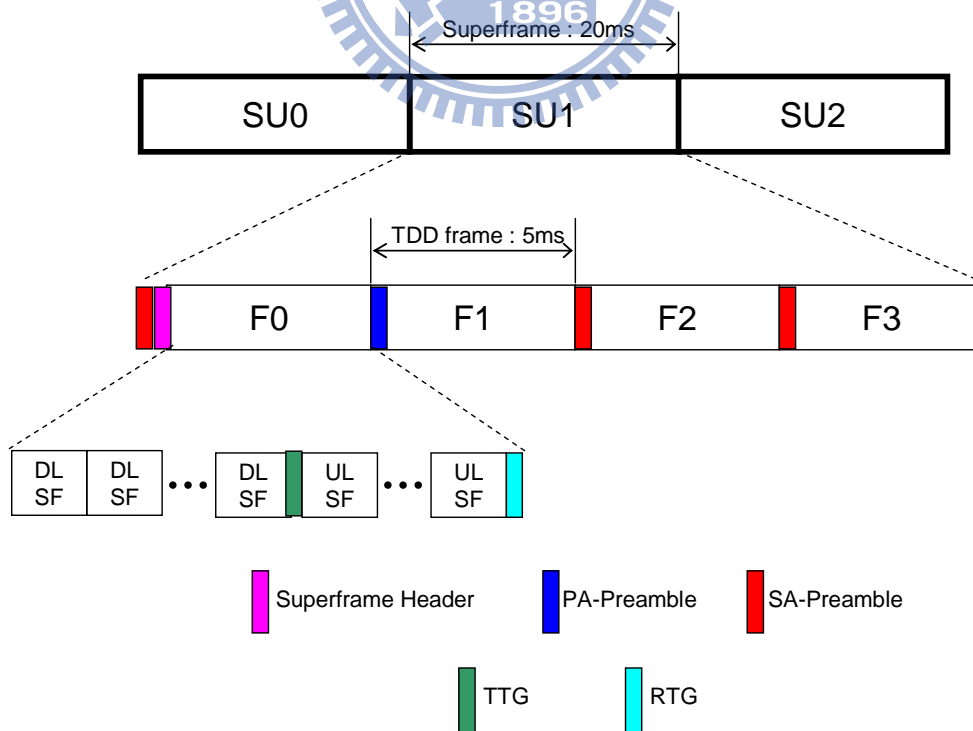


Figure 2.15: Location of the A-Preamble symbol (re-arranged from Fig. 500 in [3]).

the PA-Preamble in the frequency domain for systems of different bandwidths. Whatever PA-Preamble occupies the middle 5-MHz bandwidth which center is the DC subcarrier and the outside subcarriers are all zero.

Fig. 2.19 shows the PA-Preamble sequences in a hexadecimal format. The defined series is mapped onto subcarriers in ascending order, obtained by converting the series to a binary series and starting the series from the MSB up to 216 bits with 0 mapped to +1 and 1 mapped to -1.

The magnitude boosting levels for FFT sizes 512, 1024, 2048 are 2.3999, 3.4143, 5.1320, respectively. For 512-FFT, as an example, the boosted PA-Preamble at k_{th} subcarrier is

$$c_k = 2.3999 \cdot b_k, \quad (2.29)$$

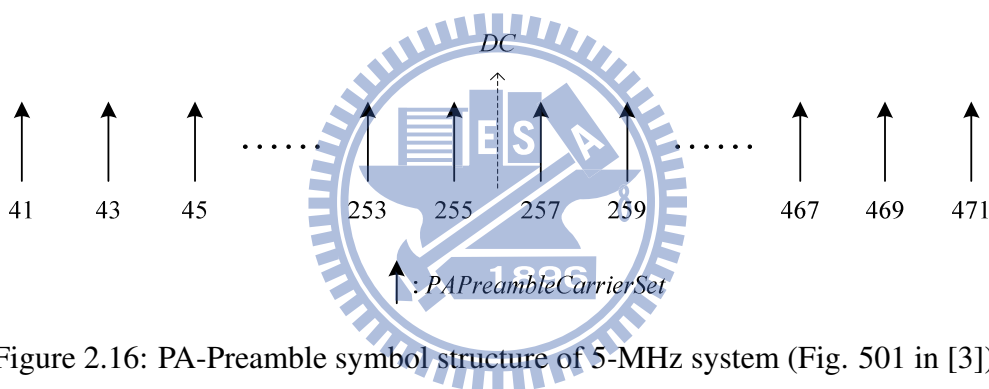


Figure 2.16: PA-Preamble symbol structure of 5-MHz system (Fig. 501 in [3]).

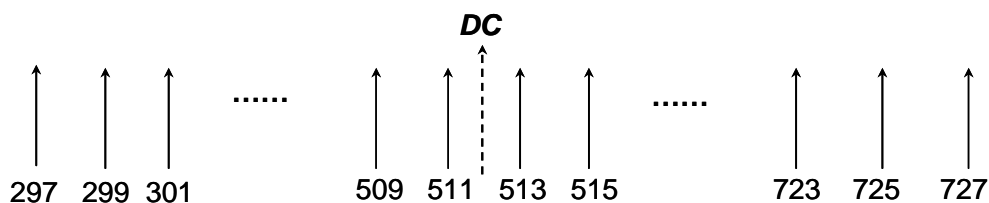


Figure 2.17: PA-Preamble symbol structure of 10 MHz system.

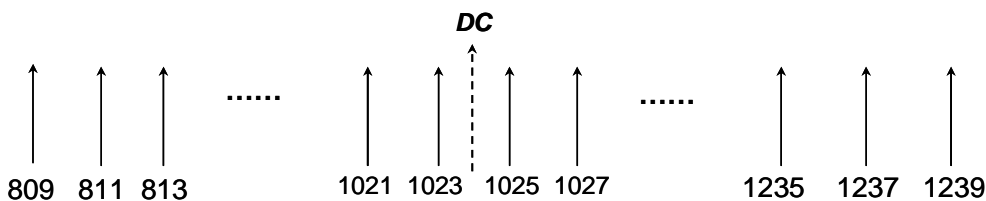


Figure 2.18: PA-Preamble symbol structure of 20 MHz system.

Index	Carrier	BW	Series to modulate
0	Fully configured	5 MHz	6DB4F3B16BCE59166C9CEF7C3C8CA5EDFC16A9D1DC01F2AE6AA08F
1		7,8.75,10 MHz	1799628F3B9F8F3B22C1BA19EAF94FEC4D37DEE97E027750D298AC
2		20 MHz	92161C7C19BB2FC0ADE5CEF3543AC1B6CE6BE1C8DCABDDD319EAF7
3		reserved	6DE116E665C395ADC70A89716908620868A60340BF35ED547F8281
4		reserved	BCFDF60DFAD6B027E4C39DB20D783C9F467155179CBA31115E2D04
5		reserved	7EF1379553F9641EE6ECDBF5F144287E329606C616292A3C77F928
6		reserved	8A9CA262B8B3D37E3158A3B17BFA4C9FCFF4D396D2A93DE65A0E7C
7		reserved	DA8CE648727E4282780384AB53CEEED1CBF79E0C5DA7BA85DD3749
8		reserved	3A65D1E6042E8B8AAD701E210B5B4B650B6AB31F7A918893FB04A
9		reserved	D46CF86FE51B562CAA84F26F6F204428C1BD23F3D888737A0851C
10	Partially configured	N/A	640267A0C0DF11E475066F1610954B5AE55E189EA7E72EFD57240F

Figure 2.19: PA-Preamble Series (Table 780 in [3]).

where b_k represents the PA-Preamble value before boosting (+1 or -1).

2.5.2 Secondary Advanced Preamble (SA-Preamble)

The lengths of sequences for SA-Preamble are 144, 288, and 576 for 512-FFT, 1024-FFT, and 2048-FFT, respectively, where subcarrier indexes 256, 512, and 1024, respectively, are the DC subcarrier. The set of SA-Preamble subcarriers are given by

$$SAPreambleCarrierSet_n = n + 3 \cdot k + 40 \cdot \frac{N_{SAP}}{144} + \lfloor \frac{2 \cdot k}{N_{SAP}} \rfloor, \quad (2.30)$$

where n is the index of the SA-Preamble carrier-set with $n = 0, 1, \text{ or } 2$ representing the segment ID, k is a running index from 0 to $N_{SAP} - 1$ for each FFT size. Fig. 2.20 illustrates the allocation under 512-FFT.

Each cell ID has an integer value ID_{cell} from 0 to 767. The ID_{cell} is defined as

$$ID_{cell} = 256n + Idx, \quad (2.31)$$

where n is the segment ID and $Idx = 2 \cdot \text{mod}(q, 128) + \lfloor q/128 \rfloor$ with q being a running index from 0 to 255.

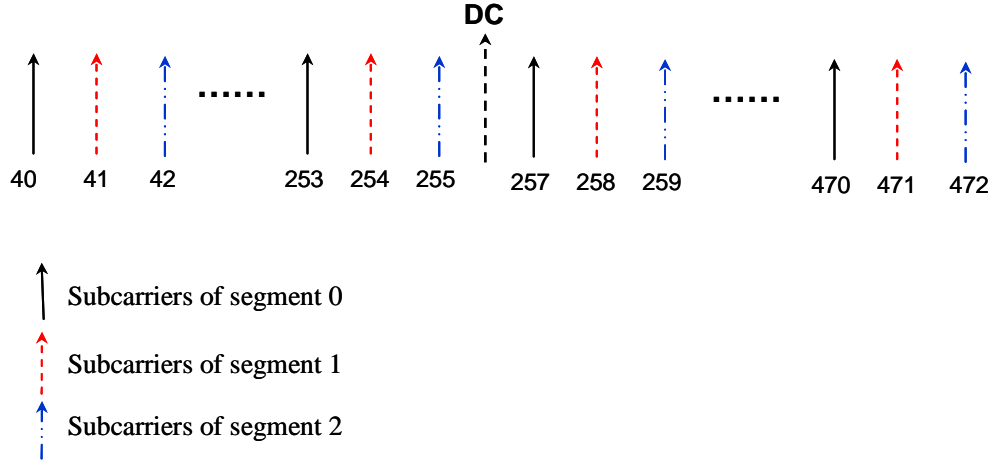


Figure 2.20: SA-Preamble symbol structure of 5 MHz.

For 512-FFT system, the 144-bit SA-Preamble sequence is divided into 8 main sub-blocks, namely, A, B, C, D, E, F, G, and H. The length of each sub-block is 18 samples (after modulation). Each segment ID has a different set of sequence sub-blocks. Tables 784 to 786 in [3] give the 8 sub-blocks of each segment ID, where 9 hexadecimal numbers are used to represent the 36 bits that are mapped to a QPSK sequence in $+1$, $+j$, -1 , and $-j$ for each sub-block. Each table contains 128 sequences indexed by q from 0 to 127. The modulation sequence is obtained by converting each hexadecimal number $X_i^{(q)}$ into two QPSK symbols $v_{2i}^{(q)}$ and $v_{2i+1}^{(q)}$, where $i=0, 1, \dots, 7, 8$. The converting equations are as follows:

$$v_{2i}^{(q)} = \exp(j\frac{\pi}{2}(2 \cdot b_{i,0}^q + b_{i,1}^q)), \quad v_{2i+1}^{(q)} = \exp(j\frac{\pi}{2}(2 \cdot b_{i,2}^q + b_{i,3}^q)), \quad (2.32)$$

where $X_i^{(q)} = 2^3 \cdot b_{i,0}^{(q)} + 2^2 \cdot b_{i,1}^{(q)} + 2^1 \cdot b_{i,2}^{(q)} + 2^0 \cdot b_{i,3}^{(q)}$.

The other 128 sequences indexed by q from 128 to 255 are obtained by letting $v_k^{(q)} = (v_k^{(q-128)})^*$ where $q = 128, 129, \dots, 254, 255$.

Fig. 2.21 shows how the sub-blocks are modulated and mapped (sequentially in ascending order) onto the SA-Preamble subcarrier-set. For higher FFT sizes, the basic blocks (A, B, C, D, E, F, G, H) are repeated in the same order. For instance, in the case of 1024-FFT, sub-blocks E, F, G, H, A, B, C, D, E, F, G, H, A, B, C, and D are modulated and mapped sequentially in ascending order onto the SA-Preamble subcarrier-set according to segment ID.

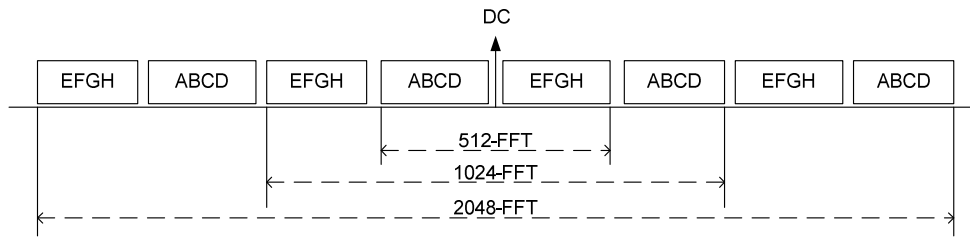


Figure 2.21: The allocation of sequence block for each FFT size (Fig. 503 in [3]).

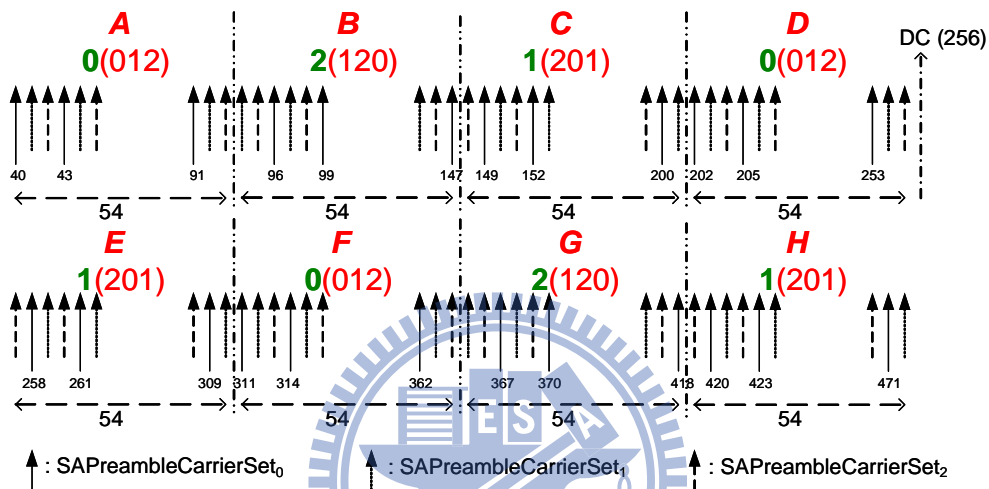


Figure 2.22: SA-Preamble symbol structure for 512-FFT (Fig. 504 in [3]).

For 512-FFT, the blocks (A, B, C, D, E, F, G, H) are subject to the following right circular shifts (0, 2, 1, 0, 1, 0, 2, 1), respectively. Fig. 2.22 depicts the symbol structure of SA-Preamble in the frequency domain for 512-FFT. For higher FFT sizes, the same rule applies.

Chapter 3

Initial Downlink Synchronization

In this chapter, we derive an initial downlink synchronization method for the IEEE 802.16m TDD system.

3.1 The Initial Synchronization Problem

In downlink (DL) signal reception, in principle, the receiver needs to estimate the carrier frequency offset (CFO), carrier phase offset (CPO), sampling frequency offset (SFO), sampling phase offset (SPO), and symbol time offset (STO). Some causes of CFO are mismatch of local oscillators and Doppler shifts due to mobility, and a cause of CPO is an phase mismatch in local oscillators. Different sampling rates in the transceiver and the receiver bring about SFO and different sampling phase in the transceiver and the receiver, SPO. The STO can arise from the unknown propagation delay between the transceiver and the receiver.

If CFO estimation is accurate enough and if STO estimation and correction is constantly performed, then SFO estimation is unnecessary, because from the beginning of an OFDMA symbol to the end of it the SPO will change little in this case. The CPO and the SPO can be considered part of channel response and dealt with in channel estimation as a result, only two issues yet need to be solved, i.e., CFO estimation and STO estimation. These are the focus of the present chapter.

Moreover, because the PA-Preamble in IEEE 802.16m also carries information about

the system bandwidth, there is a need to identify it also in the synchronization stage. Our synchronization design thus takes this into consideration also.

3.2 Derivation of the Initial Synchronization Procedure

There are three possible PA-preamble series, as shown in Fig. 2.19. Because the PA-Preamble series are known, we utilize this knowledge to derive the initial downlink synchronization algorithm. Although there are three different PA-Preambles with different bandwidth, 5-MHz, 10-MHz, and 20-MHz, but the intercommunity is all the three PA-Preamble, which length is all 216-point, locate on the middle part of their own bandwidth. Therefore, when the MS receives the signal, it can only observe 5-MHz bandwidth because there is not any information out of 5MHz at all, whatever the system bandwidth is. In the other words, we do downsampling from the 10-MHz and 20-MHz to the 5MHz without losing any information.

Fig. 3.1 depicts a model about the 576-points power sum with the window sliding. We know the information of $TTG + RTG = 165 \mu s$ in [3], so it is reasonable to suppose RTG is $45 \mu s$, about 256 sampling periods, and CP factor is $1/8$ in our study. We can also know the power of PA-Preamble is larger than the common data symbol because the amplitude of PA-Preamble is boosted before transmitting, and the detail parameter refer to [3].

At first, the received PA-Preamble (include cyclic prefix) can be represented as

$$\mathbf{y}_{576} = \mathbf{\Gamma}(\delta) \cdot \mathbf{T}_{576} \cdot \mathbf{h}_{576} + \eta_{576}, \quad (3.1)$$

where $\mathbf{y}_{576} = [y_{448}, y_{449}, \dots, y_{511}, y_0, y_1, \dots, y_{511}]'$, the received PA-Preamble symbol, δ is the carrier frequency offset, \mathbf{T}_{576} is the 576×576 Toeplitz matrix of the transmitted PA-

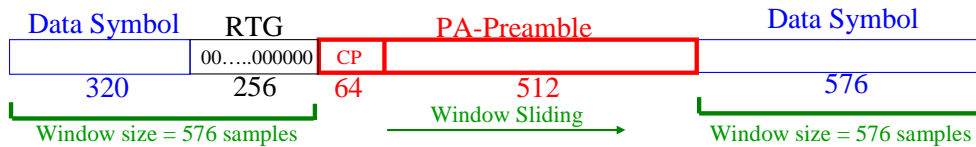


Figure 3.1: Window sliding structure.

mum power sum. This technique can actually be interpreted as quasi-maximum likelihood (ML) noncoherent detection of the preamble timing . We leave detailed treatment to potential future work.

Figs. 3.2 to 3.7 show the results of power sum with the window sliding in 0 and 10 dB of SNR, respectively, under AWGN channel, the pedestrian B (PB) [10] channel, SUI-5 channel with mobility 350 km/h. Note that Rayleighchan, a matlab function we use in our simulation, leads to an initial delay of the generated channel, even if we set the delay of the direct path zero. Figs. 3.8 and 3.9 depict this phenomenon and we must compensate it to our simulation results.

Note that the PA-Preamble timing we get by the above method has an offset to the real PA-Preamble timing due to multipath and noise effects. We will handle these problems in fine timing synchronization.

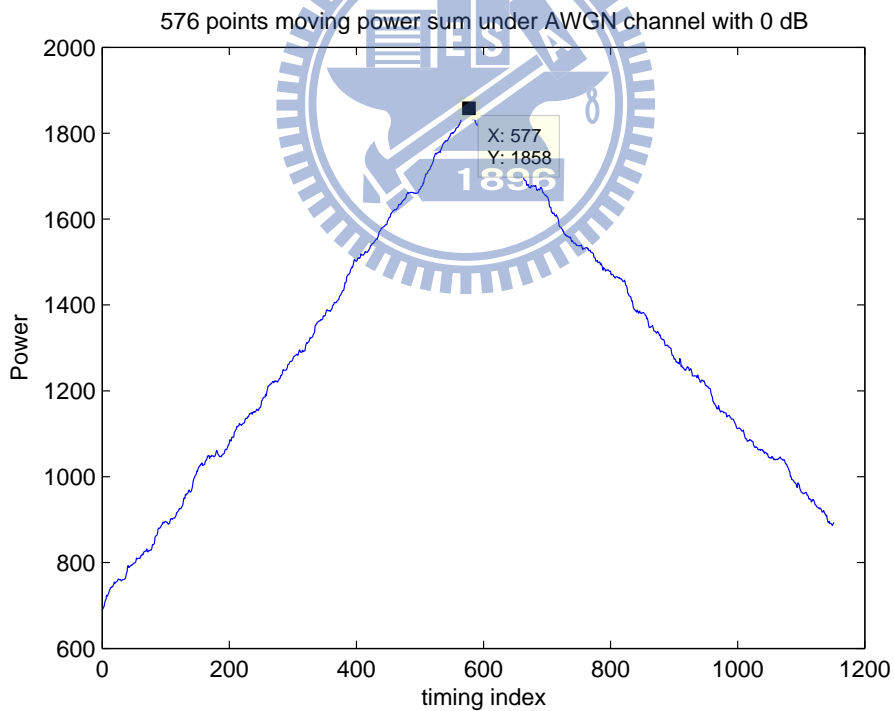


Figure 3.2: 576 points power sum under AWGN in 0 dB.

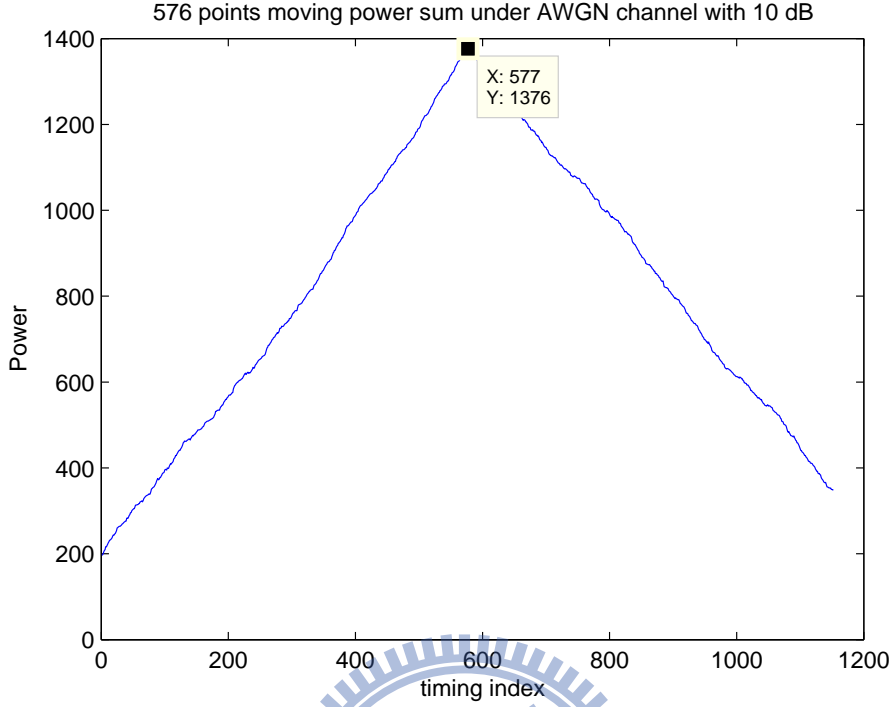


Figure 3.3: 576 points power sum under AWGN in 10 dB.

3.2.2 Estimation of Fractional Carrier Frequency Offset

Eq. (3.1) gives the received PA-Preamble signal. We attempt an ML estimation of δ from it. It turns out that a truly ML estimation is quite complex because \mathbf{T}_{576} is not circulant. However, if the coarse timing lands us in the CP and if we sacrifice the available signal power in the CP, then we can obtain a reduced-complexity solution. Let \mathbf{y}_{512} denote the received PA-Preamble symbol after removed of the CP. It is given by

$$\mathbf{y}_{512} = \mathbf{\Gamma}(\delta) \cdot \mathbf{T}_{x_n} \cdot \mathbf{h} + \eta, \quad (3.4)$$

where $\mathbf{x}_n = [x_0, x_1, \dots, x_{511}]'$, the transmitted PA-Preamble symbol, \mathbf{T}_{x_n} is a 512×512 circulant matrix given by

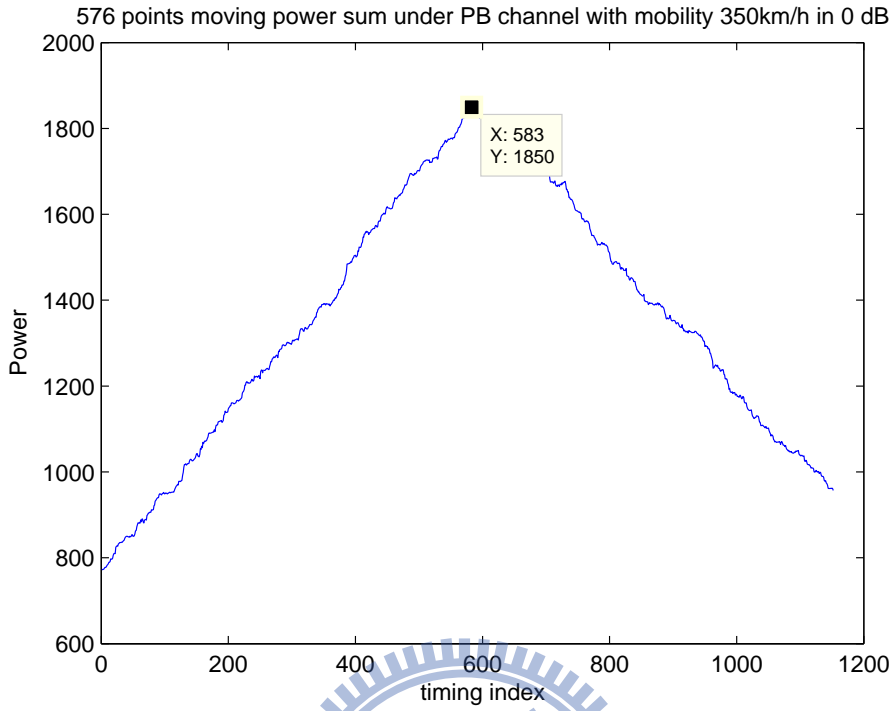


Figure 3.4: 576 points power sum under PB at mobility 350 km/h in 0 dB.

$$\mathbf{T}_{x_n} = \begin{bmatrix} x_0 & x_{511} & x_{510} & x_{509} & \cdot & \cdot & \cdot & x_2 & x_1 \\ x_1 & x_0 & x_{511} & x_{510} & \cdot & \cdot & \cdot & x_3 & x_2 \\ \cdot & x_1 & x_0 & x_{511} & \cdot & \cdot & \cdot & x_3 & x_2 \\ x_{63} & \cdot & x_1 & \cdot & \cdot & \cdot & \cdot & \cdot & \cdot \\ \cdot & x_{63} & \cdot & \cdot & \cdot & \cdot & \cdot & \cdot & \cdot \\ \cdot & \cdot & \cdot & \cdot & \cdot & \cdot & \cdot & x_{510} & \cdot \\ x_{509} & \cdot & \cdot & \cdot & \cdot & \cdot & \cdot & x_{511} & x_{510} \\ x_{510} & x_{509} & \cdot & \cdot & x_{63} & \cdot & \cdot & x_0 & x_{511} \\ x_{511} & x_{510} & x_{509} & \cdot & \cdot & x_{63} & \cdot & x_1 & x_0 \end{bmatrix}, \quad (3.5)$$

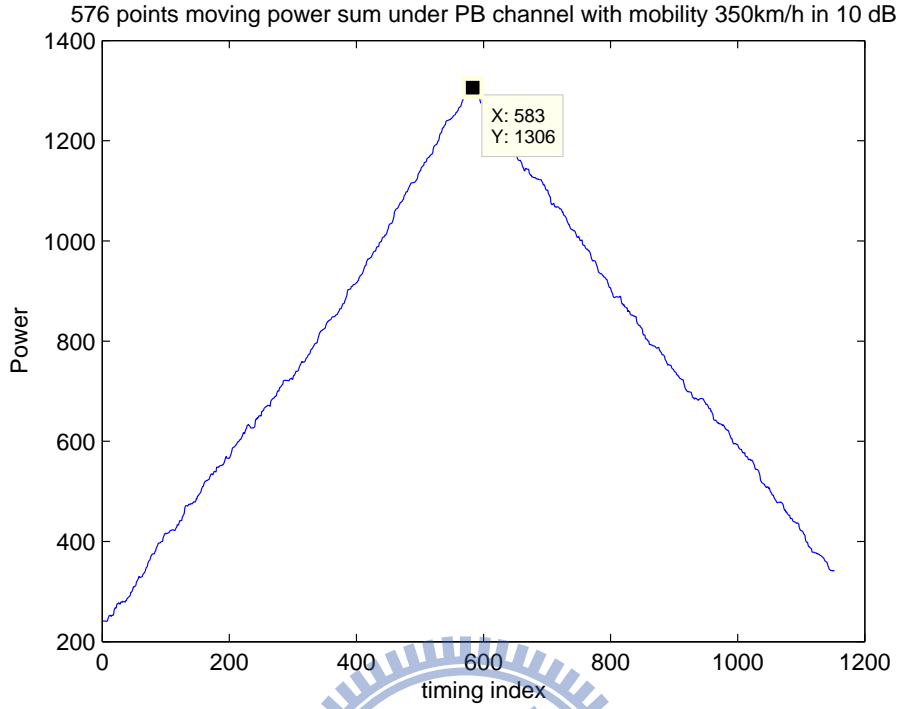


Figure 3.5: 576 points power sum under PB at mobility 350 km/h in 10 dB.

\mathbf{h} is the channel impulse response vector,

$$\mathbf{\Gamma}(\delta) = \begin{bmatrix} \exp(-j \cdot \frac{2\pi}{512} \cdot \delta \cdot 0) & & & & & & & & \\ & \exp(-j \cdot \frac{2\pi}{512} \cdot \delta \cdot 1) & 0 & & & & & & \\ & & \cdot & & & & & & \\ & & & \cdot & & & & & \\ & & & & 0 & \cdot & & & \\ & & & & & & \exp(-j \cdot \frac{2\pi}{512} \cdot \delta \cdot 511) & & \end{bmatrix}, \quad (3.6)$$

and η is an AWGN vector. Due to possibly incorrect identification of the PA-Preamble starting time from the coarse timing synchronization, there may be a circular shift of the elements in the \mathbf{h} vector from their original positions.

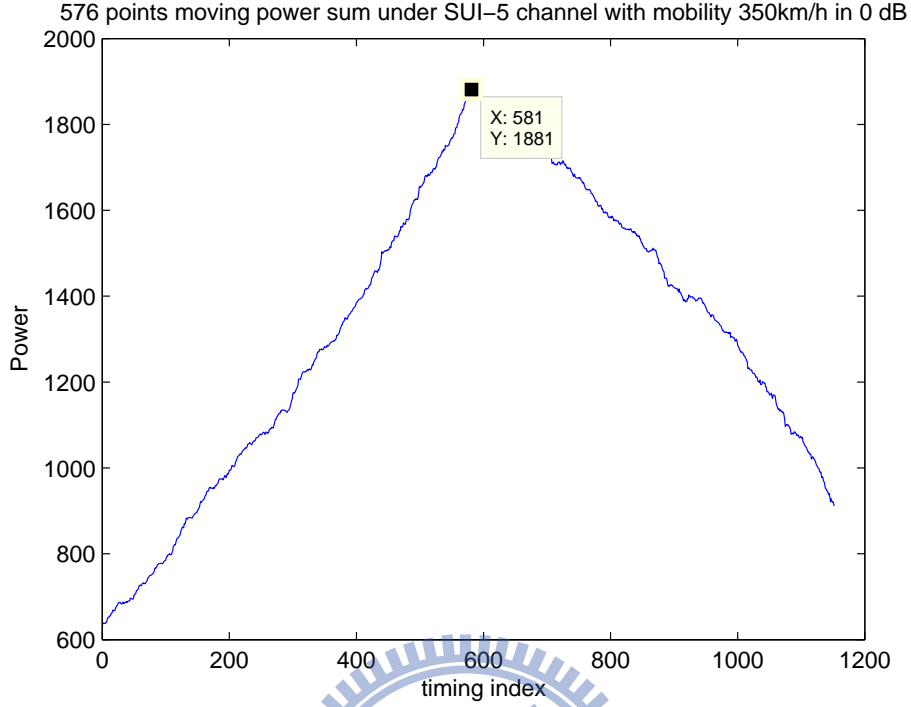


Figure 3.6: 576 points power sum under SUI-5 at mobility 350 km/h in 0 dB.

Eq. (3.4) can then be rewritten as:

$$\mathbf{y}_{512} = \mathbf{\Gamma}(\delta) \cdot \mathbf{F}^H \cdot \mathbf{F} \cdot \mathbf{T}_{x_n} \cdot \mathbf{F}^H \cdot \mathbf{F} \cdot \mathbf{h} + \eta \quad (3.7)$$

$$= \mathbf{\Gamma}(\delta) \cdot \mathbf{F}^H \cdot (\mathbf{F} \cdot \mathbf{T}_{x_n} \cdot \mathbf{F}^H) \cdot (\mathbf{F} \cdot \mathbf{h}) + \eta \quad (3.8)$$

$$= \mathbf{\Gamma}(\delta) \cdot \mathbf{F}^H \cdot \mathbf{D}_k \cdot \mathbf{H} + \eta, \quad (3.9)$$

where \mathbf{F} is the normalized 512×512 FFT matrix, \mathbf{F}^H is the corresponding IFFT matrix, \mathbf{H} is the channel frequency response vector, and \mathbf{D}_k is a diagonal matrix of the PA-Preamble sequence in the frequency domain, with k being the PA-Preamble index.

The likelihood function of \mathbf{y}_{512} can be written as:

$$p(\mathbf{y}_{512}|\delta, \mathbf{H}, k) = \frac{1}{(2\pi\sigma_{\eta_n}^2)^{512}} \cdot \exp\left(-\frac{1}{2\sigma_{\eta_n}^2} \|\mathbf{y}_{512} - \mathbf{\Gamma}(\delta) \cdot \mathbf{F}^H \cdot \mathbf{D}_k \cdot \mathbf{H}\|^2\right), \quad (3.10)$$

In the likelihood function, there are two unknowns, δ and \mathbf{H} . The ML estimation is

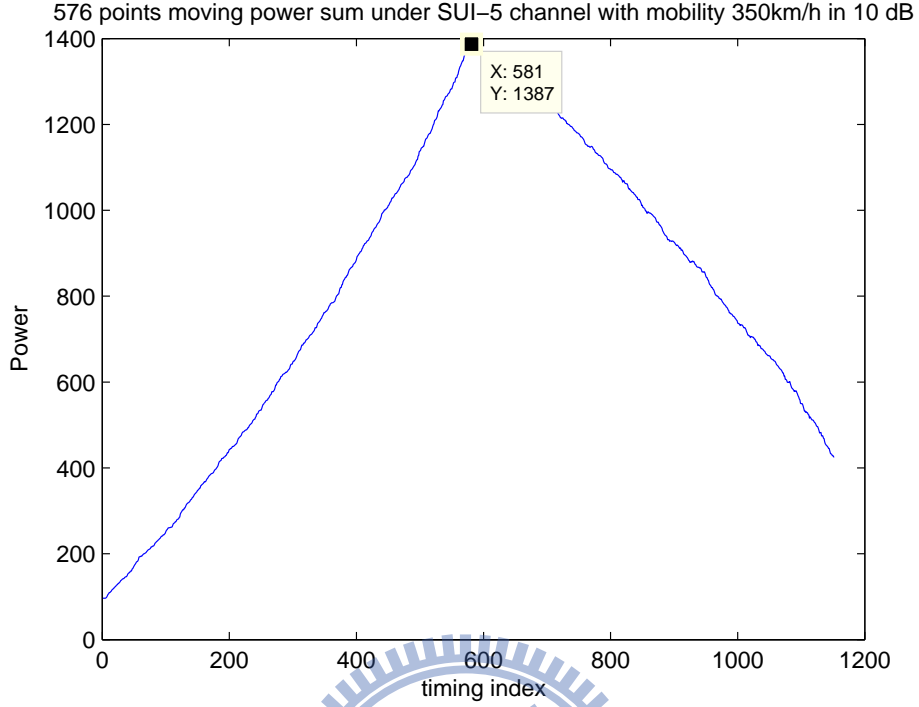


Figure 3.7: 576 points power sum under SUI-5 at mobility 350 km/h in 10 dB.

thus given by

$$\arg \max_{\delta, \mathbf{H}, k} p(\mathbf{y}_{512} | \delta, \mathbf{H}, k) \quad (3.11)$$

$$= \arg \min_{\delta, \mathbf{H}, k} \|\mathbf{y}_{512} - \mathbf{\Gamma}(\delta) \cdot \mathbf{F}^H \cdot \mathbf{D}_k \cdot \mathbf{H}\|^2 \quad (3.12)$$

$$= \arg \min_{\delta, k} \min_{\mathbf{H} | \delta} \|\mathbf{y}_{512} - \mathbf{\Gamma}(\delta) \cdot \mathbf{F}^H \cdot \mathbf{D}_k \cdot \mathbf{H}\|^2 \quad (3.13)$$

$$= \arg \min_{\delta} \|\mathbf{y}_{512} - \mathbf{\Gamma}(\delta) \cdot \mathbf{F}^H \cdot \mathbf{D}_k \cdot \mathbf{D}_k^H \cdot \mathbf{F} \cdot \mathbf{\Gamma}^H(\delta) \cdot \mathbf{y}_{512}\|^2. \quad (3.14)$$

Note that (3.14) arises because the inner minimization of (3.13) is achieved with $\mathbf{H} = \mathbf{D}_k^H \cdot \mathbf{F} \cdot \mathbf{\Gamma}^H(\delta) \cdot \mathbf{y}_{512}$ as can be obtained via standard least-square estimation technique, and $\mathbf{D}_k \cdot \mathbf{D}_k^H$ is always the same whatever k is. Then we have

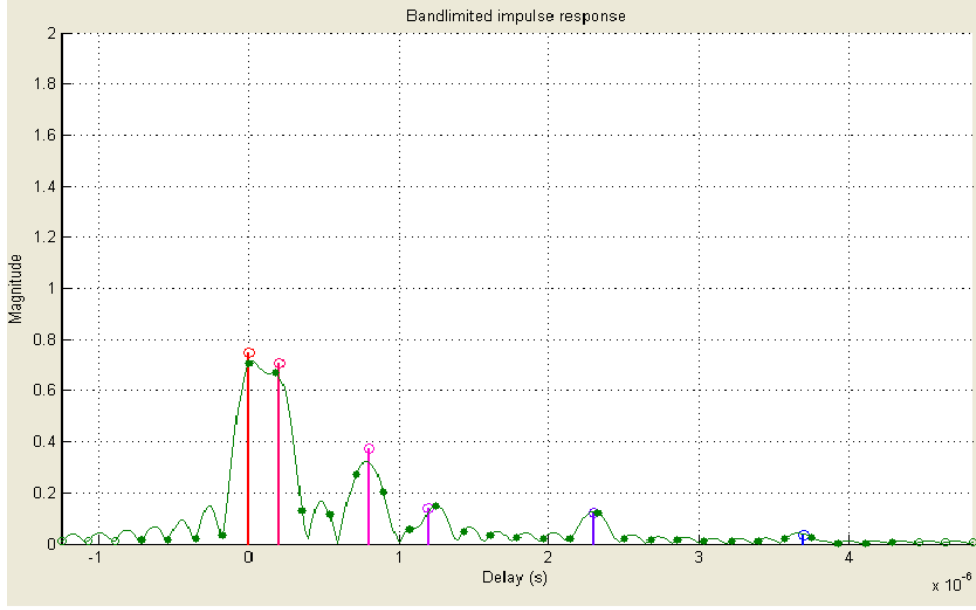


Figure 3.8: Channel impulse response of PB channel.

$$\arg \min_{\delta} \|\mathbf{y}_{512} - \mathbf{\Gamma}(\delta) \cdot \mathbf{F}^H \cdot \mathbf{D}_k \cdot \mathbf{D}_k^H \cdot \mathbf{F} \cdot \mathbf{\Gamma}^H(\delta) \cdot \mathbf{y}_{512}\|^2 \quad (3.15)$$

$$= \arg \min_{\delta} \|[I - \mathbf{\Gamma}(\delta) \cdot \mathbf{F}^H \cdot \mathbf{D}_k \cdot \mathbf{D}_k^H \cdot \mathbf{F} \cdot \mathbf{\Gamma}^H(\delta)] \cdot \mathbf{y}_{512}\|^2 \quad (3.16)$$

$$= \arg \min_{\delta} \mathbf{y}_{512}^H \cdot [I - \mathbf{\Gamma}(\delta) \cdot \mathbf{F}^H \cdot \mathbf{D}_k \cdot \mathbf{D}_k^H \cdot \mathbf{F} \cdot \mathbf{\Gamma}^H(\delta)]^2 \cdot \mathbf{y}_{512} \quad (3.17)$$

$$= \arg \max_{\delta} \mathbf{y}_{512}^H \cdot \mathbf{\Gamma}(\delta) \cdot \mathbf{F}^H \cdot \mathbf{D}_k \cdot \mathbf{D}_k^H \cdot \mathbf{F} \cdot \mathbf{\Gamma}^H(\delta) \cdot \mathbf{y}_{512} \quad (3.18)$$

$$= \arg \max_{\delta} \gamma^H(\delta) \cdot [\mathbf{Y}^H \cdot \mathbf{F}^H \cdot \mathbf{D}_k \cdot \mathbf{D}_k^H \cdot \mathbf{F} \cdot \mathbf{Y}] \cdot \gamma(\delta) \quad (3.19)$$

where $\gamma(\delta) = [\exp(-j \cdot \frac{2\pi}{512} \cdot \delta \cdot 0), \exp(-j \cdot \frac{2\pi}{512} \cdot \delta \cdot 1), \dots, \exp(-j \cdot \frac{2\pi}{512} \cdot \delta \cdot 511)]'$, and \mathbf{Y} is a diagonal matrix whose i th diagonal element is the i th element in \mathbf{y}_{512} .

Note that in Eq. (3.19), the quantity $\mathbf{D}_k \cdot \mathbf{D}_k^H$ is the same for all three PA-Preamble series. Therefore, the bracketed term in (3.19) is a known quantity for a given received PA-Preamble signal. Let $\mathbf{M} = \mathbf{Y}^H \cdot \mathbf{F}^H \cdot \mathbf{D}_k \cdot \mathbf{D}_k^H \cdot \mathbf{F} \cdot \mathbf{Y}$. Then the quantity to be maximized can be expressed as

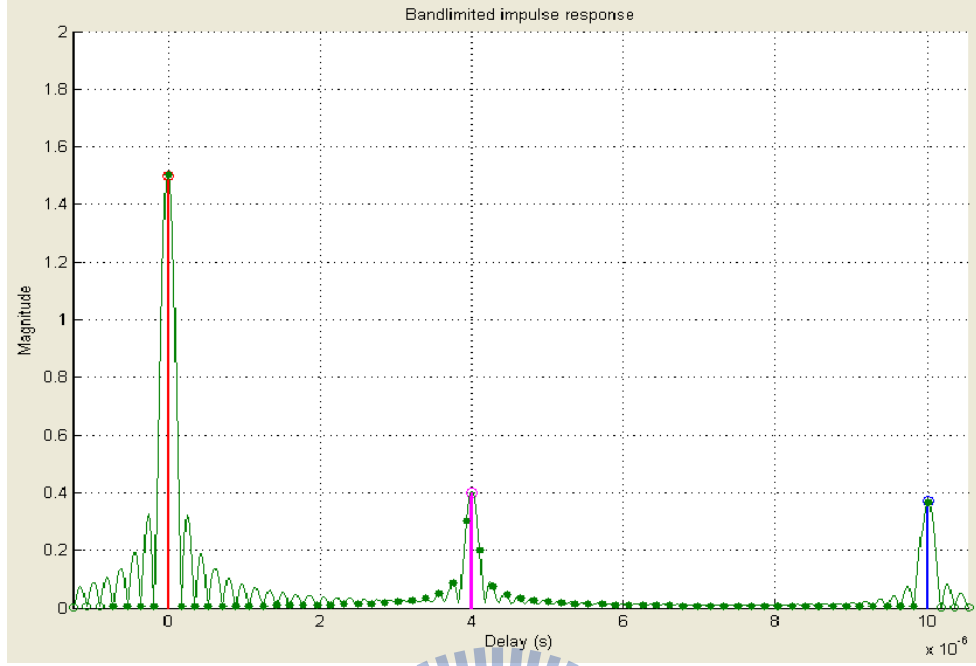


Figure 3.9: Channel impulse response of SUI-5 channel.

$$\gamma^H(\delta) \cdot \mathbf{M} \cdot \gamma(\delta)$$

$$= [1, e^{-a}, e^{-2a}, \dots, e^{-511a}] \cdot \begin{bmatrix} m_{0,0} & m_{0,1} & \cdot & \cdot & \cdot & \cdot & \cdot & m_{0,511} \\ m_{1,0} & m_{1,1} & m_{1,2} & \cdot & \cdot & \cdot & \cdot & m_{1,511} \\ m_{2,0} & m_{2,1} & m_{2,2} & m_{2,3} & \cdot & \cdot & \cdot & \cdot \\ \cdot & \cdot & \cdot & \cdot & \cdot & \cdot & \cdot & \cdot \\ \cdot & \cdot & \cdot & \cdot & \cdot & \cdot & \cdot & \cdot \\ \cdot & \cdot & \cdot & \cdot & \cdot & \cdot & \cdot & \cdot \\ m_{509,0} & \cdot & \cdot & \cdot & \cdot & \cdot & \cdot & \cdot \\ m_{510,0} & m_{510,1} & \cdot & \cdot & \cdot & \cdot & \cdot & m_{510,511} \\ m_{511,0} & m_{511,1} & m_{511,2} & \cdot & \cdot & \cdot & \cdot & m_{511,510} & m_{511,511} \end{bmatrix} \cdot \begin{bmatrix} 1 \\ e^a \\ e^{2a} \\ \cdot \\ \cdot \\ \cdot \\ e^{510a} \\ e^{511a} \end{bmatrix}$$

$$= (m_{0,0} + e^{-a} \cdot m_{1,0} + \dots + e^{-511a} \cdot m_{511,0}) + (m_{0,1} + e^{-a} \cdot m_{1,1} + \dots + e^{-511a} \cdot m_{511,1}) \cdot e^a$$

$$+ \dots + (m_{0,511} + e^{-a} \cdot m_{1,511} + \dots + e^{-511a} \cdot m_{511,511}) \cdot e^{511a}$$

$$= (m_{0,0} + m_{1,1} + \dots + m_{511,511}) \cdot e^0 + (m_{0,1} + m_{1,2} + \dots + m_{510,511}) \cdot e^a + \dots + (m_{0,511} \cdot e^{511a})$$

$$+ (m_{1,0} + m_{2,1} + \dots + m_{511,510}) \cdot e^{-a} + (m_{2,0} + m_{3,1} + \dots + m_{511,509}) \cdot e^{-2a} + \dots + (m_{511,0} \cdot e^{-511a})$$

$$= \sum_{n=-511}^{511} M_n \cdot e^{j \cdot 2\pi \cdot n \cdot \delta / 512},$$

(3.20)

where $a = j \cdot 2 \cdot \pi \cdot \delta / 512$, $m_{p,q}$ is the (p, q) th element of \mathbf{M} , $M_n = \sum_{n=0}^{511} m_{n,n}$, the sum of the n -th diagonal of \mathbf{M} .

Note that since $\mathbf{D}_k \cdot \mathbf{D}_k^H$ is diagonal, $\mathbf{W} \triangleq \mathbf{F}^H \cdot \mathbf{D}_k \cdot \mathbf{D}_k^H \cdot \mathbf{F}$ is a circulant matrix. Indeed, because $\mathbf{D}_k \cdot \mathbf{D}_k^H$ is nearly periodic (with mostly every other element equal to 1 while others equal to zero) along the diagonal, \mathbf{W} is nearly tri-diagonal and so is \mathbf{M} .

The three diagonal sums are

$$M_0 = \sum_{i=0}^{511} w_{i,i} \cdot |y_{i,i}|^2, \quad (3.21)$$

$$M_{-256} = \sum_{i=256}^{511} y_{i,i}^H \cdot w_{i,i-256} \cdot y_{i-256,i-256}, \quad (3.22)$$

$$M_{256} = \sum_{i=256}^{511} y_{i-256,i-256}^H \cdot w_{i-256,i} \cdot y_{i,i}, \quad (3.23)$$

where $y_{i,i}$ is the i th diagonal element of \mathbf{Y} , and $w_{i,i}$ is the i th diagonal of \mathbf{W} . Note that $M_{-256} = M_{256}^*$. Substituting (3.21)-(3.23) into (3.20) with all other terms set to null in order to resist the effect of noise. We utilize the mathematic format of FFT of these three dominant terms to estimate FCFO by finding the peak value and derive as

$$X[f] = \sum_{n=0}^{19999} M_n \cdot e^{-j \cdot 2 \cdot \pi \cdot n \cdot f / 20000} \quad (3.24)$$

$$\approx M_{256}^* + M_0 \cdot e^{-j \cdot 2 \cdot \pi \cdot f / 20000} + M_{256} \cdot e^{-j \cdot 4 \cdot \pi \cdot f / 20000} \quad (3.25)$$

$$= e^{-j \cdot 2 \cdot \pi \cdot f / 20000} \cdot (M_{256}^* \cdot e^{j \cdot 2 \cdot \pi \cdot f / 20000} + M_0 + M_{256} \cdot e^{-j \cdot 2 \cdot \pi \cdot f / 20000}) \quad (3.26)$$

$$= e^{-j \cdot 2 \cdot \pi \cdot f / 20000} \cdot (2 \cdot \Re\{M_{256} \cdot e^{-j \cdot 2 \cdot \pi \cdot f / 20000}\} + M_0) \quad (3.27)$$

$$= e^{-j \cdot 2 \cdot \pi \cdot f / 20000} \cdot [2 \cdot (\Re\{M_{256}\} \cdot \cos(\frac{2 \cdot \pi}{20000} \cdot f) + \Im\{M_{256}\} \cdot \sin(\frac{2 \cdot \pi}{20000} \cdot f)) + M_0] \quad (3.28)$$

$$= e^{-j \cdot 2 \cdot \pi \cdot f / 20000} \cdot [2 \cdot \sqrt{\Re\{M_{256}\}^2 + \Im\{M_{256}\}^2} \cdot (\frac{\Re\{M_{256}\}}{\sqrt{\Re\{M_{256}\}^2 + \Im\{M_{256}\}^2}} \cdot \cos(\frac{2 \cdot \pi}{20000} \cdot f) + \frac{\Im\{M_{256}\}}{\sqrt{\Re\{M_{256}\}^2 + \Im\{M_{256}\}^2}} \cdot \sin(\frac{2 \cdot \pi}{20000} \cdot f)) + M_0] \quad (3.29)$$

$$= e^{-j \cdot 2 \cdot \pi \cdot f / 20000} \cdot [2 \cdot \|M_{256}\| \cdot (\cos(\theta - \frac{\pi \cdot f}{10000})) + M_0], \quad (3.30)$$

where $\theta = -\arctan \frac{\Im\{M_{256}\}}{\Re\{M_{256}\}} = \delta \cdot \pi$. Therefore, the peak value happens when $\theta - \frac{\pi \cdot f}{10000} =$

$\delta \cdot \pi - \frac{\pi \cdot f}{10000} = 0$, and then, $\delta = 0.0001 \cdot f$. Note that the FFT size corresponds to the resolution of estimating δ and the resolution of this derivation is 0.0001. Moreover, we can conclude $\delta = -\frac{1}{\pi} \arctan \frac{\Im\{M_{256}\}}{\Re\{M_{256}\}}$, and surprisingly, this final result is the same with the result of “Moose algorithm” [7].

3.2.3 Jointly Integral CFO, PA-Preamble Index, Channel Estimation and Fine Timing Offset Searching

CFO is separated into two parts, FCFO and ICFO, and the former have been estimation in the previous subsection. We can expect that the power of channel impulse response (CIR), the inverse fourier transform of \mathbf{H} as obtained in (3.14), will be more concentrated if we compensate with the accurate CFO and use the correct one of the three possible PA-Preamble symbols. For example, Figs. 3.10 and 3.11 depict two CIRs obtained from using a combination of correct CFO and correct PA-Preamble index and from using a combination of incorrect values. The simulation environment we choose in Figs. 3.10 and 3.11 is PB channel, 120 km/h, 0 dB in SNR, the correct ICFO 8, the correct PID 1 (10-MHz), the wrong ICFO 6, and the wrong PID 0 (5-MHz). We consider there are 21 possible ICFO explained in the Eq. (3.31), 3 PA-Preamble symbols and 256 timing locations in CIR, therefore, $21 \times 3 \times 64 = 16128$ candidates in total. The method we use here is to do 64 points power sum of CIR for these candidates and find out one which has the maximum of power sum. Eq. 3.31 shows why we choose the searching range of ICFO from -20 to 20. The Maximum mismatch of Local oscillators can reach 80 ppm, so that a wireless system with carrier frequency, 2.5-GHz, has ± 18.28 subcarrier offsets in maximum, which is normalized by subcarrier spacing, 10.94-kHz. Therefore, the range of ICFO we choose is reasonable.

$$\frac{2.5G \cdot 80ppm}{10.94K} \approx 18.28 \quad , \quad (3.31)$$

For the fine timing, since it is reasonable to assume that the CIR is mostly concentrated over a length not exceeding the CP length, we decide the ICFO, the PA-Preamble index and the fine timing offset by finding which one of all candidates has the maximum power

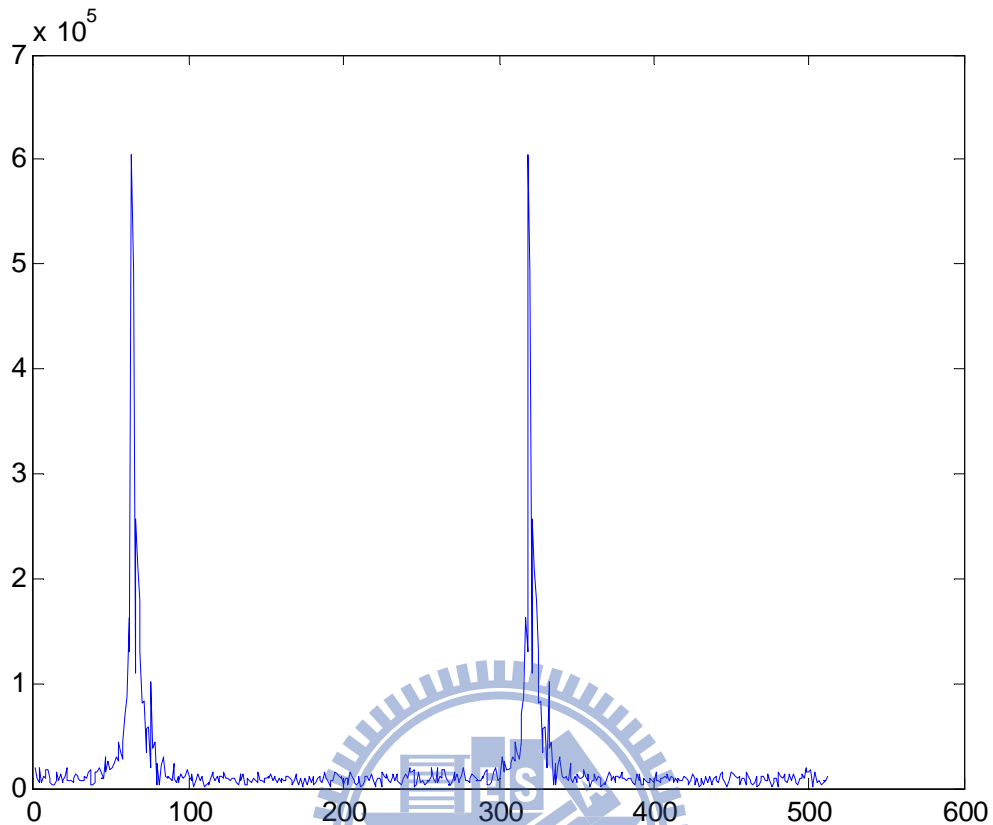


Figure 3.10: The estimated CIR with accurate ICFO, 8, compensating and correct PA-Preamble index, 1, under PB channel with 120 km/h, 0dB in SNR.

sum over the CP length.

3.2.4 Overall Block Diagram

In summary, Fig. 3.12 show the resulting overall block diagram of the derived initial downlink synchronization.

3.3 Identification of the SA-Preamble

The material from Eq. (3.34) to (3.37) in this section is mainly taken from [5]. We consider a common condition that MS accelerates from quiescence to 120 km/h in 10 seconds and the Doppler shift caused by relative motion is calculated as (3.32).

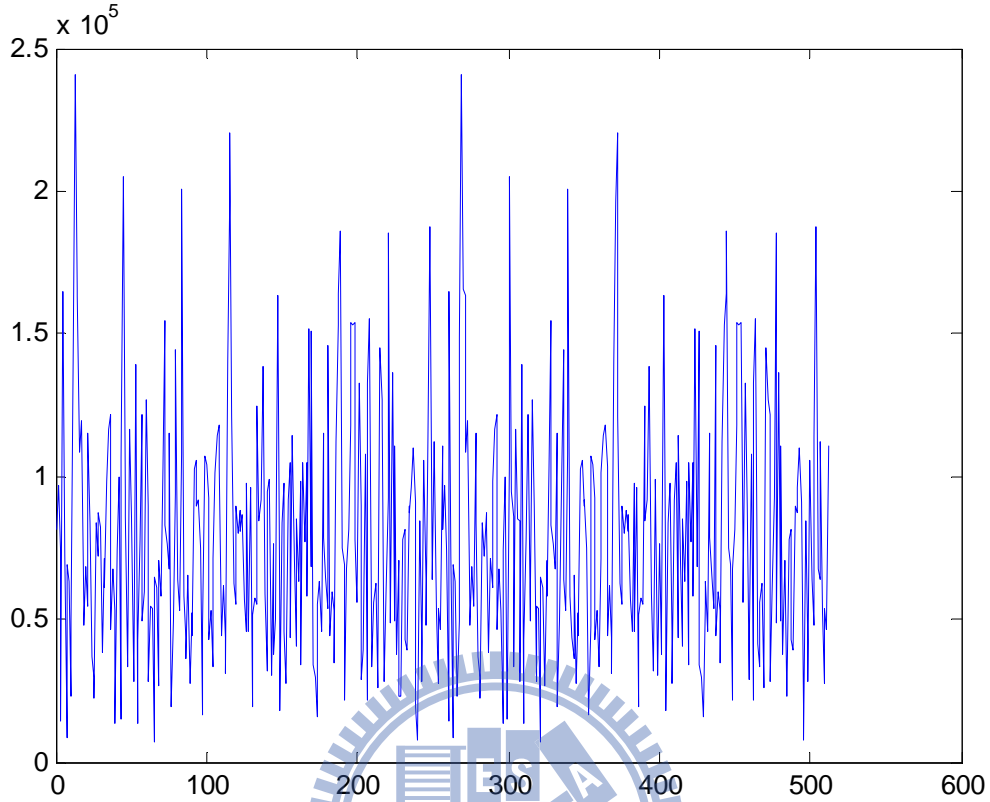


Figure 3.11: The CIR with the inaccurate ICFO, 6, compensating and incorrect PA-Preamble index, 0, under PB channel with 120 km/h, 0dB in SNR.

$$\begin{aligned}
 \Delta f_d &= \frac{\frac{\text{Frame Period}}{10s} \cdot 120km/h \cdot \text{carrier frequency} \cdot \frac{1}{3600}}{\text{Speed of light}} \\
 &= \frac{\frac{5ms}{10s} \cdot 120km/h \cdot 2.5 \times 10^9 Hz \cdot \frac{1}{3600}}{3 \times 10^5 km/s} \\
 &\approx 0.139Hz,
 \end{aligned} \tag{3.32}$$

On the other hand, the timing offset is calculated as (3.33).

$$\begin{aligned}
 \Delta t &= 120km/h \cdot 5ms \cdot \frac{1}{3600} \cdot \frac{1}{3 \times 10^5} \cdot \frac{1}{100ns} \\
 &\approx 0.056\text{samples}.
 \end{aligned} \tag{3.33}$$

We derive the change of the Doppler shift and timing offset during a frame period in 3.32 and 3.33 and it is not worth mentioning so we can use the CFO and timing estimated by initial synchronization to represent the CFO and timing of the SA-Preamble. The informations about BS group ID, BS cell ID and sector ID are described in the SA-Preamble so we need to estimate which one of 768 SA-Preambles is really transmitted by BS. Here

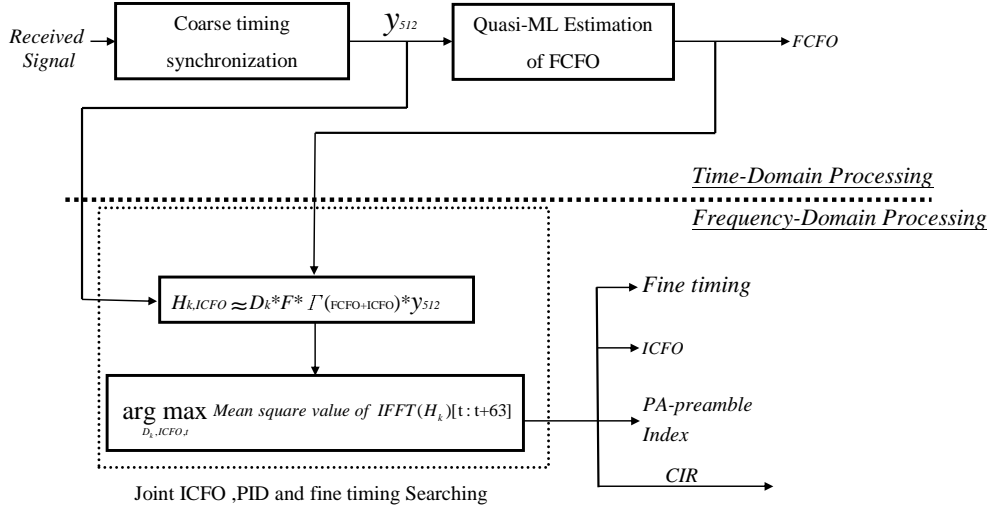


Figure 3.12: Block diagram of initial DL synchronization.

we briefly introduce a common method to do the SA-Preamble estimation, named “differential correlation method” [5]. First, for 5MHz system bandwidth an example, we find the maximum power of all the subcarriers in the 3 possible carrier-sets which start from the 40th subcarrier, the 41st subcarrier, and the 42nd subcarrier of the received preamble, respectively, and determine the carrier-set used for estimation. Note that the carrier-set we use here has length 144. We derive the differential sequence from this carrier-set by

$$D_R[k] = \text{Re}\{r_k r_{k+1}^*\} = r_{re,k} r_{re,k+1} + r_{im,k} r_{im,k+1}, \quad (3.34)$$

where $k = 0, 1, \dots, 143$.

In writing the above, we have slightly abused the index k to let it indicate the k th nonzero preamble subcarrier rather than the k th OFDMA subcarrier. This is because in IEEE 802.16m OFDMA, the nonzero preamble subcarriers are not contiguous but are spaced three subcarriers apart.

Then we derive 256 possible differential sequences from the known preamble sequences by

$$D_j[k] = 1 - 2 \times q_j[k] \oplus q_j[k + 1], \quad (3.35)$$

where $j = 0, 1, \dots, 255$, $k = 0, 1, \dots, 143$, $q_j[k] \in \{0, 1\}$ is the j th binary preamble sequence, and \oplus denotes the “exclusive or” operation. In the end, we compute 144×256 possible

metrics by using

$$M_{n,j} = \sum_{k=0}^{143} D_{R_n}[k] \times D_j[k], \quad (3.36)$$

where D_{R_n} is the sequence started from the n th value of D_R , and the length of this sequence is 144 . Then we can find the preamble index \hat{j} and \hat{n} by

$$(\hat{n}, \hat{j}) = \arg \max_{n,j} M_{n,j}. \quad (3.37)$$

Note that \hat{n} denotes the lower-end subcarrier in the carrier-set and the estimated preamble index \hat{j} determines the lower-end subcarrier of the preamble symbol in the transmitter. Therefore, we can derive the integer CFO using \hat{n} and \hat{j} .

For further particulars, please refer to [5].



Chapter 4

Simulation Study

In this chapter, we discuss the channel effect and the system parameters we consider in our study and present some simulation results about our algorithm.

4.1 System Parameters and Channel Environments

4.1.1 System Parameters

In downlink transmission, the IEEE 802.16m standard have several kinds of system parameters and is very flexible to choose. Therefore, in our study, the system profile we choose is Point to Multi-Points (PMP), Time Division Duplexing (TDD) and Single Input Single Output (SISO). We present more parameter details in the Table. 4.1.

4.1.2 Power Delay Profiles

In order to test the performance of our algorithms, we must do a lot of tests under different environments, including multipath effects and respective mobility. It is convenient to adopt power delay profiles to represent multipath effect because they can generate a tapped-delay-line model for the CIR. In PDPs, there are several discrete delay paths and we treat the minimum delay path as zero delay, so others delay paths can be determined by respective delay difference with the minimum one. Usually, the minimum delay path has the highest average power. The PDPs we use include Stanford University Interim

Table 4.1: System Parameters Used in Our Study

Parameters	Values		
	System Channel Bandwidth (MHz)	5	10
Sampling Frequency (MHz)	5.6	11.2	22.4
FFT Size	512	1024	2048
Subcarrier Spacing (kHz)	10.94	10.94	10.94
Useful Symbol Time (μsec)	91.4	91.4	91.4
Guard Time (μsec)	11.4	11.4	11.4
OFDMA Symbol Time (μsec)	102.9	102.9	102.9

(SUI) [16], Vehicular A (VA) [8], and Pedestrian B (PB) [10]. They are measured by different research units and signify representative environments. The parametric contents of them are shown in the Tables. 4.2 to 4.9.

Table 4.2: SUI-1 Channel Model

Tap	Relative delay (μs or sample number)		Average power	
	μs	sample numbers	dB	normalized dB
1	0	0	0	-0.1771
2	0.4	2	-15	-15.1771
3	0.9	5	-20	-20.1771

Table 4.3: SUI-2 Channel Model

Tap	Relative delay (μs or sample number)		Average power	
	μs	sample numbers	dB	normalized dB
1	0	0	0	-0.3930
2	0.4	2	-12	-12.3930
3	0.9	6	-15	-15.3930

Table 4.4: SUI-3 Channel Model

Tap	Relative delay (μs or sample number)		Average power	
	μs	sample numbers	dB	normalized dB
1	0	0	0	-1.5113
2	0.4	2	-5	-6.5113
3	0.9	5	-10	-11.5113

Table 4.5: SUI-4 Channel Model

Tap	Relative delay (μs or sample number)		Average power	
	μs	sample numbers	dB	normalized dB
1	0	0	0	-1.9218
2	0.4	8	-4	-5.9218
3	0.9	22	-8	-9.9218

Table 4.6: SUI-5 Channel Model

Tap	Relative delay (μs or sample number)		Average power	
	μs	sample numbers	dB	normalized dB
1	0	0	0	-1.5113
2	0.4	22	-5	-6.5113
3	0.9	56	-10	-11.5113

4.2 Simulation Results

After discussing system parameters and PDPs, we utilize them to simulate our algorithms in the coming subsections.

4.2.1 Coarse Timing Estimation

The goal of the coarse timing estimation is to find a starting timing point and use it to obtain the estimated PA-Preamble. It is reasonable the estimated starting timing point locates in CP period. Because the power of the PA-Preamble symbol is larger than the data symbol, we estimate the boundry of the PA-Preamble by this trait. Figs. 4.1 and 4.2

Table 4.7: SUI-6 Channel Model

Tap	Relative delay (μs or sample number)		Average power	
	μs	sample numbers	dB	normalized dB
1	0	0	0	-0.5683
2	0.4	78	-10	-10.5683
3	0.9	112	-14	-14.5683

Table 4.8: ETSI “Vehicular A” Channel Model [8]

Tap	Relative delay (μs or sample number)		Average power	
	μs	sample numbers	dB	normalized dB
1	0	0	0	-3.1426
2	0.31	2	-1	-4.1426
3	0.71	4	-9	-12.1426
4	1.09	6	-10	-13.1426
5	1.73	10	-15	-18.1426
6	2.51	14	-20	-23.1426

illustrate the histograms under AWGN channel with 0 dB and 10 dB, and we can find which has higher SNR performs better simulation result, lower measure of dispersion. The correct timing index under AWGN is 577, refer to Fig. 3.1. Figs. 4.3 to 4.6 depict the histograms under PB in 0 dB and 10 dB of SNR at speed 3 km/h and 120 km/h, respectively. Obviously, the measure of dispersion of their data is higher than under AWGN and the effect of SNR is prominenter than mobility. The correct timing index under PB is 583, because there is 6 samples in difference with AWGN because Matlab function default settings for multipath channel. Figs. 4.7 to 4.10 depict the histograms under PB in 0 dB and 10 dB of SNR at speed 3 km/h and 120 km/h, respectively. SUI-5 is a kind of channel model with long delay spread, so that the simulation results with SUI-5 sometimes are close to the right boundary of CP and it is getting more serious if mobility is higher. The correct timing index under SUI-5 is also 583.

Table 4.9: Pedestrian B (PB) Channel Model

Tap	Relative delay (μs or sample number)		Average power	
	μs	sample numbers	dB	normalized dB
1	0	0	0	-3.9114
2	0.2	1	-0.9	-4.8114
3	0.8	5	-4.9	-8.8114
4	1.2	7	-8	-11.9114
5	2.3	13	-7.9	-11.8114
6	3.7	21	-23.9	-27.8114

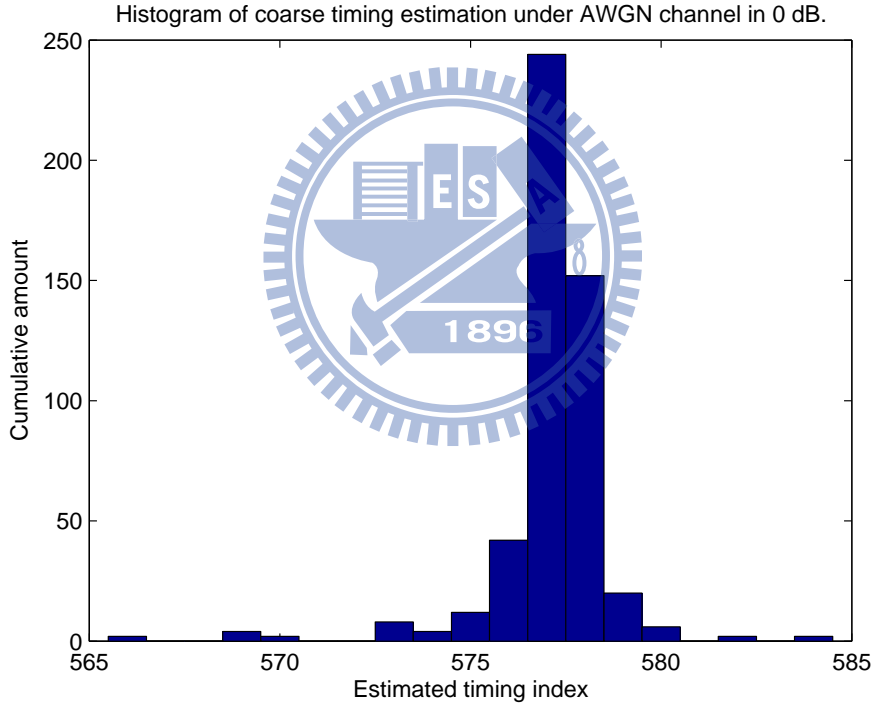


Figure 4.1: Histogram of coarse timing estimation under AWGN channel in 0 dB.

4.2.2 Fractional CFO

In this subsection, we present the performance of fractional CFO estimation under PB and SUI-5 with several different mobility which result in the Doppler shift effect, shown as Fig. 4.11. At first, we present the simulation results under AWGN channel

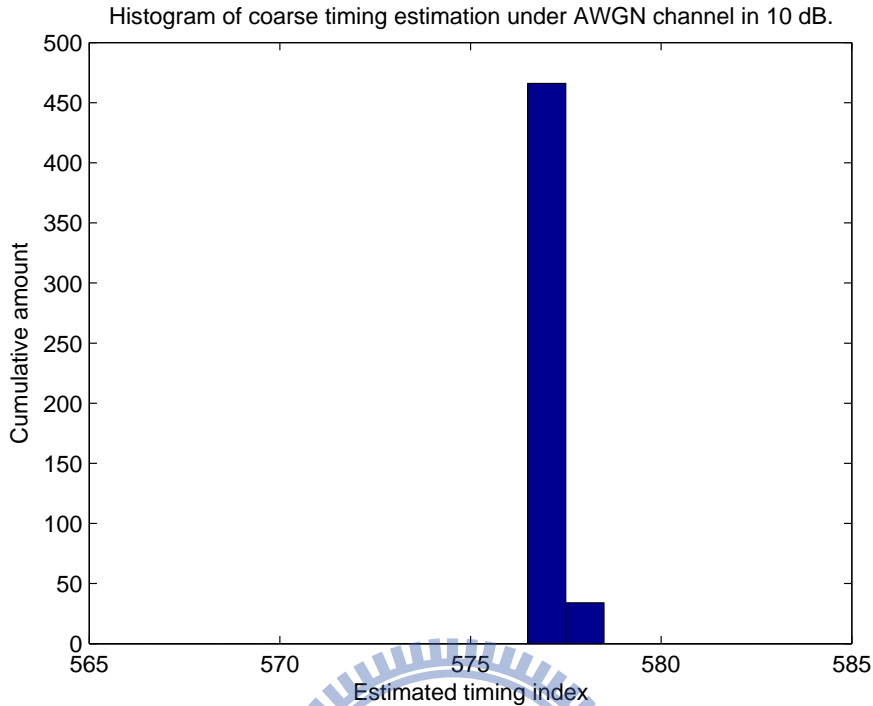


Figure 4.2: Histogram of coarse timing estimation under AWGN channel in 10 dB.

to be a comparison and the mean square error is proportional to the increasing of SNR. Moreover, we can find the relative performance of different mobility and channel delay spread. The higher mobility results in the larger Doppler shift and effects the performance seriously. Although the performance under SUI-5 with 350 km/h is the worst of all, it still satisfies the criterion of FCFO in the IEEE 802.16m specification, i.e., 0.02 subcarrier spacings.

4.2.3 Joint Estimation of Integral CFO, PA-Preamble Index, Channel Response and Fine Timing

We perform Monte Carlo simulation with five hundreds times to test our joint searching. The simulation parameters are shown as:

- ICFO: 8 subcarriers spacings.
- PID: 1 (10MHz).

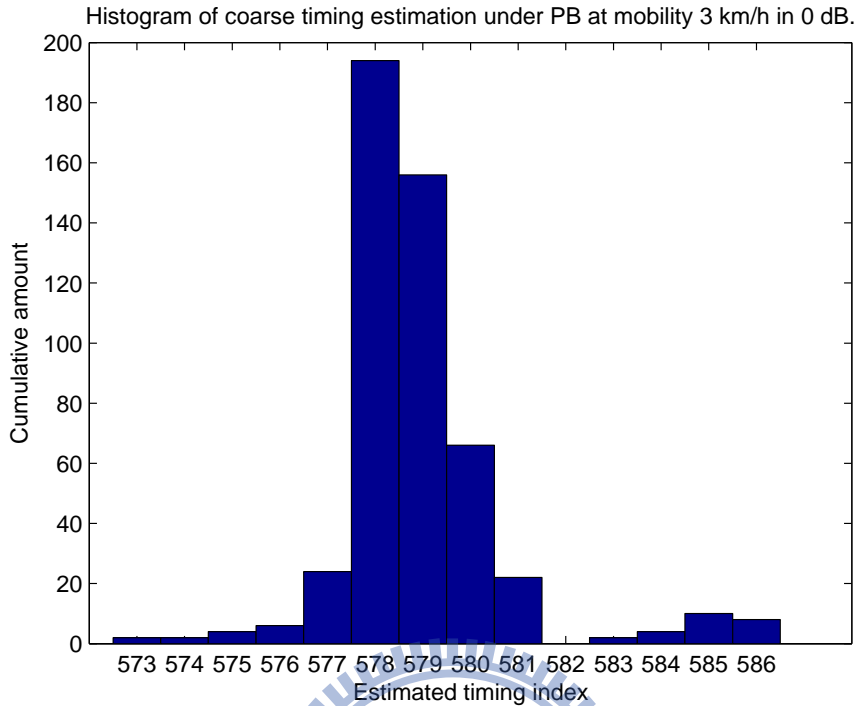


Figure 4.3: Histogram of coarse timing estimation under PB at 3 km/h in 0 dB.

- Channel model: AWGN, PB, SUI-5.
- Mobility: 3 km/h, 120 km/h.
- SNR: 0 dB, 10 dB.

Figs. 4.12 and 4.13 illustrate the simulation results under AWGN channel and we find there are some correlations between coarse and fine timing estimation. It means that the estimated coarse timing index will determine the result of fine timing estimation. In Fig. 4.2, we find the estimated coarse timing are almost 577, so that the results in Figs. 4.13 are almost 54 samples, close to the right boundary of CP. Figs. 4.14 to 4.21 depict the histograms under PB in 0 dB and 10 dB of SNR at speed 3 km/h and 120 km/h, respectively. The trend is similar with coarse timing estimation: higher mobility or lower SNR, larger dispersion and the results under SUI-5 is more centralized than under PB because the number of channel paths is less. Moreover, it is interesting that the histograms appear some special shapes and it seems to be relative to the channel models. Figs. 4.22 and 4.23 depict this jointly searching algorithm can perfectly detect the ICFO

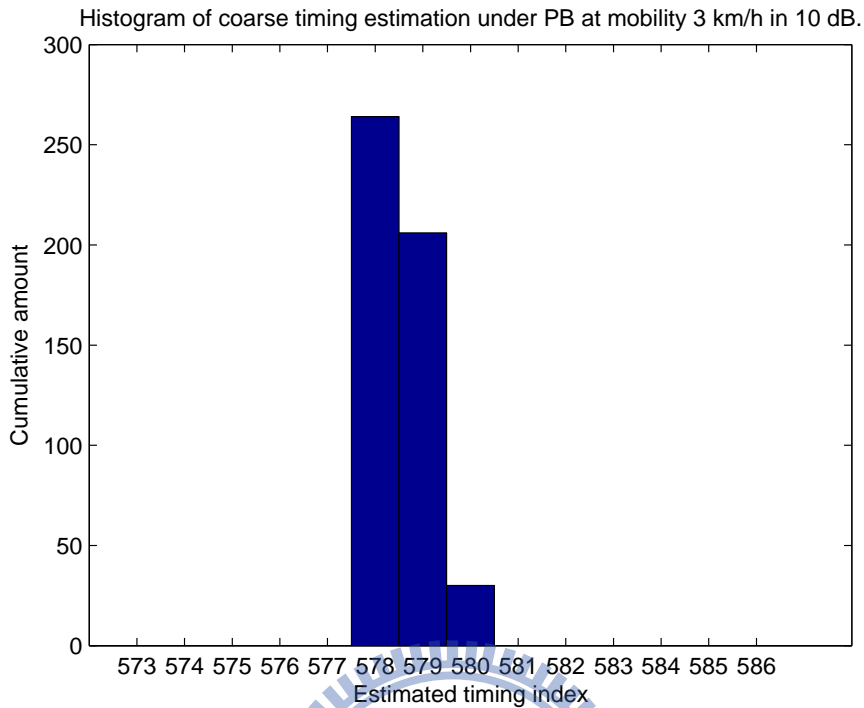


Figure 4.4: Histogram of coarse timing estimation under PB at 3 km/h in 10 dB.

and PID even if the environment has high delay spread, low SNR, and high mobility. We just present two figures to explain this result.

4.2.4 Overall Timing Estimation

It is meaningful to combine coarse timing estimation and fine timing estimation to observe the results of estimated timing index, and we define “error” is that the estimated timing index does not locate between the boundary of delay spread and the right end of CP, the region of non-ISI. From tables 4.9 and 4.6, we can know the normalized delay spread, and Figs. 4.24 to 4.33 depict the overall timing estimation.

Therefore, we can calculate the error rate according our definition of error, and show in table 4.10.

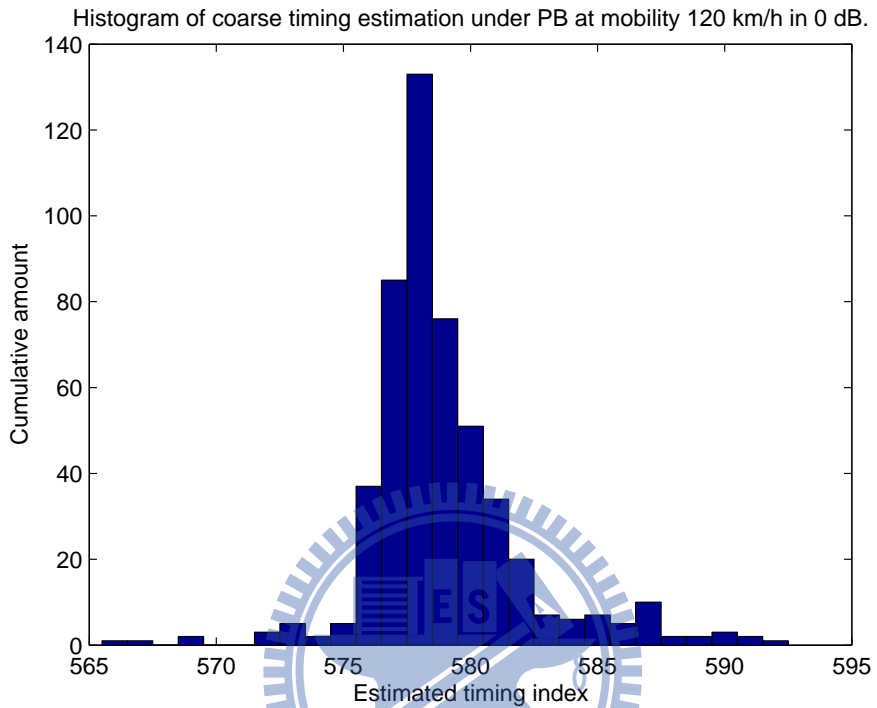


Figure 4.5: Histogram of coarse timing estimation under PB at 120 km/h in 0 dB.

Table 4.10: The error rate of timing estimation.

	AWGN	PB_3km	PB_120km	SUI5_3km	SUI5_120km
0 dB	0	0.116	0.154	0.16	0.152
10 dB	0	0.016	0.05	0.08	0.08

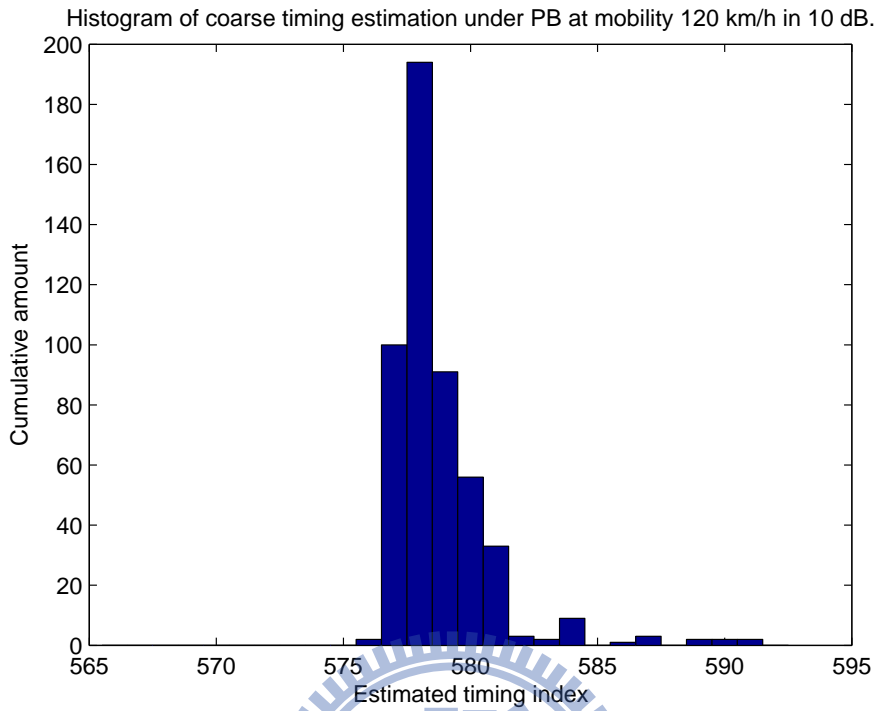


Figure 4.6: Histogram of coarse timing estimation under PB at 120 km/h in 10 dB.

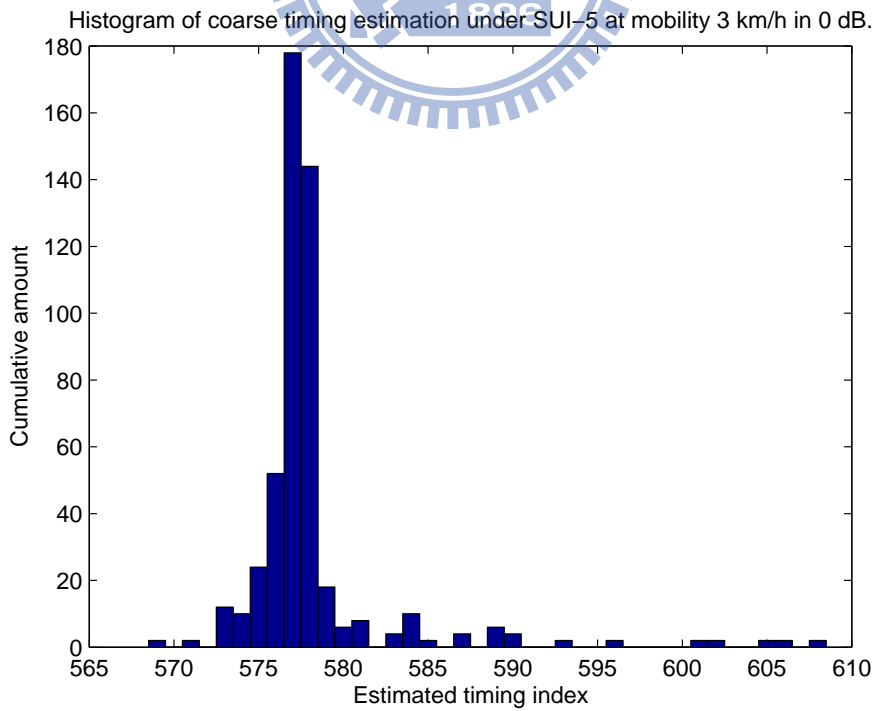


Figure 4.7: Histogram of coarse timing estimation under SUI-5 at 3 km/h in 0 dB.

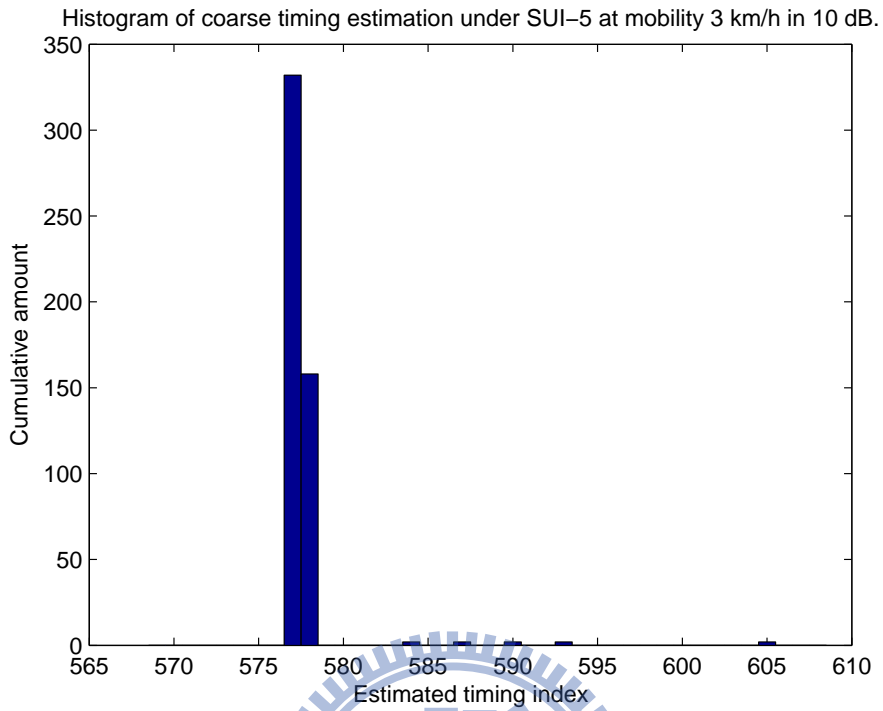


Figure 4.8: Histogram of coarse timing estimation under SUI-5 at 3 km/h in 10 dB.

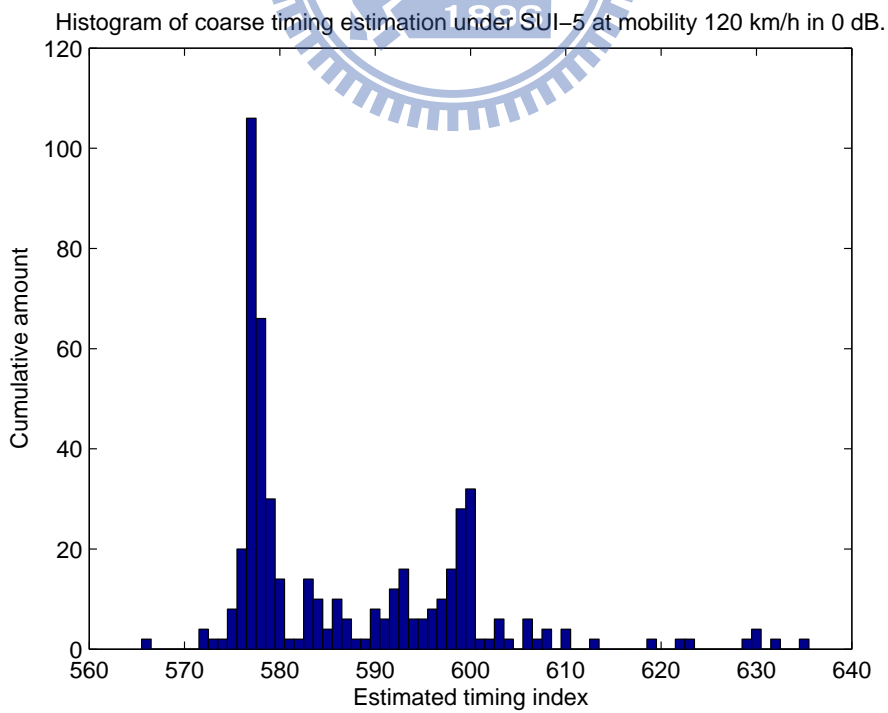


Figure 4.9: Histogram of coarse timing estimation under SUI-5 at 120 km/h in 0 dB.

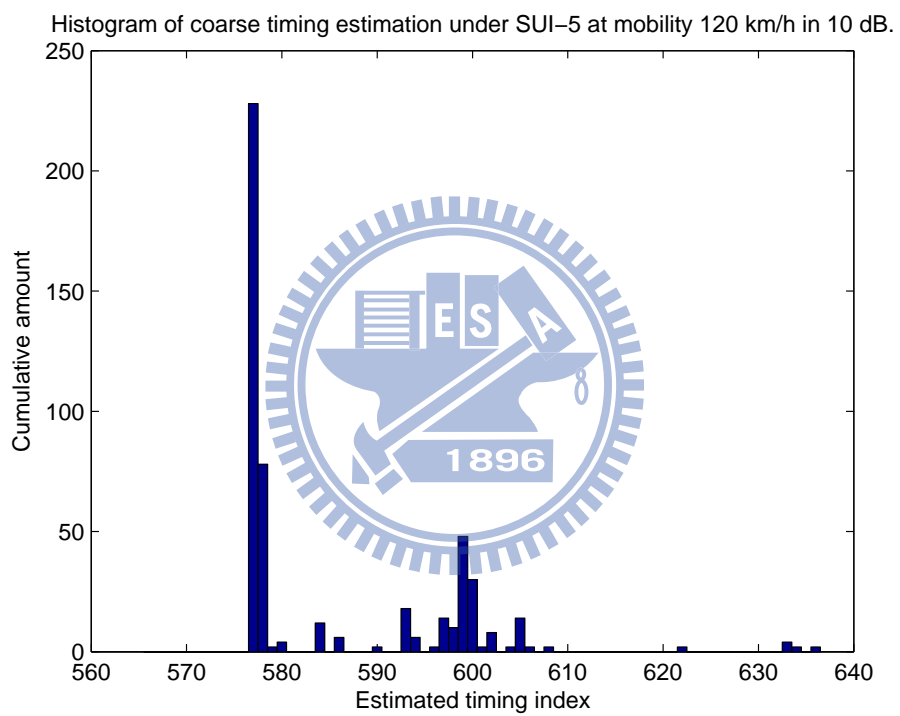


Figure 4.10: Histogram of coarse timing estimation under SUI-5 at 120 km/h in 10 dB.

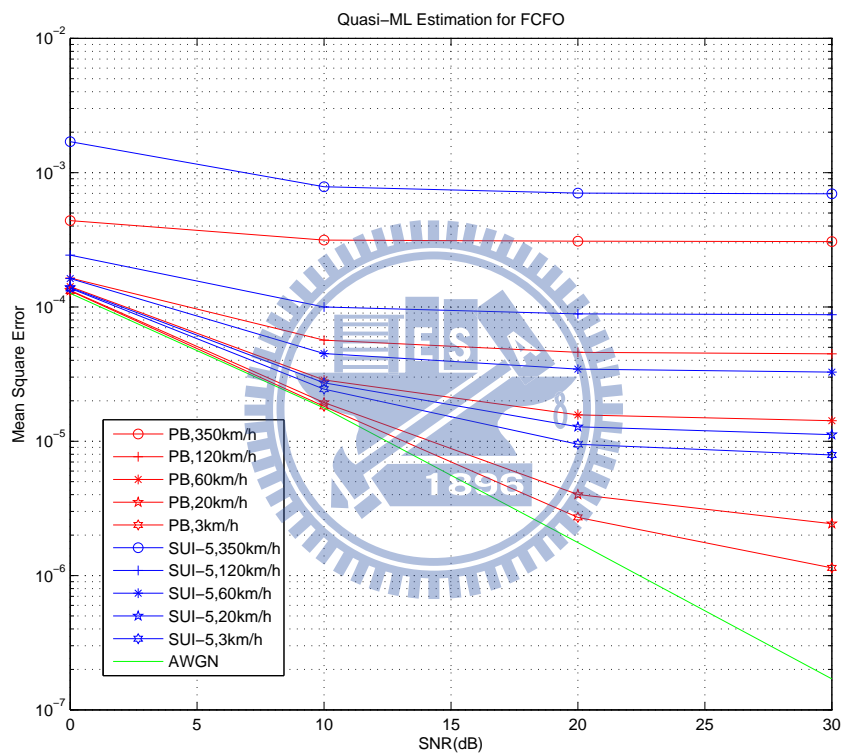


Figure 4.11: Simulation results of FCFO estimation under PB, SUI5 and AWGN channel.

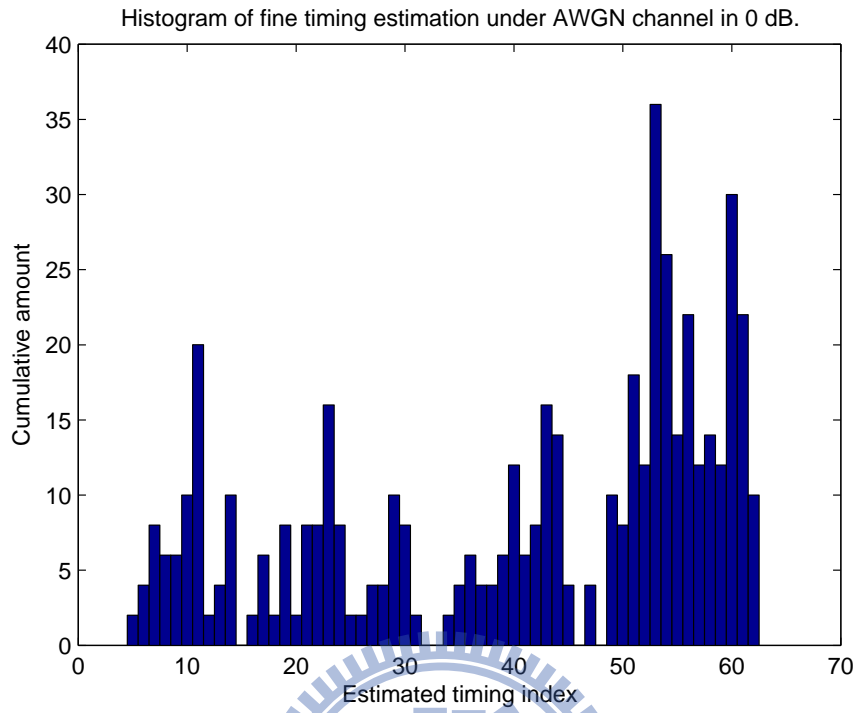


Figure 4.12: Histogram of fine timing estimation under AWGN channel in 0 dB.

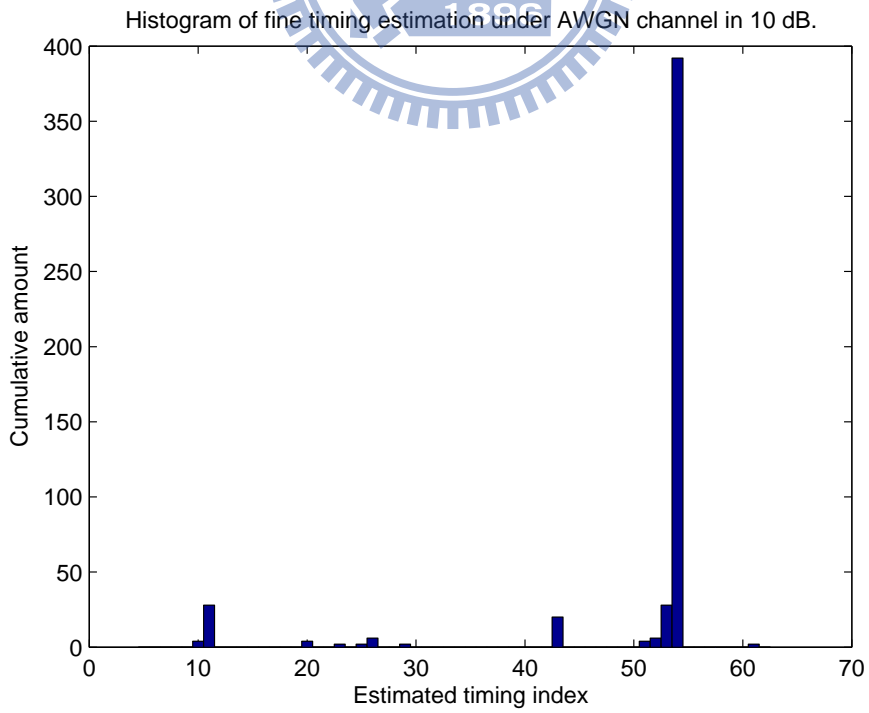


Figure 4.13: Histogram of fine timing estimation under AWGN channel in 10 dB.

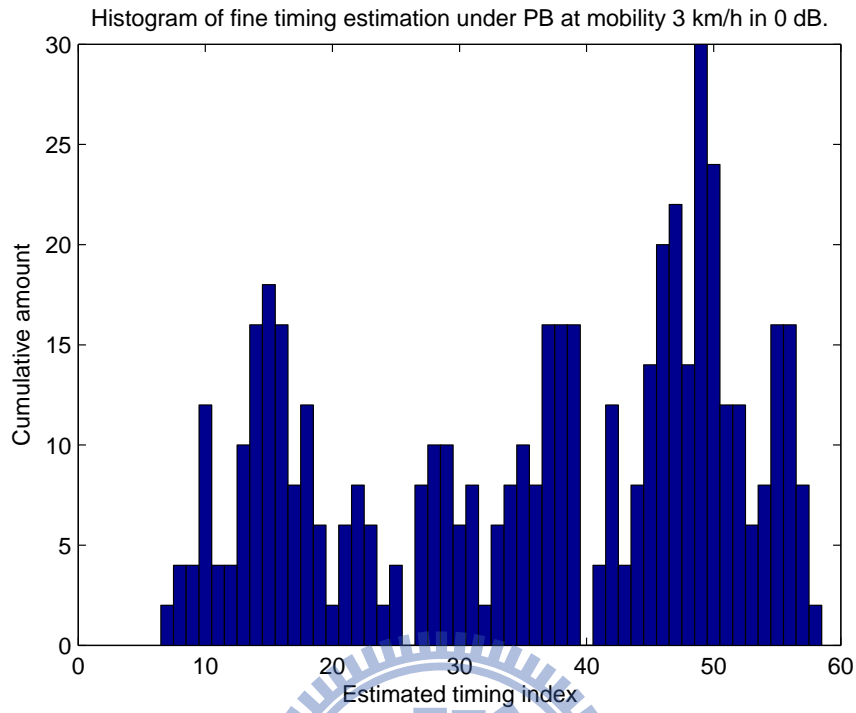


Figure 4.14: Histogram of fine timing estimation under PB at 3 km/h in 0 dB.

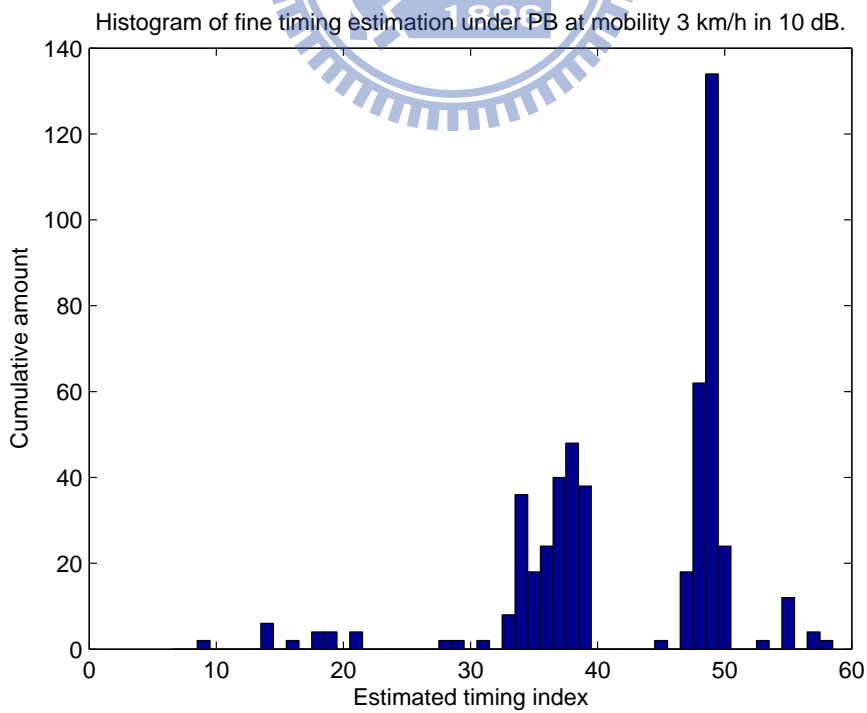


Figure 4.15: Histogram of fine timing estimation under PB at 3 km/h in 10 dB.

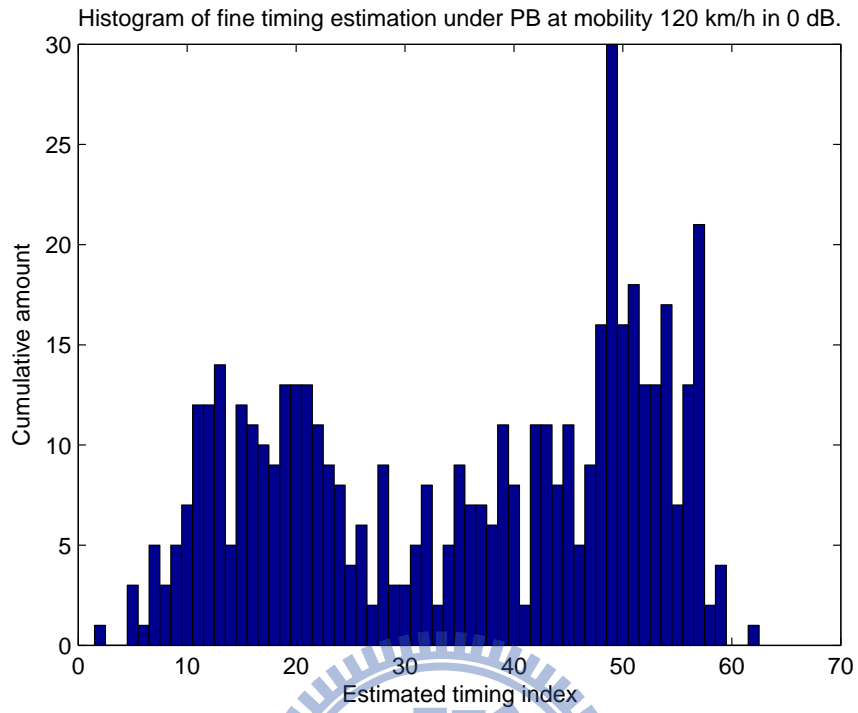


Figure 4.16: Histogram of fine timing estimation under PB at 120 km/h in 0 dB.

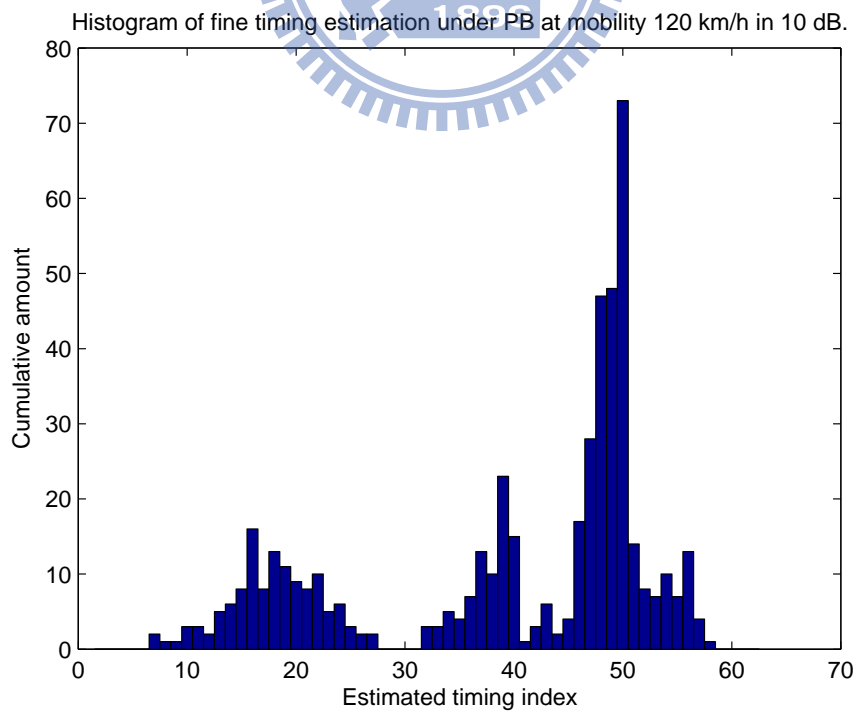


Figure 4.17: Histogram of fine timing estimation under PB at 120 km/h in 10 dB.

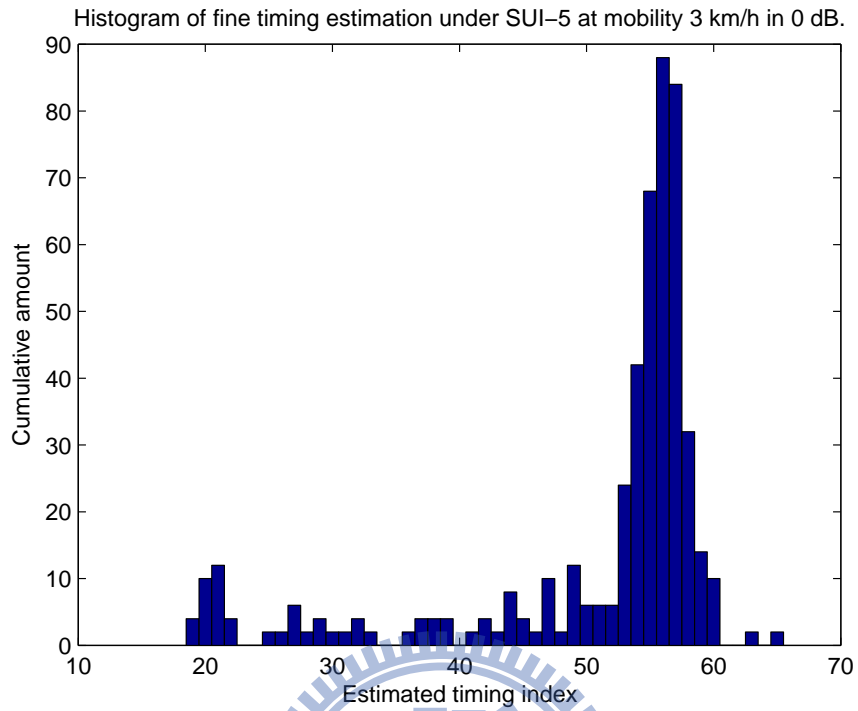


Figure 4.18: Histogram of fine timing estimation under SUI-5 at 3 km/h in 0 dB.

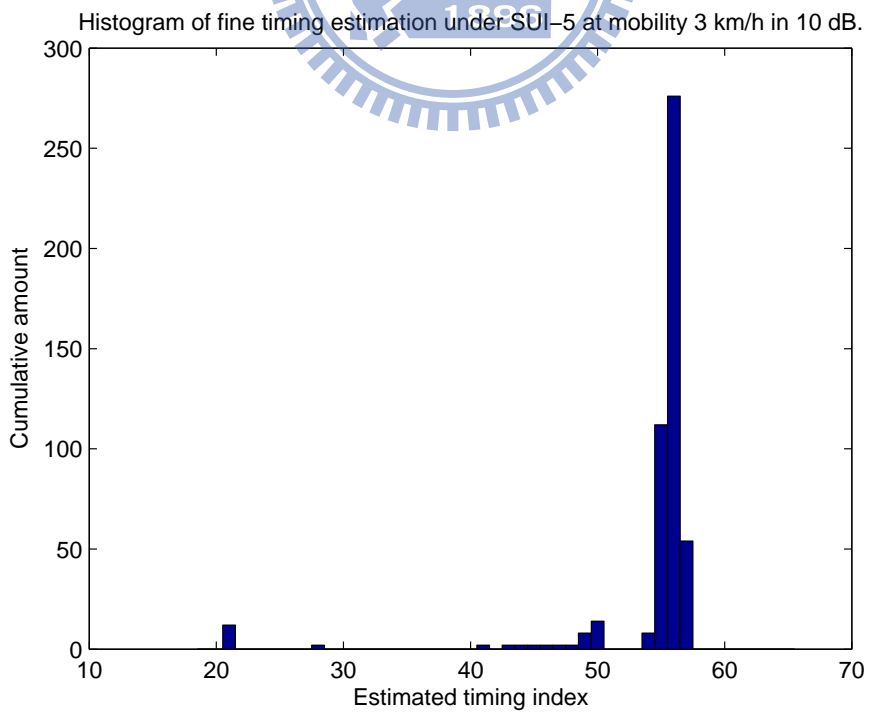


Figure 4.19: Histogram of fine timing estimation under SUI-5 at 3 km/h in 10 dB.

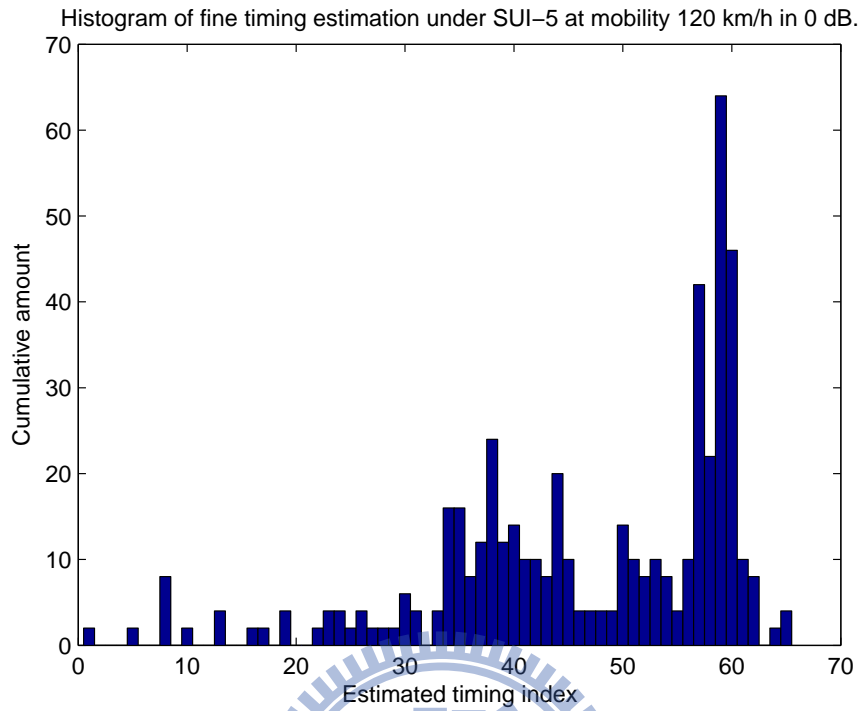


Figure 4.20: Histogram of fine timing estimation under SUI-5 at 120 km/h in 0 dB.

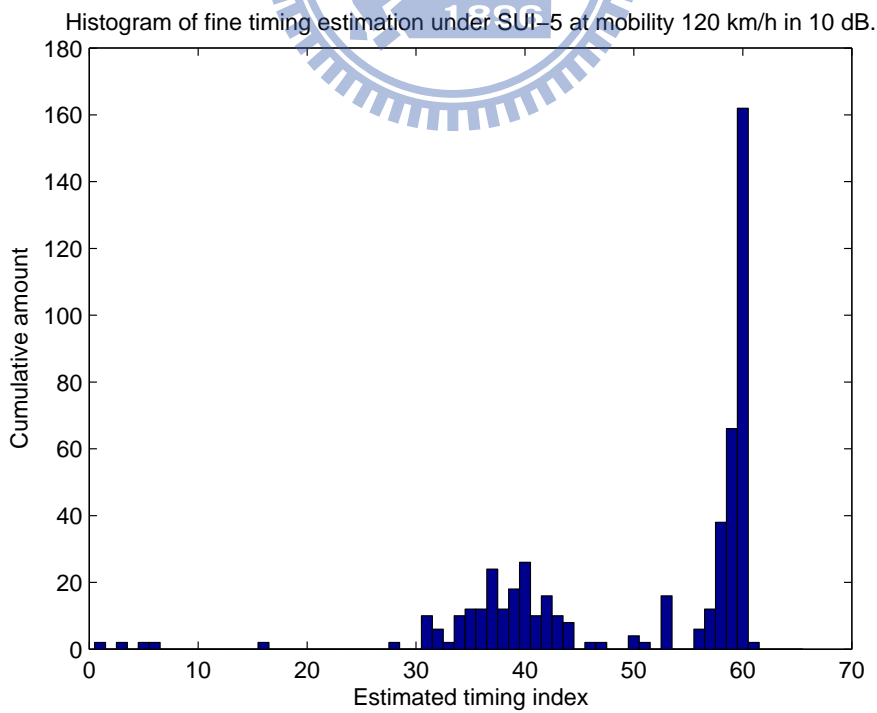


Figure 4.21: Histogram of fine timing estimation under SUI-5 at 120 km/h in 10 dB.

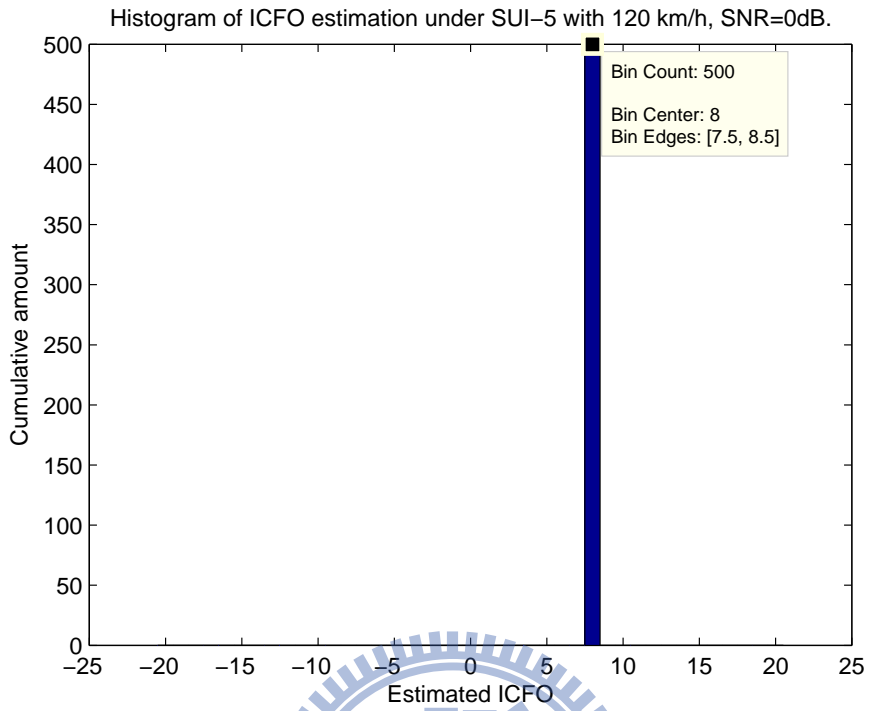


Figure 4.22: Histogram of ICFO estimation under SUI-5 at 120 km/h in 0 dB.

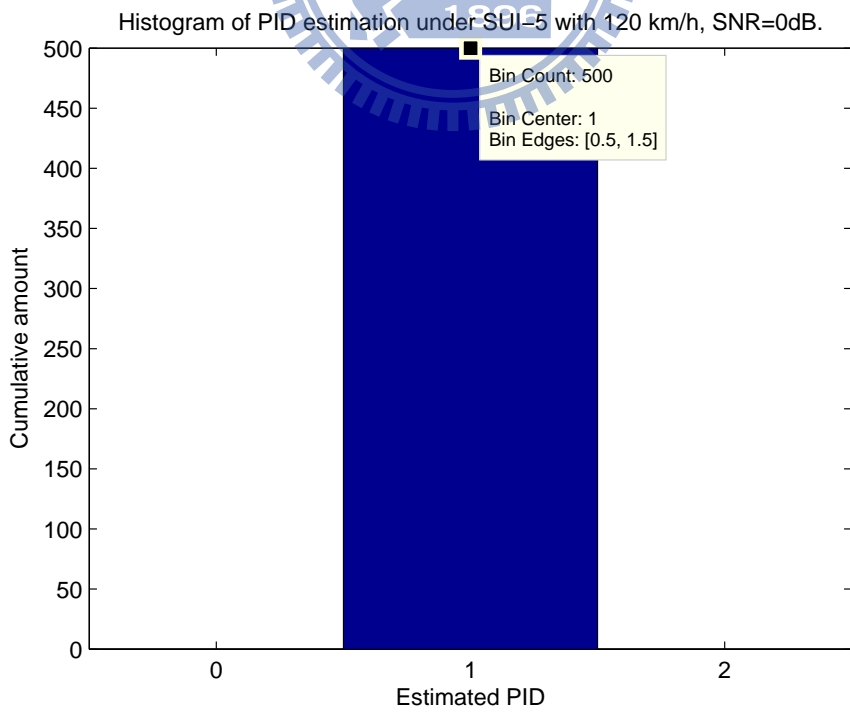


Figure 4.23: Histogram of PID estimation under SUI-5 at 120 km/h in 0 dB.

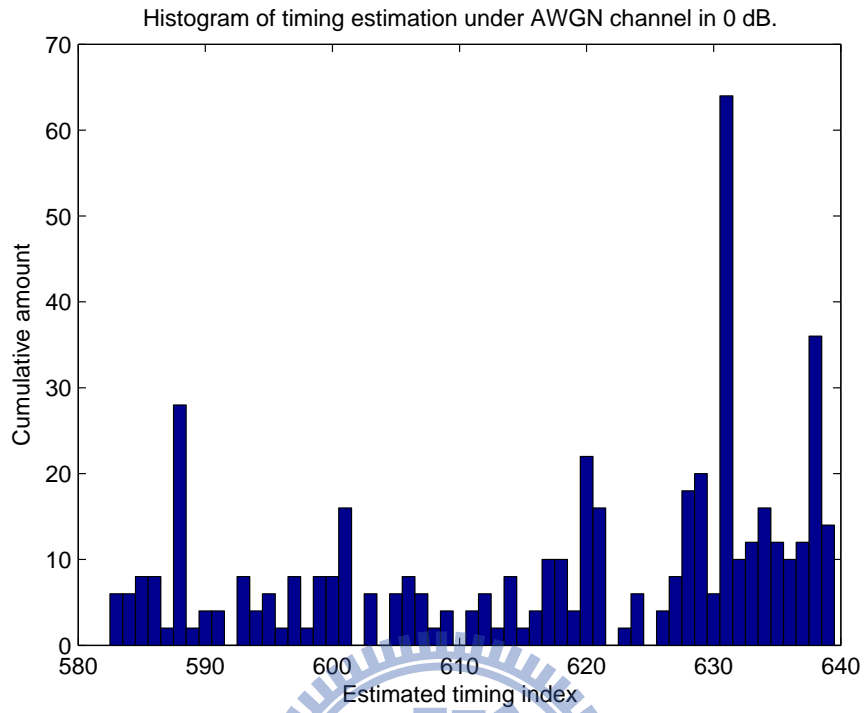


Figure 4.24: Histogram of timing estimation under AWGN in 0 dB.

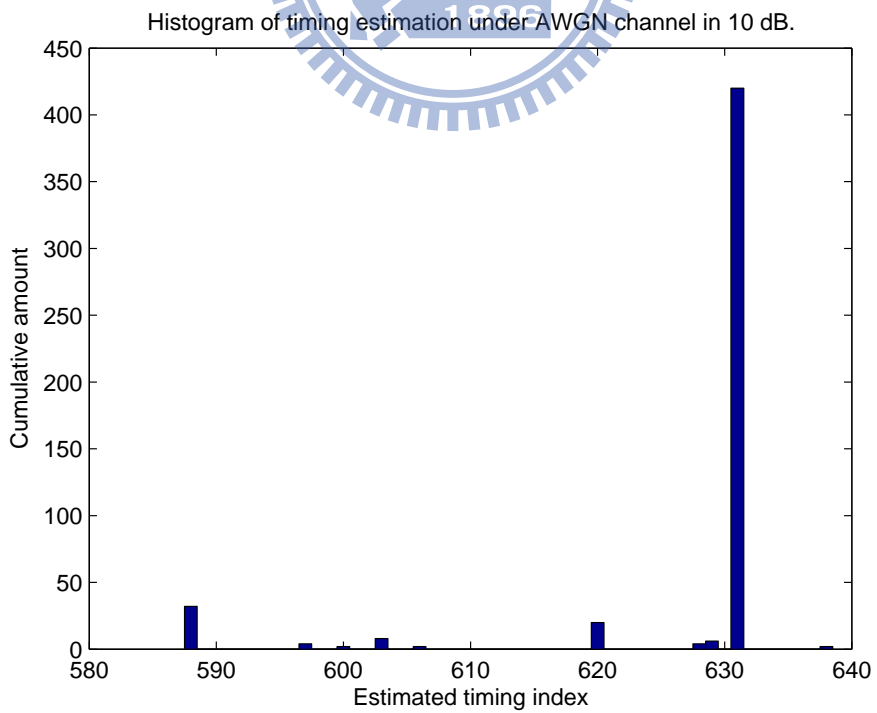


Figure 4.25: Histogram of timing estimation under AWGN in 10 dB.

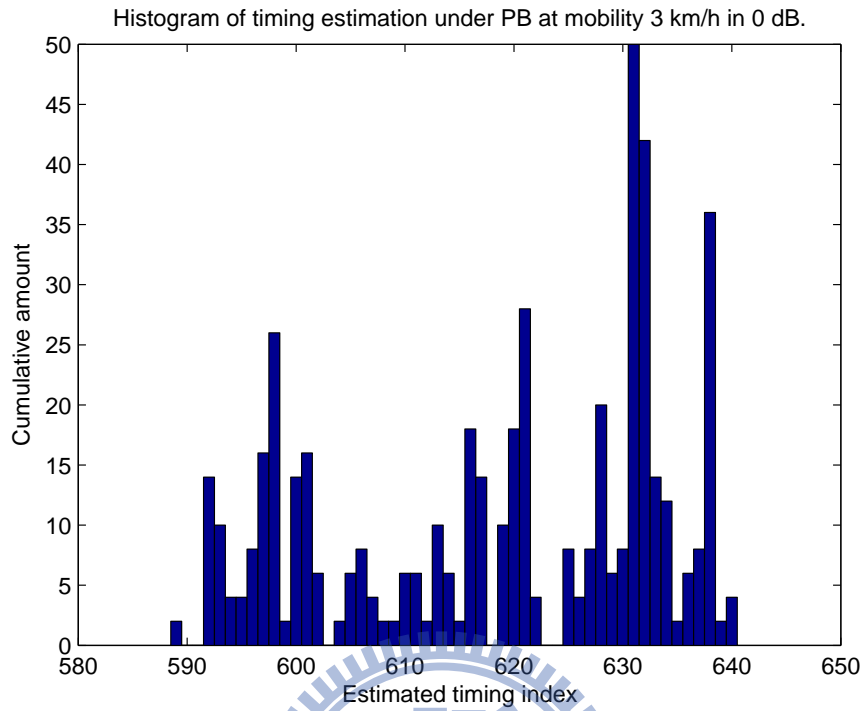


Figure 4.26: Histogram of timing estimation under PB at 3 km/h in 0 dB.

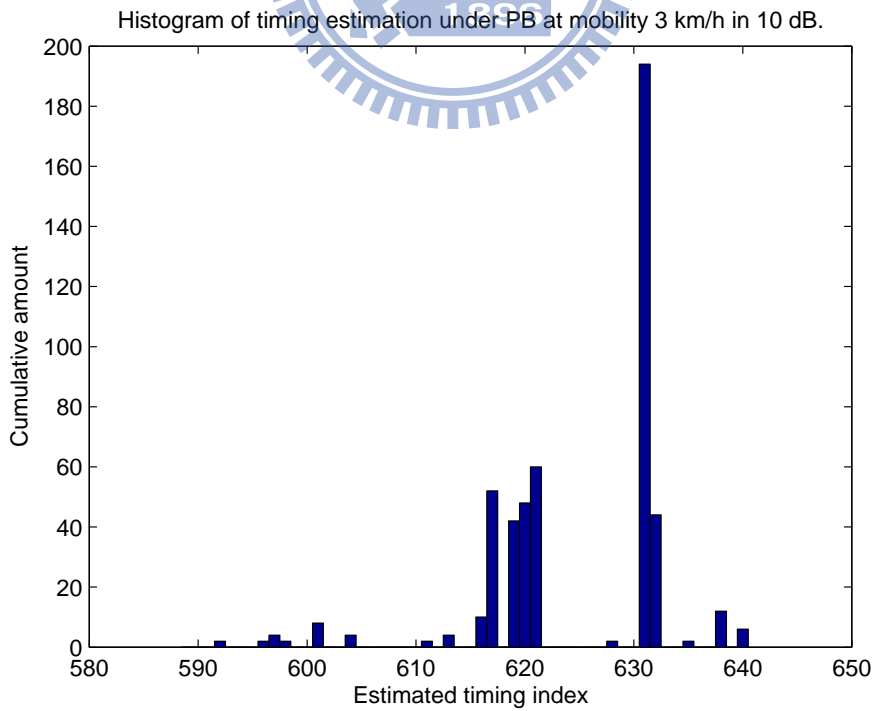


Figure 4.27: Histogram of timing estimation under PB at 3 km/h in 10 dB.

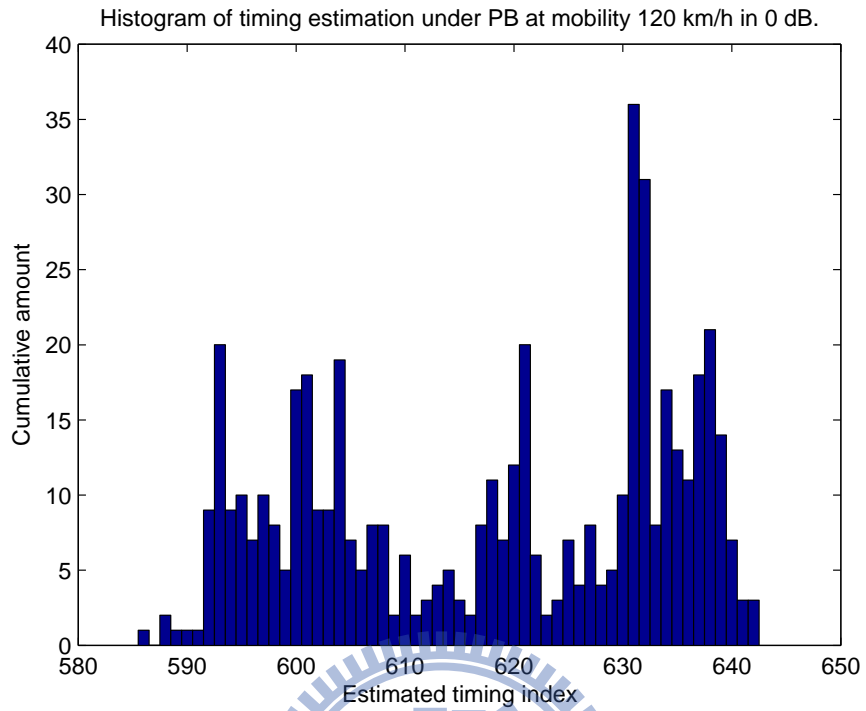


Figure 4.28: Histogram of timing estimation under PB at 120 km/h in 0 dB.

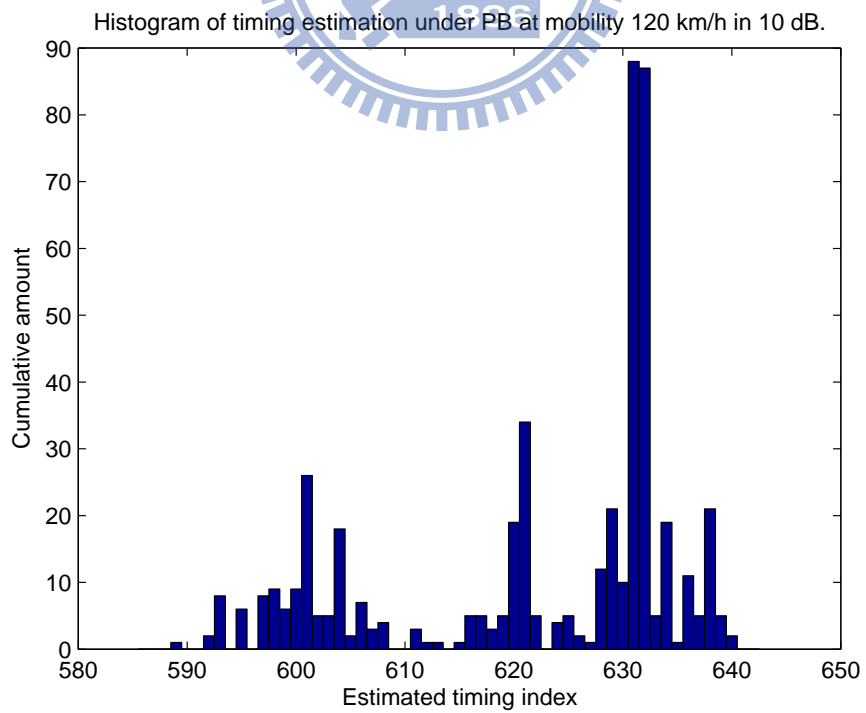


Figure 4.29: Histogram of timing estimation under PB at 120 km/h in 10 dB.

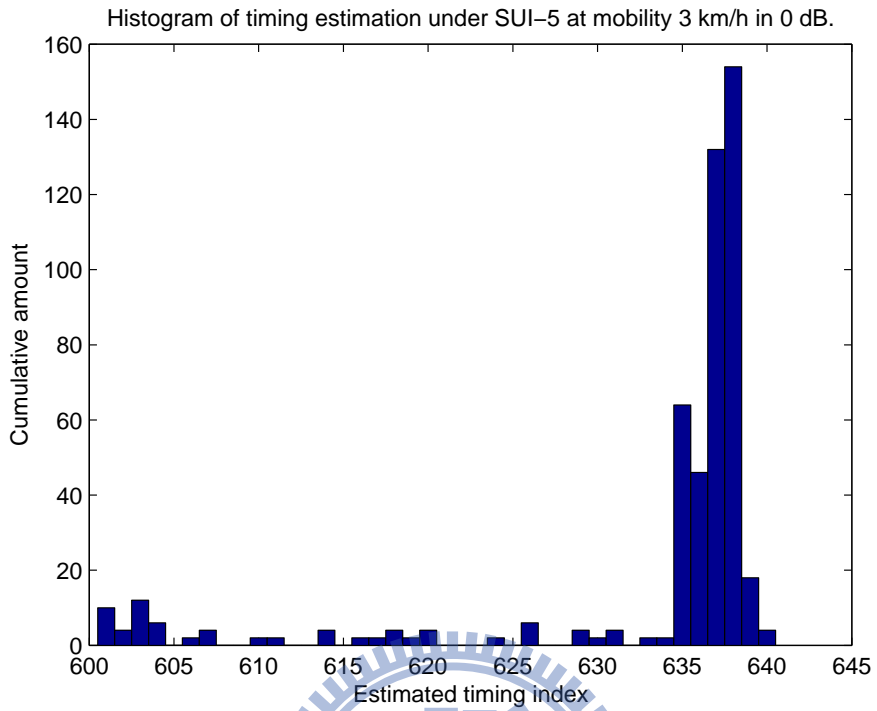


Figure 4.30: Histogram of timing estimation under SUI-5 at 3 km/h in 0 dB.

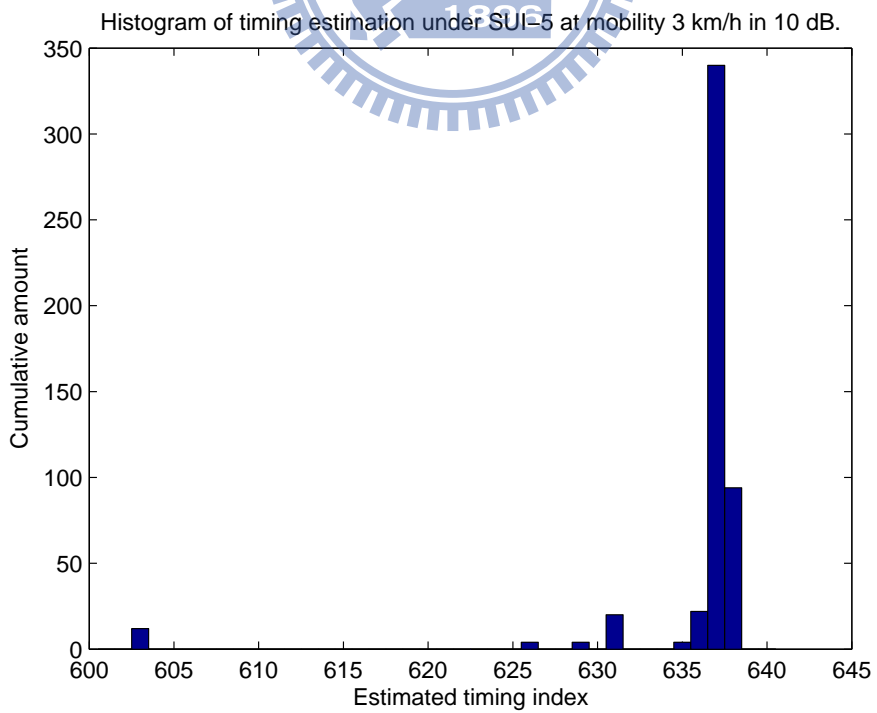


Figure 4.31: Histogram of timing estimation under SUI-5 at 3 km/h in 10 dB.

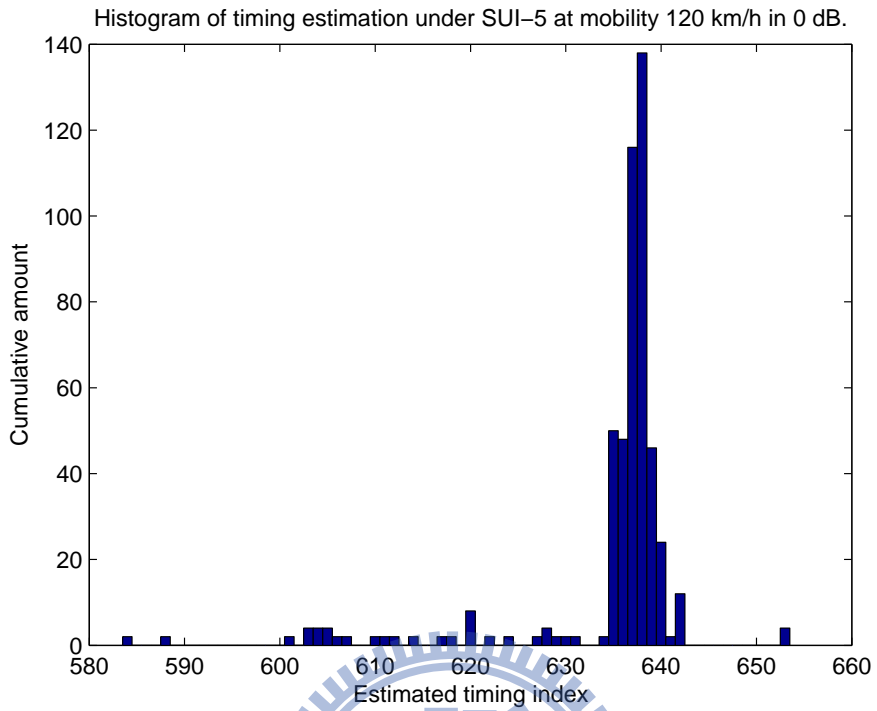


Figure 4.32: Histogram of timing estimation under SUI-5 at 120 km/h in 0 dB.

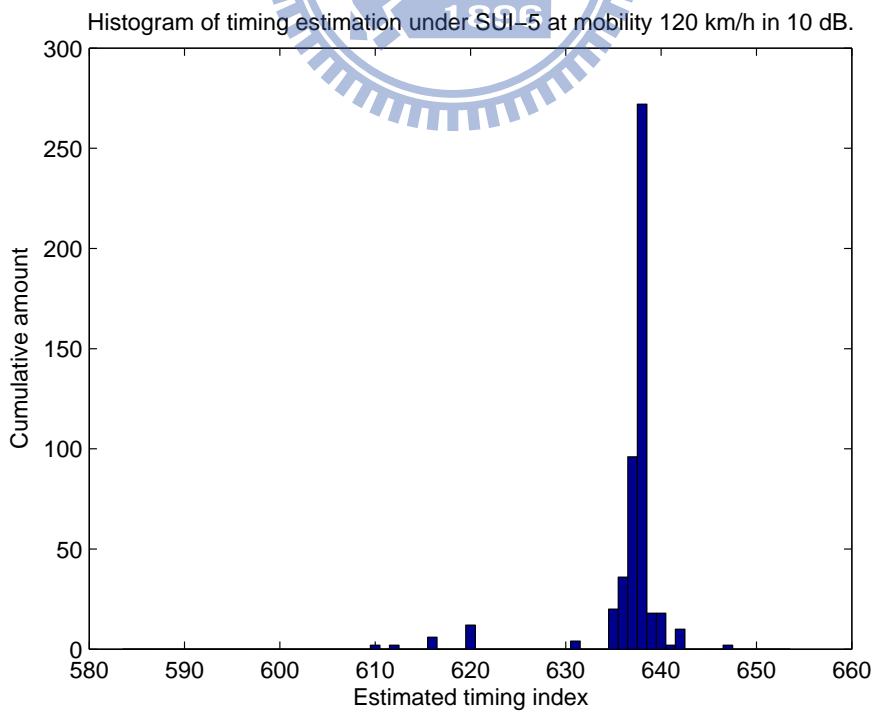


Figure 4.33: Histogram of timing estimation under SUI-5 at 120 km/h in 10 dB.

Chapter 5

Conclusion and Future Work

5.1 Conclusion

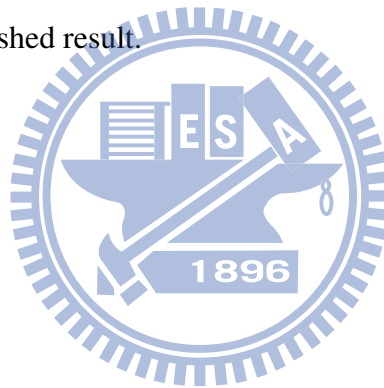
The primary contribution in our study is to derive an overall procedure of downlink initial synchronization of the IEEE 802.16m TDD system, and it can be divided into three parts in Fig. 3.12.

Above all, we capitalized on the large powerlevel of the PA-Preamble to do moving power sum and determine the beginning of the frame by detecting the peak value. Thus, we obtained the estimated PA-Preamble from the coarse timing index and this result was used in the second part. After coarse timing estimation, we derived a quasi-ML estimation to acquire the fractional CFO, and surprisingly, the result of this derivation and well-known “Moose algorithm” happen to have the same view. The performance of this estimation achieve the criterion of IEEE 802.16m, 2% subcarrier spacings, even if under long delay spread (55 samples) with the respectively mobility 350 km/h. In the third part, we derived the range of ICFO by some realization of mismatch between local oscillators, and utilized the trait of the power centralization of channel impulse response, which was derived as the function of δ in the second part, to find ICFO, PID, fine timing offset and the channel impulse response of the PA-Preamble jointly by searching 16128 candidates, which was consisting of 3 PA-Preamble, 21 ICFOs, and 256 timing index. In other words, if we choose the wrong PA-Preamble, ICFO, and timing index, the power of CIR will disperse to be like AWGN.

5.2 Future Work

There are several possible extensions for our research:

- Consider the ranging process for UL synchronization since we do not lay stress on UL synchronization in this thesis.
- Take the effect caused by sampling frequency offset and IQ mismatch into consideration. This is for a more practical simulation.
- Analyze the effects of different length of guard interval (CP). The guard interval length may effect the performance of fractional CFO and symbol timing.
- Consider the optimal ML estimation for fractional CFO and compare its performance with the established result.



Bibliography

- [1] Man-On Pun, Michele Morelli, and C.-C. Jay Kuo, “Maximum-likelihood synchronization and channel estimation for OFDMA uplink transmissions,” *IEEE Trans. Commun.*, vol. 54, no. 4, pp. 726–736, Aprl. 2006.
- [2] Lior Eldar, M. R. Raghavendra, S. Bhashyam, Ron Bercovich, and K. Giridhar, “Parametric channel estimation for pseudo-random user-allocation in uplink OFDMA,” in *IEEE Int. Conf. Commun.*, 2006, vol. 7, pp. 3035–3039.
- [3] IEEE 802.16 Task Group m Draft 2, *Part 16: Air Interface for Fixed and Mobile Broadband Wireless Access Systems — Advanced Air Interface (working document)*. IEEE 802.16m/D2, Oct.30, 2009.
- [4] IEEE Std 802.16e-2005 and IEEE Std 802.16-2004/Cor1-2005, *IEEE Standard for Local and Metropolitan Area Networks — Part 16: Air Interface for Fixed Broadband Wireless Access Systems — Amendment 2: Physical and Medium Access Control Layers for Combined Fixed and Mobile Operation in Licensed Bands and Corrigendum 1*. New York: IEEE, Feb. 28, 2006.
- [5] K.-C. Hung and D. W. Lin, “Joint detection of integral carrier frequency offset and preamble index in OFDMA WiMAX downlink synchronization,” in *Proc. IEEE Wireless Commun. Networking Conf.*, Mar. 2007, pp. 1959–1964.
- [6] R. van Nee and R. Prasad, *OFDM for Wireless Multimedia Communications*. Boston: Artech House, 2000.

- [7] Moose, P.H., "A technique for orthogonal frequency division multiplexing frequency offset correction," in *IEEE Trans. Commun.*, vol. 42, issue 10, pp. 2908-2914, Oct. 1994.
- [8] ETSI TR 101 112, "Selection procedures for the choice of radio transmission technologies of the UMTS," *ETSI Technical Report*, V3.0.2, pp. 38-43, Apr. 1994.
- [9] S. B. Weinstein and P. M. Ebert, "Data transmission by frequency-division multiplexing using the discrete Fourier transform," *IEEE Trans. Commun. Technol.*, vol. COM-19, pp. 628-634, Oct. 1971.
- [10] Chunxuan Ye; Reznik, A.; Sternberg, G.; Shah, Y., "On the Secrecy Capabilities of ITU Channels," in *Vehicular Technology Conference*, Oct. 2007, pp. 2030-2034.
- [11] C.-C. Tung, "IEEE 802.16a OFDMA TDD uplink transceiver system integration and optimization on DSP platform," M.S. thesis, Department of Electronics Engineering, National Chiao Tung University, Hsinchu, Taiwan, R.O.C., June 2005.
- [12] J. Puthenkulam, and M. Goldhammer, "802.16 overview and coexistence aspects," IEEE standard doc. no. IEEE 802.19-05/0025, July 20, 2005. Available: <http://grouper.ieee.org/groups/802/secmail/ppt00009.ppt>.
- [13] V. Bykovnikov, "The advantages of SOFDMA for WiMAX," available: <http://mail.com.nthu.edu.tw/jmwu/LAB/SOFDMA-for-WiMAX.pdf>.
- [14] WiMAX Forum, "Mobile WiMAX — Part 1: A technical overview and performance evaluation," June 2006. Available: http://www.wimaxforum.org/news/downloads/Mobile_WiMAX_Part1_Overview_and_Performance.pdf
- [15] P. Dent, G. E. Bottomley, and T. Croft, "Jakes' fading model revisited," *Electron. Lett.*, vol. 29, no. 13, pp. 1162-1163, June 1993.
- [16] V. Erceg *et al.*, "Channel models for fixed wireless applications," IEEE standards contribution no. IEEE 802.16.3c-01/29r4, July 2001.

- [17] M.-T. Lin, "Fixed and mobile wireless communication based on IEEE 802.16a TDD OFDMA: Transmission filtering and synchronization," M.S. thesis, Department of Electronics Engineering, National Chiao Tung University, Hsinchu, Taiwan, R.O.C., June 2003.
- [18] J. J. van de Beek, P. O. Borjesson, M. L. Boucheret, D. Landstromo J. M. Arenas, P. Odling, and S. K. Wilson, "Three non-pilot-based time and frequency estimators for OFDM," Research Report 1998:08, Division of Signal Processing, Lulea University of Technology, Sep. 1998.
- [19] T. M. Schmidl and D. C. Cox, "Robust frequency and timing synchronization for OFDM," *IEEE Trans. Commun.*, vol. 45, no. 12, pp. 1613–1621, Dec. 1997.
- [20] M. Morelli and U. Mengali, "An improved frequency offset estimator for OFDM applications," *IEEE Commun. Lett.*, vol. 3, pp. 75–77, Mar. 1999.
- [21] U. Tureli, H. Liu., and M. D. Zoltowski, "OFDM blind carrier offset estimation: ESPRIT," *IEEE Trans. Commun.*, vol. 48, pp. 1459–1461, Sep. 2000.
- [22] X. Ma, C. Tepedelenlioglu, G. B. Giannakis, and S. Barbarossa, "Non-data-aided carrier offset estimator for OFDM with null subcarriers: Identifiability, algorithms, and performance," *IEEE J. Select. Areas Commun.*, vol. 19, pp. 2504–2515, Dec. 2001.
- [23] T. Bhatt, V. Sundaramurthy, J. Zhang, and D. McCain, "Initial synchronization for 802.16e downlink," *Proc. Asilomar Conf. Signals Systems Computers*, Nov. 2006, pp. 701–706.
- [24] J. J. van de Beek *et al.*, "ML estimation of time and frequency offset in OFDM systems," *IEEE Trans. Signal Processing*, vol. 45, no. 7, pp. 1800–1805, July 1997.
- [25] J.-C. Lin, "Maximum-likelihood frame timing instant and frequency offset estimation for OFDM communication over a fast Rayleigh-fading channel," *IEEE Trans. Vehicular Technology*, vol. 52, no. 4, pp. 1049–1062, July 2003.

- [26] G.-W. Ji, "Research in synchronization techniques and DSP implementation for IEEE 802.16e OFDM uplink and OFDMA downlink," M.S. thesis, Department of Electronics Engineering, National Chiao Tung University, Hsinchu, Taiwan, R.O.C., June 2006.
- [27] H. Lim and D. S. Kwon, "Initial synchronization for WiBro," in *Proc. Asia-Pacific Conf. Commun.*, Oct. 2005, pp. 284–288.



作者簡歷

學生陸凱暉，民國七十二年八月出生於桃園縣。民國九十四年六月畢業於國立交通大學電機與控制工程學系，並於民國九十六年九月進入國立交通大學通訊與網路科技產業研發碩士班就讀，從事 OFDMA 通訊系統方面相關研究。民國九十九年二月取得碩士學位，碩士論文題目為『IEEE 802.16m 之初始下行同步』。

